ISSN 2500-0632 (ON-LINE)

ГОРНЫЕ НАУКИ И ТЕХНОЛОГИИ

ТОМ
VOL. 4, №1
2019

MINING SCIENCE AND TECHNOLOGY

MISIS

НАЦИОНАЛЬНЫЙ ИССЛЕДОВАТЕЛЬСКИЙ
ТЕХНОЛОГИЧЕСКИЙ УНИВЕРСИТЕТ «МИСИС»
NATIONAL UNIVERSITY OF SCIENCE
AND TECHNOLOGY MISIS

CONTENTS

СОДЕРЖАНИЕ

ORIGINAL PAPERS

DOI: 10.17073/2500-0632-2019-1-4-15

The Study of Parameters of Quarry Faces in Muruntau and Myutenbai Open Pits in Case of Applying Major Blasts

B. R. Raimzhanov, A. R. Khasanov, R. R. Vakhitov

State Unitary Enterprise "O’zGEORANGMETLITI", Tashkent, Uzbekistan,
✉b.raimjanov@mail.ru

Abstract: The paper presents process layouts for excavation of zones near pit envelope based on the analysis of findings of the ore loss study in case of open-pit mining, as well as the results of field measurements in the quarry faces in Muruntau and Myutenbai open pits. In the course of the field measurements, parameters of the quarry faces at Muruntau and Myutenbai open pits were determined under the following working conditions of an excavator: at full bench with shotpile height of 19–21 m; at full bench with shotpile height of 12–14 m at excavation of the “blast cap”; at heading face and taking ramp material. In all the above-listed quarry faces, the slope angles and the ore mass shotpile height when excavating were measured. Besides, the used excavator type (dragline or hydraulic) was taken into account. For each face, 2–3 measurements were performed, and the average slope angle at the ore mass excavation was determined for each type of excavator. At the next stage of the field measurements, the bench height in the rock mass and the shotpile parameters were measured before and after blasting operations under the following arrangements for preparing the rock mass for excavation: a) under normal conditions, when the ore mass blasting is performed for the selected face or relieving wall of the required thickness; b) in compression with a “blast cap” formation; c) in the marginal parts of the bench. Based on the results of the actual bench height and the blasted rock shotpile parameter field measurements, the following conclusions were drawn: a) the actual slope angles of the quarry faces were 49° when excavating the “blast cap” using dragline excavators, and 53° when excavating the ore mass at full bench regardless of the excavator type used; the slope angles of 49° for the dragline excavator and 53° for the hydraulic excavators were taken for further calculations; b) the width of the marginal (near-envelope) zone, where losses and dilution of balance ore are generated, increased from 7 to 13.0 m (at 49°) and from 7 to 11.3 m (at 53°); as a result, the areas of loss and dilution triangles have increased; c) when blasting in compression conditions, in the upper part of the shotpile, intense mixing of the involved rock and all ore grades occurs, therefore, when excavating the “blast cap”, bulk ore mass mining is only possible. The lower part of the blasted bench preserves the geological structure of the rock mass to a greater degree and can be selectively excavated with separation of the ore mass by grade; d) when blasting the rock mass, to maintain the required pulse direction and the blasting sequence, barren boreholes are included in the breaking outline, which increase the balance ore dilution, and structural dilution arises, which should be taken into account when drawing up the "Methods for determining, limitation and accounting for ore losses and dilution in the course of the Muruntau and Myutenbai (the fifth stage) open-pit mining"; e) when compiling the "Methods ...", the option of dividing a bench of 15 m high into two sub-benches of 7.5 m should be considered.

Keywords: excavator, face, blast, open pit, measurement, bench, ore, dragline, hydraulic, slope.

For citation: Raimzhanov B. R., Khasanov A. R., Vakhitov R. R. The study of parameters of quarry faces in Muruntau and Myutenbai open pits in case of applying major blasts. *Mining Science and Technology*. 2019;4(1):4-15. (In Russ.). DOI: 10.17073/2500-0632-2019-1-4-15.

Исследование параметров экскаваторных забоев при массовых взрывах в карьерах Мурунтау и Мютенбай

Раимжанов Б. Р., Хасанов А. Р., Вахитов Р. Р.

Государственное унитарное предприятие Узбекский научно-исследовательский и проектно-изыскательский институт геотехнологии и цветной металлургии «O'zGEORANGMETLITI», Ташкент, Узбекистан, ✉b.raimjanov@mail.ru

Аннотация: В статье приводятся технологические схемы отработки приконтурных зон на основе анализа результатов исследований по потерям руды при открытой разработке месторождений и результаты проведения натурных замеров в экскаваторных забоях карьеров Мурунтау и Мютенбай. В ходе проведения натурных замеров определены параметры экскаваторных забоев на карьерах Мурунтау и Мютенбай при следующих условиях работы экскаватора: полным уступом с высотой развала 19–21 м; полным уступом с высотой развала 12–14 м при отгрузке «шапки взрыва»; проходке и подборе съезда. Во всех вышеперечисленных экскаваторных забоях произведены замеры углов откоса и высоты развала при экскаваторной выемке рудной массы. Также учитывался применяемый тип экскаватора – канатный или гидравлический. По каждому забою производились 2–3 замера и определялся средний угол откоса при экскаваторной выемке рудной массы для данного типа экскаватора. На следующем этапе проведения натурных замеров измерялись высота уступа в массиве и параметры развала до и после производства взрывных работ при следующих схемах рудоподготовки массива к экскавации: а) в нормальных условиях, когда взрывание рудного массива производится на подобранный забой или подпорную стенку требуемой толщины; б) в зажатой среде с образованием «шапки взрыва»; в) в краевых частях уступа. По результатам проведения натурных замеров фактических углов откоса и параметров развала взорванных пород сделаны следующие выводы: а) фактические углы откосов экскаваторных забоев составили при отгрузке шапки взрыва 49° при применении канатных экскаваторов, а при выемке рудной массы полным уступом 53° независимо от типа применяемого экскаватора; углы откоса экскаваторного забоя 49° для канатного экскаватора и 53° для гидравлических экскаваторов приняты для производства дальнейших расчетов; б) увеличилась ширина приконтурной зоны с 7 до 13,0 м (49°) и с 7 до 11,3 м (53°), где образуются потери и разубоживание балансовой руды, вследствие этого увеличились площади треугольников потерь и разубоживания; в) при взрывании в зажатой среде в верхней части развала происходит интенсивное перемешивание прихватываемой породы и всех сортов руды, поэтому при отгрузке шапки взрыва возможна только валовая выемка рудной массы. Нижняя часть взорванного уступа больше сохранит геологическую структуру массива и может быть отработана селективно с разделением рудной массы по сортам; г) при взрывании массива для соблюдения требуемого направления импульса и очередности взрывания в контур отбойки включаются безрудные скважины, которые увеличивают разубоживание балансовой руды, возникает конструктивное разубоживание, которое необходимо учесть при составлении «Методики определения, нормирования и учета потерь и разубоживания руды при разработке карьеров Мурунтау и Мютенбай (V-очередь)»; д) при составлении «Методики…» следует рассмотреть возможность разделения уступа высотой 15 м на два подуступа по 7,5 м.

Ключевые слова: экскаватор, забой, взрыв, карьер, замер, уступ, руда, канатный, гидравлический, откос.

Для цитирования: Раимжанов Б. Р., Хасанов А. Р., Вахитов Р. Р. Исследование параметров экскаваторных забоев при массовых взрывах в карьерах Мурунтау и Мютенбай. *Горные науки и технологии.* 2019;4(1):4-15. DOI: 10.17073/2500-0632-2019-1-4-15.

For increasing effectiveness of gold ore deposit development by open-cut mining, the actual task of a mining enterprise in the gold ore extraction is to determine, control, standardize and account for the values of ore loss and dilution, as well as the parameters of quarry faces.

The previous studies on this topic performed by domestic and foreign scientists were devoted to excavators with small bucket capacity. Interesting production data are given in the work of B. P. Yumatov. The studies of changing ore losses and dilution depending on the number of rows of boreholes were carried out by a number of authors. Based on the measurements taken in the conditions of the Sorsky deposit, it was noted that at multi-row blasting the losses increased by 6 times, and dilution, by 3 times compared with single-row blasting. The authors explain these defects of multi-row blasting by the individual features of the geological and morphological structure of the Sorsky stockwork and the imperfection of the implemented drilling and blasting.

In fact, the defects are the result of the fact that the outliners of the ore bodies in the shotpile were not known, and therefore the excavation of the blasted rock mass was carried out "blindly". This work correctly indicates that the use of the method of tool surveying and designing commercial and non-commercial sections for a multi-row block shotpile is only possible with accurate taking into consideration the degree of transformation and mixing of the ore sections of the block during the blasting. At the same time, the possibility of implementing such an operation with modern drilling and blasting methods is being called into question.

An attempt to theoretically determine the positions of the individual layers of a bench in the shotpile was undertaken by G.G. Lomonosov. He proposed an algorithm for predicting shotpile parameters based on the laws of external ballistics. The essence of the algorithm is that based on the magnitude of the initial rock fragment velocity, using the laws of external ballistics, it is possible to determine the trajectories of points located on the outer contour of the blasted bench. This allows determining the nature of the bench rock distribution in the blasted rock mass.

In the process of drawing up the "Methods for determining, limitation and accounting for ore losses and dilution in the course of the Muruntau and Myutenbai (the fifth stage) open-pit mining"; for the "M" mine of the Central Mine Group of the Navoi Mining and Metallurgical Combine, the initial data were determined and refined.

Process layouts for mining in near-envelope (contact) pit zones

Based on the analysis of the findings of the studies on ore losses during open pit mining, it was found that the contact (or near-envelope) zone demonstrates a complex shape of the ore-rock contact surface and in some cases may not have a distinguished contact surface. It is possible to distinguish a certain volume of rock mass located in the transitional zone from balance ore to off-balance ore or from one ore grade to the next. Depending on an ore body dip angle and the height of a working bench, the contact zone may have different widths.

The size of the contact zone in plan view and in the cross-section depends on a number of factors:

– grades of valuable components in the contact zone;

– the ore body dip angle in the contact zone;

– the height of working bench;

– visual distinguishability of ore and rock.

Excavation of contact zones can be carried out by longitudinal or transverse cuts. The selection of cut type depends on the following factors:

– curvature of the contact zone line in plan view;

– the degree of visual distinguishability of ore and rock in the contact zone;

– the degree of curvature of the "ore-rock" contact plane in vertical sections;

– parameters of ore bodies – strike, thickness, dip angle.

The less curved the contact zone line in plan view and the greater its length, the more appropriate the selective excavation of the contact zone, since in this case the excavating cut does not practically change its direction. The selection of the longitudinal or transverse layouts for contact zone excavation is carried out on the basis of the requirements for the quality of the extracted minerals. The longitudinal mining pattern should be selected under conditions of a large length of the contact zone without changing direction, whereas the transverse one, in case of a strongly curved contact zone line with changeable direction in plan view.

Currently, when using the block model for reserve estimation in the contour of the mined bench, which is considered to be a mining unit, the following ore grades are distinguished:

– three grades of rich ore located in the central part of the ore deposit being developed (core of the deposit), namely:

a) balance ore with the metal grade in excess of 4.0 conditional units (CU);

b) balance ore with the metal grade of 2.0 to 4.0 CU;

c) balance ore with the metal grade of 1.50 to 2.0 CU;

– balance ore with the metal grade of 1.0 to 1.50 CU;

– balance ore with the metal grade of 0.50 to 1.0 CU;

– off-balance ore graded at from 0.40 to 0.50 CU;

– rock – mineral mass with the metal grade below 0.40 CU

To draw up grade plans for ore excavation (digging) within the mining bench, at the current planning, three balance ore grades (a, b, c), due to their small amount, are usually combined into one grade of balance ore with the metal grade exceeding 1.50 CU, which is selectively excavated, stockpiled in a separate sectional type ore stockpile, and serves to charge leaner ore grades supplied to GMZ-2 (processing plant) for processing. This allows stabilizing the metal grade in the commercial ore going to processing, and ensures stability of the final product output.

The analysis of the ore excavation parameters in the contact zones involved the following ore grades:

– balance ore with the metal grade in excess of 1.50 CU (denoted as R – "Rich");

– balance ore with the metal grade of 1.0 to 1.50 CU (denoted as M – "Medium");

– balance ore with the metal grade of 0.50 to 1.0 CU (denoted as LG – “Low-grade ore”);

– off-balance ore with the metal grade of 0.40 to 0.50 CU (denoted as OB – “Off-Balance”);

– rock with the metal grade of less than 0.40 CU (denoted a R "Rock").

The presented division of ore mass into grades corresponds to the approved conditions for the Muruntau and Mutenbai deposits development in the fifth stage envelope.

Analysis of the “ore - enclosing rocks” contact zones for the Muruntau and Mutenbai deposits made it possible to classify their manifestations.

The developed classification covers the features of the contact zone geological structure, the qualitative characteristics of the enclosing rocks, the ore grades, rock types, the valuable component content in relation to the mine engineering parameters of mining operations (concordant or discordant dipping of the contact zone, the bench slope line and front of acting benches, the contact dip angle) (Fig. 1).

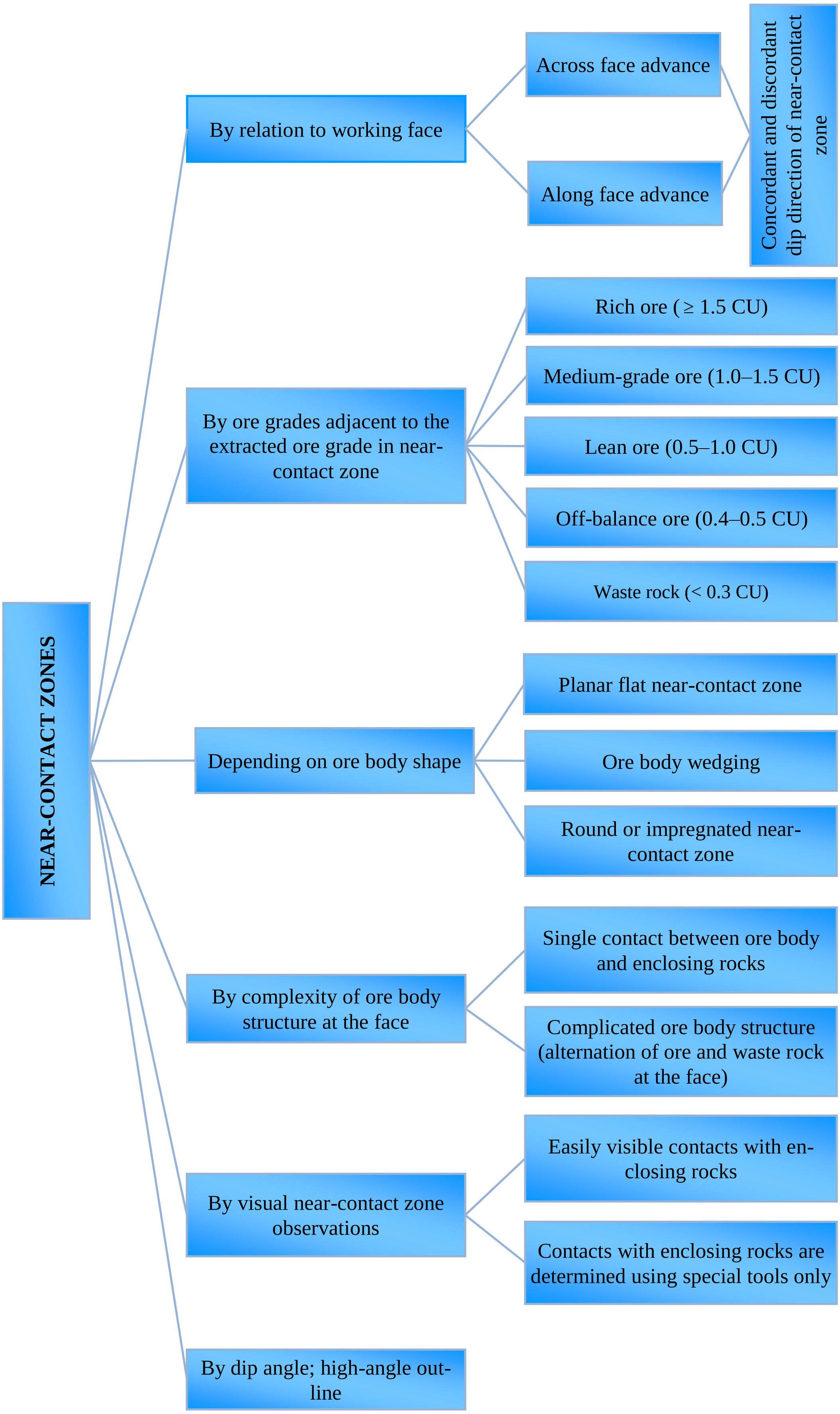

Fig. 1. Classification of contact zones

For the analysis, the main types of the contact zones were selected on the grade plans presented by the Navoi MMC specialists. The studied contact zones are the boundaries between the ore grades, the extraction of which is carried out selectively according to the surveyed reference points. Bulk mining of all grades of ore and rock with preservation of the rock mass structure is envisaged. The boundary between the grades of ore and rock is assumed to be vertical within the limits of the extracted bench.

In this case, the face in vertical section can be conditionally divided into right and left parts, respectively, with ore of one grade and ore of the next grade, ore of one grade and rock, or vice versa, depending on the direction of excavation. The metal grade in the rock mass of the near-contact zone is assumed to amount to the average value between the grade of excavated ore and the grade of the bordering ore (admixed to the excavated ore).

The boundary grade at the contact between the ore or rock grades is assumed to be equal to the cut-off grade for the division of the ore and rock grades. The width of the near-contact zone, where different ore types and rock are mixed, was determined by the graphical-analytic method depending on the slope angle during excavation of the blasted rock mass. The maximal slope angle is accepted for both transverse and longitudinal cuts: 49^{o} and 53^{o}, respectively. The contact zone width amounted to 13.0 m (Fig. 2).

The ratio of the different ore grades interval lengths in the extraction contour was determined based on the equation of $C_{\text{вк}}$, the metal grade at the boundary of the extraction contour; $C_{\text{бс}}$, the accepted grade for the separation of ores into the grades for the reserve estimate. The $C_{\text{бс}}$ value is taken according to the current separation of ore into the grades when planning production in an open pit.

In this case, the length of ore and rock intervals on the boundary between the ore grades in the course of excavation is determined from the following equation:

$$H \cdot C_{\text{бс}} = h_{\text{р}} \cdot C_{\text{р}} + h_{\text{п}} \cdot C_{\text{п}},$$

$$h_{\text{р}} = \frac{H \cdot (C_{\text{сб}} - C_{\text{п}})}{(C_{\text{р}} - C_{\text{п}})}, \quad (1)$$

$$h_{\text{п}} = H - h_{\text{р}},$$

where H is the height of the extracted layer at the boundary between the selectively extracted ore types; $h_{\text{р}}$ is the length of the extracted ore grade at the face or the length of the ore interval at the ore/rock boundary; $h_{\text{п}}$ is the length of the rock interval at the face at the boundary with the extracted ore grade type, or the length of the rock interval at the ore/rock boundary; $C_{\text{р}}$ is the gold grade in the ore in the extraction contour (the normalized average gold grade for the extracted ore grade type); Cп is the gold grade in the admixed rock mass (the normalized average gold grade for the ore grade type adjacent to the extracted ore grade type); $C_{\text{бс}}$ – cut-off grade of gold for the division into the ore grades, the ore/rock separation.

In Fig. 2: L – the length of an elementary ore block or the length of the scooping line at several scooping faces, m; S_p – the area of the ore loss triangle in the elementary ore block, m; $S_{\text{п}}$ – the area of the triangle of admixing of the adjacent ore grade or dilution of the elementary ore block by rock, m; α – the angle at which the upper contour of the blasted rock mass begins to be loaded when the excavator bucket scoops along the bench bottom (determined experimentally), degrees; $C_{\text{бс}}$ – boundary (cut-off) grade for separating the ore grades, ore and rock, conditional units; $C_{\text{п}}$ – gold grade in diluting rock mass, conditional units; C_p – gold grade in the elementary ore block, conditional units; $l\Delta$ – the width of the near-envelope (near-contour) zone, m; $\Delta_{\text{р}}$ – the distance to the point of positioning the flag, indicating the border of the rock mass loaded as ore, m.

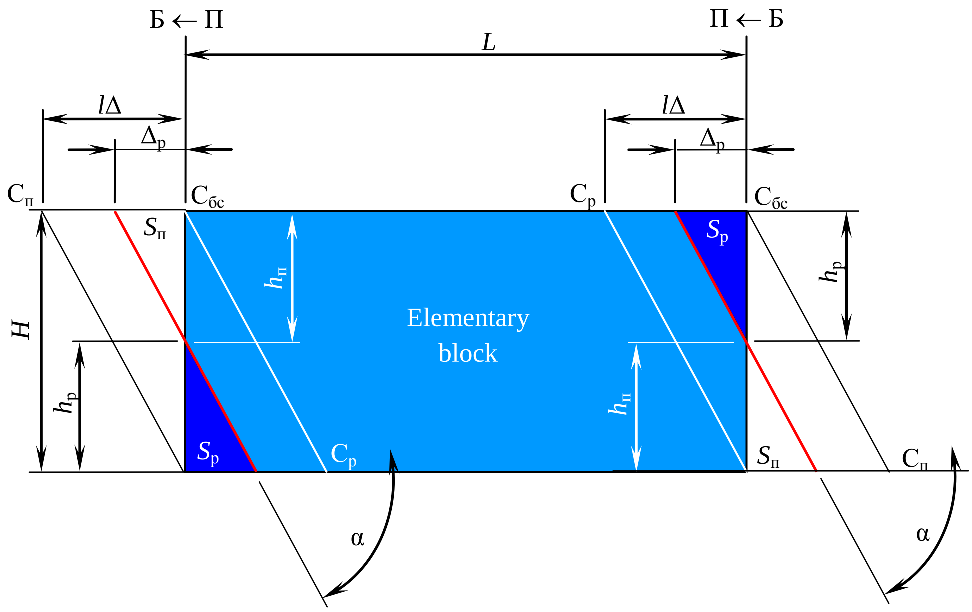

Fig. 2. Schematic of losses and dilution generation in bench slopes when scooping blasted ore mass:
L – the length of an elementary ore block or the length of the loading line at several sides of loading, m; $S_р$ – the area of an ore loss triangle in an elementary ore block, m^2; $S_п$ – the area of a triangle of admixing the neighboring ore grade or dilution by a rock for an elementary ore block, m^2; α – the angle at which the upper contour of the blasted rock mass begins to be undermined when scooping along the bench bottom (to be determined experimentally), degrees; $С_{бс}$ – cut-off grade of gold for the separation of grades of ore, ore and rock, conditional units; $С_п$ – gold grade in the diluting rock mass, conditional units; $С_р$ – gold grade in the elementary ore block, conditional units; *l*Δ – width of the border zone, m; $\Delta_р$ – the distance to the flag-indicator to be installed for indicating the boundary of the rock mass loaded as ore, m)

As part of the analysis, various options for selective ore extraction in the contact zones between different ore grades, depending on the direction of excavation, are considered.

It is accepted that: when excavating ore from richer one towards leaner one, a shift from the contact by the size of the loss triangle should be taken, while when excavating in opposite direction, the shift from the contact by the size of the dilution triangle should be taken.

The slope angles of excavating cuts are taken on the basis of the field measurements at the Muruntau and Mutenbai open pits and amount to 49° for dragline excavators and 53° for hydraulic excavators.

Results of the field measurements in the quarry (excavating) faces of the quarries of the Muruntau and Mutenbai open pits

The parameters of the quarry faces were measured at the Muruntau and Mutenbai open pits under the following conditions of excavating:

– by full bench with the shotpile height of 19–21 m;

– by full bench with the shotpile height of 12–14 m when excavating the “blast cap”;

– by ramp cutting and scooping.

In all the above-listed quarry faces, the slope angles and the ore mass shotpile height at digging were measured. Besides, the used excavator type (dragline or hydraulic) was taken into account. For each face, 2-3 measurements were performed, and the average slope angle at the ore mass digging was determined for the type of excavator.

The results of determining the slope angles of the quarry faces are given in Table 1.

At the next stage of the field measurements, the bench height in the rock mass and the shotpile parameters were measured before and after blasting operations under the following arrangements for preparing the rock mass for excavation:

a) under normal conditions, when the of the ore mass blasting is performed for the swept face or relieving wall of the required thickness;

b) in compression with a “blast cap” formation;

c) in the marginal parts of the bench.

Table 1

Slope angles of quarry faces

Type of excavator	**Type of work**	**Slope angle, degrees**		
		from	**to**	**average**
Muruntau open pit				
EG-12	Full bench	52	55	53
Myutenbai open pit				
EKG-77	“Blast cap” loading	45	50	49
EKG-60	Full bench	52	55	53
EG-14	Ramp cutting	47	51	–

Table 2

The results of the field measurements of the blasted rock shotpile parameters

Level	**Bench height, m**	**Blasting method**	**Blasted bench height, m**		
			from	**to**	**average**
Muruntau open pit					
+330	15	With “blast cap” formation	17	+330	15
+135	15	With “blast cap” formation in marginal parts	16	+135	15
Myutenbai open pit					
+315	15	With “blast cap” formation	23	+315	15
+315 (Block 1)	10	Under compression conditions	15	+315 (Block 1)	10
+315 (Block 2)	10	Under compression conditions	16.5	+315 (Block 2)	10
+300	15	For excavated face	13.8	+300	15

At the “M” mine open pits, row-by-row arrangement of blast holes on a 5.6×5.6 m grid was adopted. The drilling within a working bench is based on the drilling project. The boreholes located within an ore body outline are exploratory-production, in which drill cuttings are sampled every 5 m. In the samples of drill cuttings in the laboratory, the metal grade is determined, and then the average metal grade in the block model cell tied to this borehole is calculated.

For each specific block, a Project for loading borehole charges is drawn up, which indicates the blast network installation layout, providing the required direction of the initiating pulse passage and the sequence of blasting of the borehole charges.

In accordance with the specific mining conditions and parameters of the excavation equipment used, the following types of the blasted block rock mass shotpile formation are distinguished:

– normal conditions when the shotpile height is compatible with the digging height of the excavator used;

– with "blast cap" formation along the shotpile axis;

– with "blast cap" formation near the bench face – to be applied in the edge parts of the bench.

In the course of the field measurements, the elevation of the rock mass was measured before and after blasting, and then the height of the formed shotpile was determined.

The results of the field measurements of the blasted rock shotpile parameters are given in Table 2.

Conclusion

Based on the results of the field measurements of the actual slope angles and the parameters of the blasted rock shotpile, the following conclusions can be drawn:

– the actual slope angles of the quarrying faces amounted to the following values:

– when excavating the "blast cap" and using excavators – 49^{o};

– when mining ore mass by full bench – 53^{o}, regardless of the excavator type used;

– the slope angles of the quarry face, 49^{o} for dragline excavators and 53^{o} for hydraulic excavators, are accepted for further calculations;

– it should be noted that the actual slope angles of the slope angles are lower than the slope angles adopted in the calculation method used by the mine, where the slope angle is 70–75^{o};

– the width of the marginal (near-envelope) zone where losses and dilution of balance ore are generated increased from 7 to 13.0 m (at 49°) and from 7 to 11.3 m (at 53°); as a result, the areas of loss and dilution triangles have increased;

– the height of the blasted rock shotpile when blasting to a relieving wall or swept face does not exceed the digging height of the excavators used;

– when blasting in compression conditions with the formation of "blast cap", the height of the blasted rock shotpile exceeds the excavator digging height that restricts the scope of use of hydraulic excavators;

– when blasting in the edge parts of the bench, the direction of the rock mass breaking and the shotpile formation occur at the bench face;

– when blasting in compression conditions, in the upper part of the shotpile, intense mixing of the involved rock and all ore grades occurs, therefore, when excavating the “blast cap”, bulk ore mass extraction is only possible. The lower part of the blasted bench preserves the geological structure of the rock mass to a greater extent and can be selectively excavated with separation of the ore mass by grade;

– when compiling the "Methods ... ", the option of dividing a bench 15 m high into two sub-benches 7.5 m high should be considered.

– when blasting the rock mass, to maintain the required pulse direction and the blasting sequence, barren boreholes are included in the breaking outline, which increase the balance ore dilution, and structural dilution arises, which should be taken into account when drawing up the “Methods for determining, limitation and accounting for ore losses and dilution in the course of the Muruntau and Myutenbai (the fifth stage) open-pit mining".

References

1. Life-of-Mine plans for Muruntau and Myutenbai deposits for 2018; TsRU, GP NGMK, 2018. (in Russ.)

2. Feasibility study (TEO) "Muruntau pit mining (V stage)". (In Russ.).

3. Geological level plans presenting actual outlines of ore bodies (Characteristic grade plans for quarry faces) of Muruntau and Myutenbai open pits. (In Russ.)

4. Factual materials of Muruntau mine provided on request: Parameters of quarry faces. Drilling projects for Muruntau and Myutenbai deposits. Typical drilling-and-blasting projects for the open pits. (In Russ.)

5. Temporary instruction on geological support of open-pit mining at Muruntau and Mutenbai gold deposits: Zarafshan, 2014. (In Russ.)

6. Ruling technical document "Operational standards and instructions for accounting losses, dilution of ore in conditions of open-pit mining at Muruntau and Kokpatas deposits of Navoi MMC": Moscow-Navoi, 1994. (In Russ.)

7. Sectoral instruction for calculation, accounting for, rate setting, and planning of ore losses and dilution at underground and open-pit mining of radioactive, rare, and precious metals (RD 8-19-92): All-Russian FEED and R&D establishment for Industrial Technology "VNIPIpromtekhnologii", Moscow, 1993. (In Russ.)

8. Typical guidelines for rate setting, assessing the economic consequences, and estimation and accounting for mining losses of minerals, approved by the USSR State Technical Inspection on March 28, 1972: Collection of guidances on subsoil protection, Moscow, Nedra Press, 1973. (In Russ.)

9. Unified safety rules for mining ores, nonmetallics, and placer accumulations: Tashkent, 1996. (In Russ.)

10. Mining rules for open pits, placers and underground mines for nonferrous, rare, and precious metals: Moscow, Nedra Press, 1981. (In Russ.)

11. Sinclair A., Blackwell G. Applied Mineral Inventory Estimation, Cambridge University Press, 2002.

12. Canadian Securities Administrators, National Instrument 43-101 Standards of Disclosure for Mineral Projects (NI 43-101), 2012.

13. Gerald D. Crawford Pincock Allen and Holt, Pincock perspectives, Dilution and ore Recovery, issue NO. 60, 2004.

14. Parker H. M. Reconciliation principles for the mining industry .Published by Maney on behalf of the Institute of Materials, Minerals and Metallurgy and the AusIMM, maneypublishing.com, 2012.

15. Pakalnis R., Poulin, R. and Hadjieorgiou J. Quantifying the Cost of Dilution in Underground Mines, SME Annual Metallurgy and Exploration, Denver, 1995.

16. Scoble M. J., and Moss A. Dilution in underground bulk mining: implications for production management; in Whateley, M. K. G., and P. K., 1994.

17. Beck D. A. Stress influences on rockmass damage and stope stability at GF mine-calibrated model criteria. Consultant report for Xstrata Zinc, George Fisher mine, 2003.

18. Barton N., Lien R., Lunde J. Engineering classification of rock masses for the design of tunnel support. Rock Mech. 6(4):189-236, 1974.

19. Brady T. M., Pakalnis R., Clark L. Design in weak rock masses: Nevada underground mining operations. SME preprint 05-43. Littleton, CO: Society for Mining, Metallurgy, and Exploration, Inc., 2005.

20. Capes G. W., Grant D. R., Neindorf L. B. George Fisher: sustainable mine design. Paper presented at the Second International Seminar on Strategic Versus Tactical Approaches in Mining (Perth, Australia), 2006.

21. Capes G. W., Milne D. M., Grant D. R. Stope hangingwall design approaches at the Xstrata Zinc, George Fisher mine, North Queensland, Australia. In: Chen G, Huang S, Zhou W, Tinucci J, eds. Proceedings of the 40th U.S. Rock Mechanics Symposium (Anchorage, AK, June 25-29, 2005). Alexandria, VA: American Rock Mechanics Association, 2005.

22. Clark L., Pakalnis R. An empirical design approach for estimating unplanned dilution from open stope hangingwalls and footwalls. Presented at the 99th Canadian Institute of Mining Annual Conference (Vancouver, British Columbia, Canada), 1997.

23. Deere D. U. Technical description of rock cores for engineer-purposes. Rock Mech. Eng.Geol. 1(1), 1964.

24. Forrestal P. J. Mount Isa and Hilton silver-lead- zinc deposits. In: Hughes FE, ed. Geology of the mineral deposits of Australia and Papua New Guinea. AusIMM Monogr 14:927-934, 1990.

25. Grenfell K., Hay don M. Challenges in modelling large complex orebodies at the George Fisher north mine. In: Proceedings of the Sixth International Mining Geology Conference (Darwin, Northern Territory, Australia, August 21-23, 2006), 2006.

26. Hadjigeorgiou J. Memorandum of March 11, 1999, from John Hadjigeorgiou, Laval University, Quebec, Canada: a discussion document on geotechnical rock mass characterisation for Mount Isa, 1999.

27. Miller F., Jacobs D., Potvin Y. Laser measurement of open stope dilution. CIM Bull 85 :Jul-Aug., 1992.

28. Potvin Y. Empirical open-stope design in Canada [Dissertation]. Vancouver, British Columbia, Canada: University of British Columbia, 1988.

29. Yunliang M., Fuying G. and Zhanwu M. Strengthening the Technical Cooperation to Reduce Loss and Dilution Rates, Express Information of Mining Industry, Vol. 17, pp. 34-39., 2000.

30. Chen Y. W. The Calculation and Experience of the Mining Total Loss and Impoverishing Index, Gold Science and Technology, Vol. 6, pp. 21-30, 2002.

31. Wang X. X., Yu H. Optimise Ore Dilute and Loss Rate, Enhance Mine Economic Effectiveness, Mineral Resources and Geology, Vol. 3, pp. 51-58, 2000.

Библиографический список

1. План развития горных работ по месторождениям Мурунтау и Мютенбай на 2018 год; ЦРУ, ГП НГМК – 2018.

2. Технико-экономическое обоснование (ТЭО) «Отработка карьера Мурунтау (V-очередь)».

3. Геологические планы горизонтов с нанесением фактических контуров рудных тел (Характерные сортовые планы экскаваторных забоев) карьеров Мурунтау и Мютенбай.

4. Фактические материалы рудника Мурунтау, присланные по запросу: Параметры экскаваторных забоев. Буровые проекты по месторождению Мурунтау и Мютенбай. Типовые проекты буровзрывных работ на карьерах.

5. Временная инструкция по геологическому обслуживанию горно-эксплуатационных работ, производимых открытым способом на золоторудных месторождениях Мурунтау и Мютенбай. Зарафшан, 2014.

6. Руководящий технический документ «Эксплуатационные нормативы и инструкции по учету потерь, разубоживания руды в условиях открытой разработки месторождений Мурунтау и Кокпатас Навойского ГМК». Москва-Навои, 1994.

7. Отраслевая инструкция по определению, учету, нормированию и планированию потерь и разубоживания руды при подземной и открытой разработке месторождений радиоактивных, редких и благородных металлов (РД 8-19-92) // Всероссийский проектно-изыскательский и научно-исследовательский институт промышленной технологии «ВНИПИпромтехнологии». М.: 1993.

8. Типовые методические указания по нормированию, по оценке экономических последствий и по определению и учету потерь твердых полезных ископаемых при добыче, утвержденные Госгортехнадзором СССР 28 марта 1972 г. Сборник руководящих материалов по охране недр. М.: Недра, 1973.

9. Единые правила безопасности при разработке рудных, нерудных и россыпных месторождений подземным способом. Ташкент, 1996.

10. Правила технической эксплуатации рудников, приисков и шахт, разрабатывающих месторождения цветных, редких и драгоценных металлов. М.: Недра, 1981.

11. Sinclair A., Blackwell G. Applied Mineral Inventory Estimation, Cambridge University Press, 2002.

12. Canadian Securities Administrators, National Instrument 43-101 Standards of Disclosure for Mineral Projects (NI 43-101), 2012.

13. Gerald D. Crawford Pincock Allen and Holt, Pincock perspectives, Dilution and ore Recovery, issue NO. 60, 2004.

14. Parker H. M. Reconciliation principles for the mining industry .Published by Maney on behalf of the Institute of Materials, Minerals and Metallurgy and the AusIMM, maneypublishing.com, 2012.

15. Pakalnis R., Poulin, R. and Hadjieorgiou J. Quantifying the Cost of Dilution in Underground Mines, SME Annual Metallurgy and Exploration, Denver, 1995.

16. Scoble M. J., and Moss A. Dilution in underground bulk mining: implications for production management; in Whateley, M. K. G., and P. K., 1994.

17. Beck D. A. Stress influences on rockmass damage and stope stability at GF mine-calibrated model criteria. Consultant report for Xstrata Zinc, George Fisher mine, 2003.

18. Barton N., Lien R., Lunde J. Engineering classification of rock masses for the design of tunnel support. Rock Mech. 6(4):189-236, 1974.

19. Brady T. M., Pakalnis R., Clark L. Design in weak rock masses: Nevada underground mining operations. SME preprint 05-43. Littleton, CO: Society for Mining, Metallurgy, and Exploration, Inc., 2005.

20. Capes G. W., Grant D. R., Neindorf L. B. George Fisher: sustainable mine design. Paper presented at the Second International Seminar on Strategic Versus Tactical Approaches in Mining (Perth, Australia), 2006.

21. Capes G. W., Milne D. M., Grant D. R. Stope hangingwall design approaches at the Xstrata Zinc, George Fisher mine, North Queensland, Australia. In: Chen G, Huang S, Zhou W, Tinucci J, eds. Proceedings of the 40th U.S. Rock Mechanics Symposium (Anchorage, AK, June 25-29, 2005). Alexandria, VA: American Rock Mechanics Association, 2005.

22. Clark L., Pakalnis R. An empirical design approach for estimating unplanned dilution from open stope hangingwalls and footwalls. Presented at the 99th Canadian Institute of Mining Annual Conference (Vancouver, British Columbia, Canada), 1997.

23. Deere D. U. Technical description of rock cores for engineer-purposes. Rock Mech. Eng.Geol. 1(1), 1964.

24. Forrestal P. J. Mount Isa and Hilton silver-lead- zinc deposits. In: Hughes FE, ed. Geology of the mineral deposits of Australia and Papua New Guinea. AusIMM Monogr 14:927-934, 1990.

25. Grenfell K., Hay don M. Challenges in modelling large complex orebodies at the George Fisher north mine. In: Proceedings of the Sixth International Mining Geology Conference (Darwin, Northern Territory, Australia, August 21-23, 2006), 2006.

26. Hadjigeorgiou J. Memorandum of March 11, 1999, from John Hadjigeorgiou, Laval University, Quebec, Canada: a discussion document on geotechnical rock mass characterisation for Mount Isa, 1999.

27. Miller F., Jacobs D., Potvin Y. Laser measurement of open stope dilution. CIM Bull 85 :Jul-Aug., 1992.

28. Potvin Y. Empirical open-stope design in Canada [Dissertation]. Vancouver, British Columbia, Canada: University of British Columbia, 1988.

29. Yunliang M., Fuying G. and Zhanwu M. Strengthening the Technical Cooperation to Reduce Loss and Dilution Rates, Express Information of Mining Industry, Vol. 17, pp. 34-39., 2000.

30. Chen Y. W. The Calculation and Experience of the Mining Total Loss and Impoverishing Index, Gold Science and Technology, Vol. 6, pp. 21-30, 2002.

31. Wang X. X., Yu H. Optimise Ore Dilute and Loss Rate, Enhance Mine Economic Effectiveness, Mineral Resources and Geology, Vol. 3, pp. 51-58, 2000.

Information about the Authors

B. R Raimjanov – Dr. Sci. (Tech.), Prof., Deputy Director for Science, State Unitary Enterprise "O’zGEORANGMETLITI", Tashkent, Uzbekistan, b.raimjanov@mail.ru;

A. R. Hasanov – Chief of Research Department of Mining Works, State Unitary Enterprise "O’zGEORANGMETLITI", Tashkent, Uzbekistan;

R. R. Vahitov – Eng. of 1st Category of Research Department of Mining Works, State Unitary Enterprise "O’zGEORANGMETLITI", Tashkent, Uzbekistan.

Информация об авторах

Раимжанов Бахадиржан Раимжанович - доктор технических наук, профессор, заместитель директора по науке Государственного унитарного предприятия Узбекский научно-исследовательский и проектно-изыскательский институт геотехнологии и цветной металлургии «O’zGEORANGMETLITI», Ташкент, Узбекистан, b.raimjanov@mail.ru;

Хасанов Алексей Рашидович – начальник научно–исследовательского отдела горных работ науке Государственного унитарного предприятия Узбекский научно-исследовательский и проектно-изыскательский институт геотехнологии и цветной металлургии «O’zGEORANGMETLITI», Ташкент, Узбекистан;

Вахитов Руслан Рамилевич – инженер 1 категории научно–исследовательского отдела горных работ Государственного унитарного предприятия Узбекский научно-исследовательский и проектно-изыскательский институт геотехнологии и цветной металлургии «O’zGEORANGMETLITI», Ташкент, Узбекистан.

ORIGINAL PAPERS

DOI: 10.17073/2500-0632-2019-1-16-22

Tendencies of Mining Technology Development in Relation to Deep Mines

Ngoc Minh Nguyen[1], Duc Thang Pham[2]

[1]Central South University, Changsha, Hunan, China; Quang Ninh University of Industry, Quang Ninh, Vietnam;
[2]National University of Science and Technology "MISiS" (NUST "MISiS"), Moscow, Russia; Quang Ninh University of Industry, Quang Ninh, Vietnam, ✉phamducthangmct@gmail.com

Abstract: Mineral demand rapidly increases; as a result, underground mining activities gradually dig into the earth's crust to deeper levels. For instance, the depth of coal mines has reached 1500 m, whereas the depth of mines for nonferrous metals has already achieved around 4500 m. Deep mining faces a number of technical and environmental challenges, first of all, great rock mass stresses, high temperature and long winding distance. The traditional technologies are hardly capable to provide the development and extraction efficiency and safety. That is why the need in developing and implementation of new modern mining technologies arose. In roadheading, TBM (tunnel-boring machine) method is gradually introduced. A TBM combines the functions of rock breaking, support installation, mucking and conveying rock. In mining industry, smart mining based on mechanized and automated mining methods is successfully implemented at coal mines. Besides, a technical concept of fluidized mining for deep-seated mineral resources (6000 m and more) was proposed. This paper presents the review of the current global status of deep mining and highlights some of the newest technological achievements in roadheading and the mineral extraction processes.

Keywords: mining technology, deep mines, smart mining, mechanized, extraction processes, fluidized mining.

For citation: Nguyen Ngoc Minh, Pham Duc Thang. Tendencies of mining technology development in relation to deep mines. *Mining Science and Technology*. 2019;4(1):16-22. DOI: 10.17073/2500-0632-2019-1-16-22.

Направление развития технологий добычи применительно к рудникам глубокого заложения

Нгуен Нгок Минь[1], Фам Дык Тхань[2]

[1]Центральный Южный Университет, Чанша, Хунань, Китай; Промышленный Университет Куанг Нинь, Куанг Нинь, Вьетнам;
[2]Национальный исследовательский технологический университет «МИСиС», Москва, Россия; Промышленный Университет Куанг Нинь, Куанг Нинь, Вьетнам, ✉phamducthangmct@gmail.com

Аннотация: Потребление полезных ископаемых быстро растет, что заставляет вести горные работы на всё более глубоких уровнях земной коры. В частности, глубина угольных шахт достигла 1500 м, а шахт для добычи цветных металлов – приблизительно 4500 м. Осуществление горных работ на больших глубинах требует решения ряда технических и экологических проблем, в первую очередь связанных с высокими давлениями и напряжениями в горном массиве, высокими температурами и значительными расстояниями транспортировки горной массы на поверхность. Традиционные технологии вряд ли способны обеспечить эффективность и безопасность разработки и добычи в таких условиях. Вот почему возникла необходимость в разработке и внедрении новых современных технологий добычи. В проходке горных выработок постепенно внедряется метод ТВМ (применение туннелепроходческих машин). Туннелепроходческая машина сочетает функции отбойки горной массы, установки крепи, уборки (из забоя), погрузки и транспортировки горной массы. В горнодобывающей промышленности «умная» добыча полезных ископаемых, основанная на механизированных и автоматизированных системах разработки, успешно применяется на угольных шахтах. Мы выдвигаем техническую концепцию добычи методом флюидизации/псевдоожижения горной массы для отработки глубокозалегающих ТПИ (6000 м и более). В данной статье представлен анализ текущего состояния разработки глубокозалегающих месторождений ТПИ в мире и освещены некоторые из новейших технологических достижений в области проходки горных выработок и технологий добычи твердых полезных ископаемых.

Ключевые слова: технология добычи, глубокие рудники, «умная» добыча, механизированные процессы добычи/ведения горных работ, добыча методом флюидизации/псевдоожижения.

Для цитирования: Нгуен Нгок Минь, Фам Дык Тхань. Направление развития технологий добычи применительно к рудникам глубокого заложения. *Горные науки и технологии*. 2019;4(1):16-22. DOI: 10.17073/2500-0632-2019-1-16-22.

Introduction

Since coal and other mineral resources at shallow depths are gradually exhausted, underground mining activities gradually dig into the earth's crust to deeper levels. At present, deep mining at a depth of 1000 m is normal; the depth of coal mines, geothermal resources exploitation, nonferrous metal mines, and oil and gas production has reached 1500, 5000, 4500, and 7500 m, respectively. Deep mining is likely to become the popular technique in the future. Coal mining in Poland, Germany, Britain, Japan, and France had reached depth of 1000 m and more in early 1980s. In China, there are 47 coal mines operating at a depth of 1000 m and more [1, 2]. There were at least 80 mines for metals operating at a depth of 1000 m and more by 1996, mostly located in South Africa, Canada, the United States, India, Australia, Russia, and Poland. The average depth of mines for metals in South Africa ranges 2000 to 4000 m (Fig. 1) [3].

Activity of mining industry in China gradually changes to deeper levels to a depth ranging 1000 to 2000 m, and it is already common to see the mines at this depth [4]. During the "The 13th Five-Year Plan" period, approximately 50 metal mines will operate at a depth of 1000 m, and a half of them will reach the depth of 1500 m in the next 10 to 20 years (Fig. 2).

Deep mining faces a number of technical and environmental challenges, first of all, great rock mass stresses. If compatible mining methods would not adapted to high stress conditions, great technogenic disasters may happen, resulting in decreasing or even complete stoppage of the affected mine production. This will naturally produce extremely negative effect on the mine performance and viability. A large number of documents have showed that many deep metal mines have faced a large number of rock bursts, mine-shocks, formation of large areas of goaf instability, and roof caving problems. The second challenge when operating deep mines is high temperature. It is known that the temperature will rise by 10 to 40° C when digging to a depth of 1000 m. The high temperature conditions of deep mining seriously affect the miner labor productivity and the effectiveness of cooling, thus increasing the mining cost. One more challenge is long winding distance: increasing mining depth requires increasing the height of winding of ore and all kind of materials, resulting in growing the mining cost and causing HSE risks.

Based on findings of the implemented research of deep mining status in the world, the authors summarized and highlighted relevant technologies applying to deep mining, namely, TBM (tunnel-boring machine use) for deep roadheading, smart mining, and fluidized mining.

Application of TBM for deep roadheading

It is well known that TBM is the most advanced tunneling machine in the world. A TBM combines the functions of rock breaking, support installation, mucking and conveying rock (Fig. 3) [5]. Compared with drill and blast method, TBM roadheading has significant advantages, including high support installation efficiency and lower project costs. TBM-based mining is more environmentally friendly and allows improving surrounding rock stability control [6].

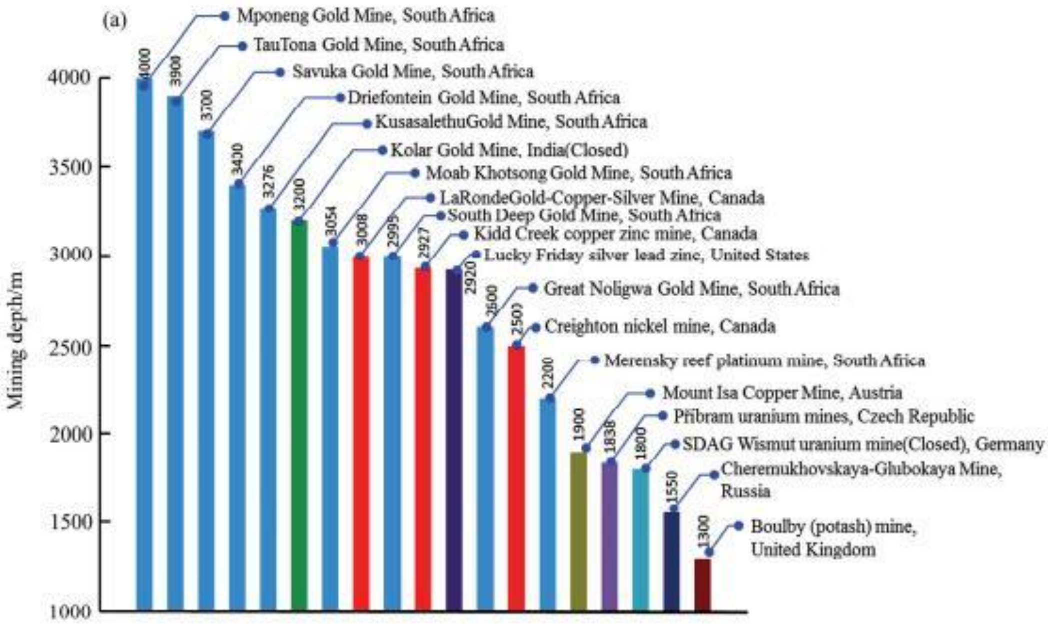

Fig. 1. Examples of Deep Mines in the World

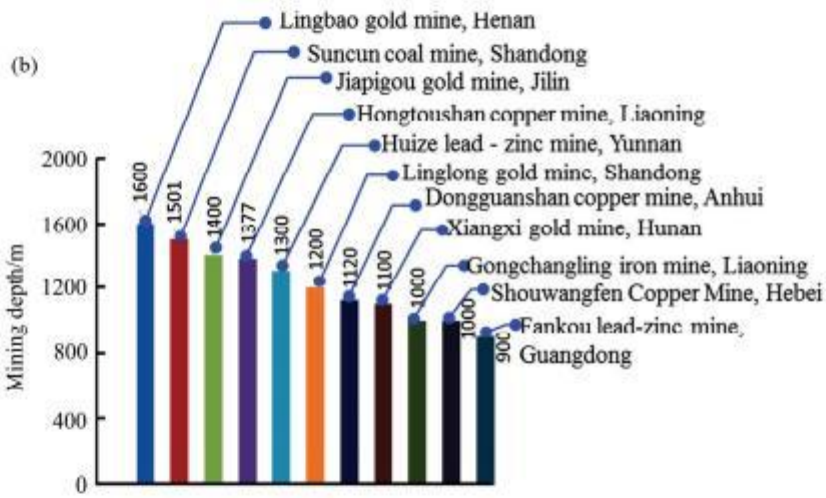

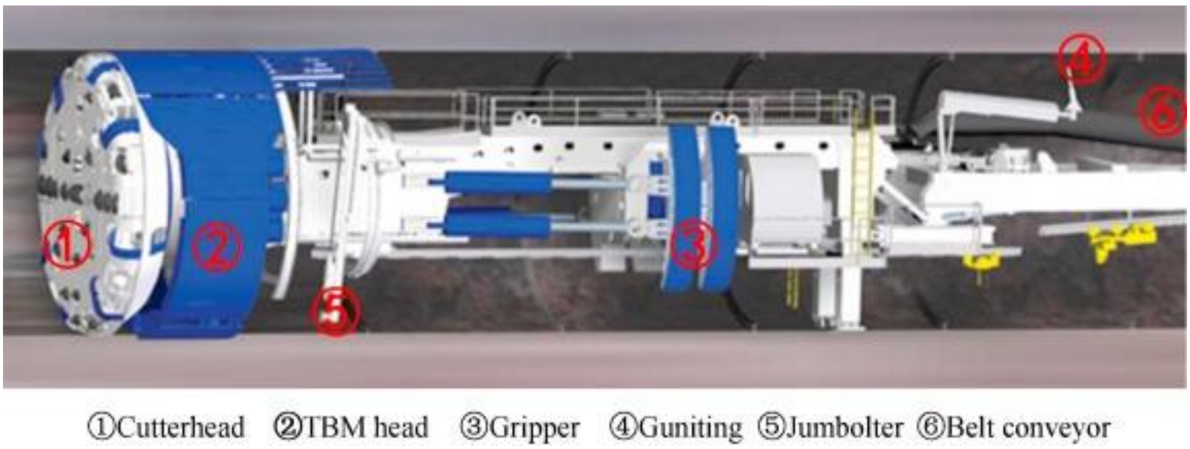

Fig. 3. A Gripper TBM (modified from The Robbins Company, 2015)

Since the first modern TBM was developed and successfully applied in the 1950s, over 10,000 TBMs have been used to construct tunnels for traffic, hydropower, sewerage and water, underground storage and mining. The technique is currently available for tunneling at different diameters in different ground conditions from hard rock to soft soil. Based on ground and groundwater conditions (hard rock, soft soils, mixed and varying grounds), to provide stability of tunnel face and walls, TBMs can be broadly classified into seven types [7], as indicated in Fig. 4.

With increasing coal mining intensity, the number, length and depth of coal mine roadways increases drastically. The traditional drill-and-blast method and comprehensive mechanized driving method, with corresponding support setting methods are incapable of controlling the surrounding rock stability. Hard rock TBMs (full-face tunnel boring machine) have significant advantages in terms of high advance rates, high support setting capacity; they are more environmentally friendly and enable lower tunneling costs. TBMs have been successfully used for some roadway tunneling and inclined shaft construction. Therefore, we can expect that the TBM tunneling method will become the first choice and preferred method for deep roadheading in coal mines in the future [8].

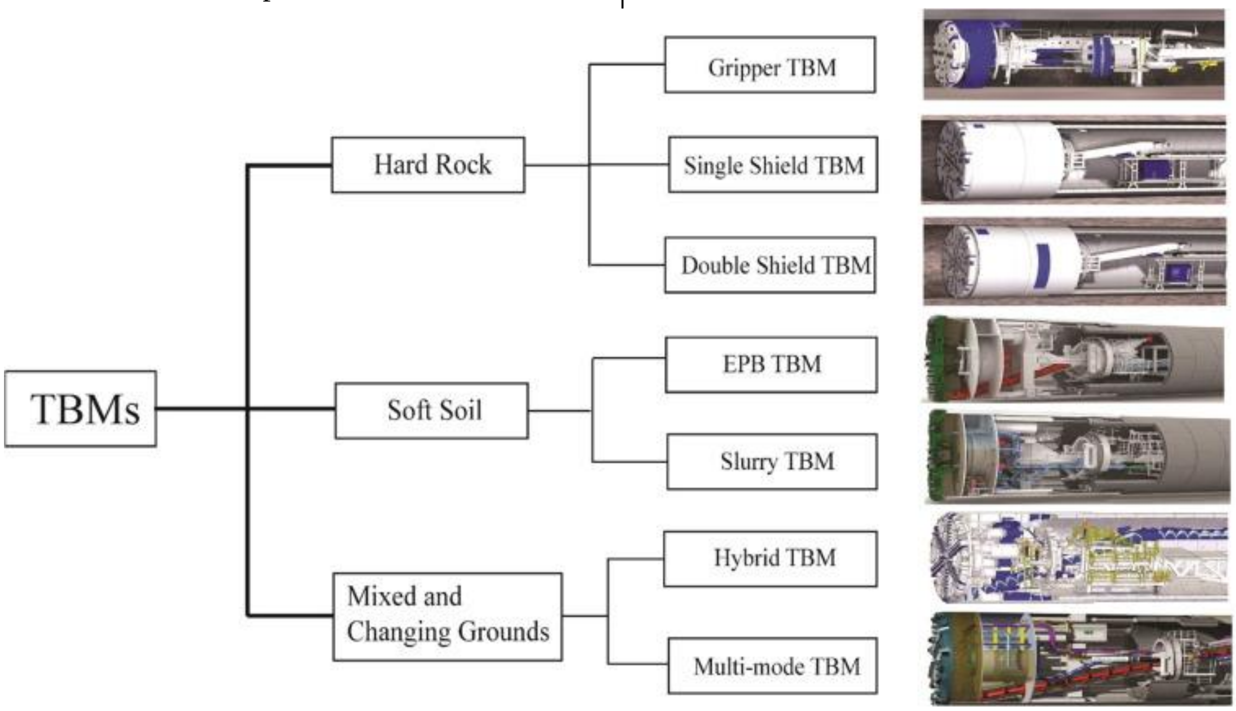

Fig. 4. A Classification of TBMs

Smart mining

Smart mining, based on mechanized and automatic mining methods and a combination of informatization with commercial development, has brought a revolution in the mining industry [9]. This new approach enables automatic mining based on smart control of a working face, mining machine operation, with automatic control of mining equipment. Smart mining has three main features: (1) mining machines can operate in automatic mode; (2) real-time data can be captured and updated promptly, including geological information, coal-rock boundary location, positions of the machines and the face, etc.; and (3) mining machinery can be automatically controlled depending on the conditions of the working face. When decision-making process and machine operation can be conducted automatically, the working face is called “smart mining working face” [10].

In Australia, LASC (Longwall Automation Steering Committee) is engaged in automatic and smart mining method development for coal mines [11]. The LASC automation technologies are available for the national and international mining industry through the major OEM (Original Equipment Manufacturer) for longwall mining, which has integrated the LASC open intercommunication standards into its proprietary shearer automation equipment. The LASC technology has been widely adopted, with CSIRO (Mining Technology Research Group) automation technology deployed in more than 70 % of the automated underground coal mining machinery operating in Australia, with growing the deployment in the world [12]. Three main advantages are provided by applying the precision optical fiber gyroscope and the method of navigation and orientation. The first one is three-dimensional (3D) positioning of a shearer (at the deviation below ±10 cm); the second one is a system of straightening adjustment (at the deviation below ±50 cm); and the third advantage is a horizontal level control system for the working face. These three components compose the initial automatic controlling system. The mining process can be monitored and controlled remotely.

The IMSC is a remote monitoring and control system, used for control of working faces at longwall coal mining, which was developed by the American company Joy Global Inc. (recently taken over by the Japanese company Komatsu Mining Corp.). This system captures the real-time information and data from all mining machines at any time. It enables mining engineers to adjust coal production procedures based on the information reported by the system regarding alarms or breakdowns (Fig. 5) [13].

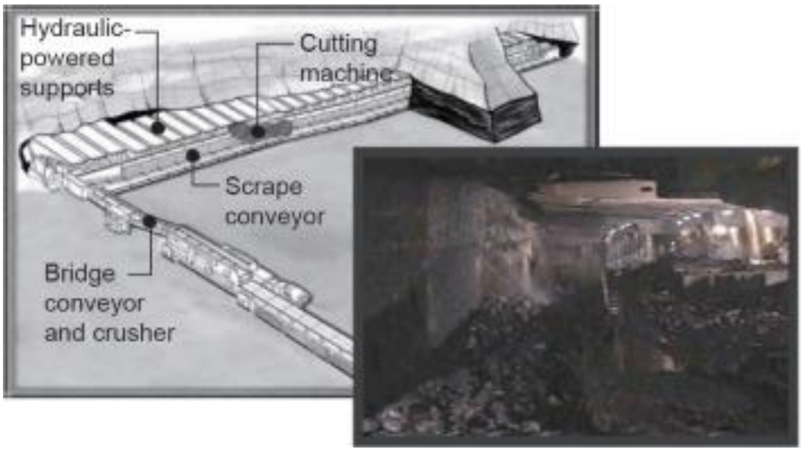

Fig. 5. Facilities at a Working Face Monitored by the IMSC

According to Wu et al. [14], the new task of a digital coal mine is to establish, for coal mines, a real-time access to digital mine integration platforms to create a multidimensional and dynamic coal mine virtual model prototype. Four main development directions are determined for digital mining in the new situation of deep mining: (1) a digital mine integration platform; (2) a mining simulation system; (3) underground positioning and navigation methods; and (4) mining environment smart perception.

Fluidized mining

Xie et al. [15, 16] assumed that there exists a theoretical limit of mining depth by traditional methods. It is estimated theoretically that all the currently available mining methods will become obsolete once the depth of underground mineral resources exceeds 6000 m. Therefore, to implement development and utilization of mineral resources at great depths, disruptive innovations in mining theory and technology should be advanced. For this purpose, Xie et al. [16] proposed a theoretical and technical concept of fluidized mining for extraction of deep-seated mineral resources (Fig. 6). Based on a mining mode similar to the TBM, the concept provides for achieving *in situ*, real-time, and integrated utilization of deep-seated mineral resources through mining, sorting, refining, backfilling, power generation, and gasification of solid resources, thus converting the resources into gas, liquid, or a mixture of gas/liquid/solid substances.

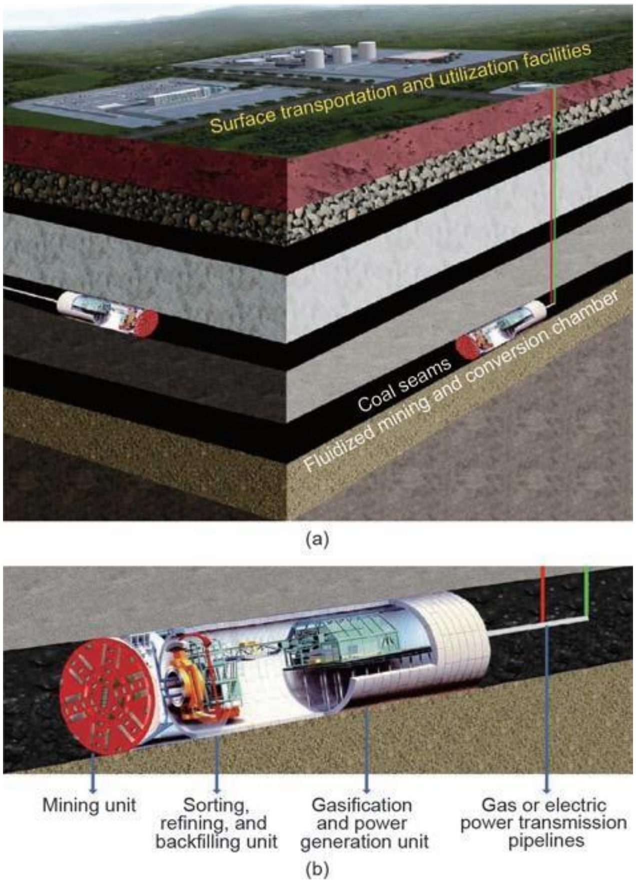

Fig. 6. A Conceptual Illustration of Fluidized Mining of Deep-Seated Mineral Resources. (a) mining model; (b) fluidized mining and conversion facility

As a result, future coal mines will no longer have workers going down the mines, coal drawing, waste rock dumps, or dusting. Instead, power and energy transmission will be clean, safe, smart, environmentally-friendly.

For coal mining, the fluidized mining concept includes the following five main procedures: (1) unmanned breaking, (2) automated sorting, (3) fluidization of coal, (4) controlled backfilling, and (5) power transmission, smart power control, and power storage. For metal mining, the fluidized mining concept includes the following three steps: (1) unmanned breaking, (2) fluidization of ore, and (3) controlled backfilling [15].

There are four methods to implement the fluidized mining of deep-seated solid mineral resources: (1) the conversion of solid minerals into gases, such as underground gasification of coal; (2) the conversion of solid minerals into liquid fuels, such as the underground liquefaction of coal and high-temperature biological and chemical transformation of coal; (3) the conversion of solid minerals into mixes, such as explosive coal dust and water-coal slurry; and (4) the *in situ* conversion of solid minerals into electric power, such as the *in situ* underground production of coal-fired electric power. Fluidized mining is a disruptive innovation in mining technologies, particularly in regards to future deep mining.

Conclusions

This short review presents the current status of deep mining in the world, and highlights some of the newest technological achievements and opportunities. It also addresses some geotechnical issues in relation to deep mining. Some of the current challenges, advances, and expected issues in deep mining can be summarized as follows:

(1) Deep mining will be common in the future as coal and metal mineral resources at shallow depths gradually become exhausted. The progress is restricted and affected by the advancement of rock mechanics and machine-building technologies. New ideas and techniques

are therefore required for deep mining, particularly considering great *in situ* and mining-induced stresses and other boundary conditions that are found at great depths.

(2) TBMs have significant advantages in excavation and support setting, and meet the deep roadheading requirements. Thus, TBM roadheading is believed to become the first choice and preferred future method for roadheading in deep mines.

(3) Smart mining methods using in longwall coal mining have been demonstrated their advantages for coal production because of their better return on investment, energy saving, safety, minimizing underground staff, and better performance.

(4) Fluidized mining for deep-seated coal resources is the novel idea, applicable to in-situ conversion of deep-seated mineral resources into gas, liquid, or a gas/liquid/solid mix to implement unmanned smart underground mining, sorting backfilling, and conversion into heat/power/syngas using an underground fluidized mining method and a conversion facility. The suggested method may replace the traditional resources breaking, transportation, and utilization modes with a new mining approach. In addition, the technique may pioneer the development of fluidized mining technology and facilitate achieving clean, efficient, and eco-friendly exploitation of deep-seated solid minerals.

References

1. Xie H., Gao F., Ju Y., Gao M., Zhang R., Gao Y., *et al*. Quantitative definition and investigation of deep mining. Journal of the China Coal Society, 40 (1) (2015), pp. 1-10.

2. Xie H. Research framework and anticipated results of deep rock mechanics and mining theory. Advanced Engineering Science, 49 (2) (2017), pp. 1-16.

3. Hu S., Peng J., Huang C., Chen P., Li M. An overview of current status and progress in coal mining of the deep over a kilometer. China Mining Magazine, 20 (7) (2011), pp. 105-110.

4. Li Xi-bing. Rock dynamics fundamentals and applications. Beijing, Science Press, 2014.

5. Barla G., Pelizza S. TBM tunnelling in difficult ground conditions. GeoEng2000 – An International Conference on Geotechnical & Geological Engineering, Melbourne, Australia, 2000, p. 20 .

6. Liu Q. S., Huang X., Gong Q.M., *et al*. Application and development of hard rock TBM and its prospect in China. Tunnelling and Underground Space Technology, 57-2016, p.33–46.

7. Zheng Y. L., Zhang Q. B., Zhao J. Challenges and opportunities of using tunnel boring machine. Tunnelling and Underground Space Technology 57 (2016), pp. 287–299.

8. Xing H., Quansheng L., Kai S., Yucong P., Jianping L. Application and prospect of hard rock TBM for deep roadway construction in coal mines. Tunnelling and Underground Space Technology, 73 (2018), p. 105–126.

9. Wang J. H., Wang Y.G., Fu J. H. Crucial technology research and demonstration of digital mines. Journal of the China Coal Society, 41 (6) (2016), pp. 1323-1331.

10. Wang J. H., Huang Z. H. Innovation and development of intelligent coal mining science and technology in China. Coal Science and Technology, 42 (9) (2014), pp. 1-6.

11. Wang J. H., Huang L. T., Li S. B., Huang Z. H. Development of intelligent technology and equipment in fully-mechanized coal mining face. Journal of the China Coal Society, 39 (8) (2014), pp. 1418 1423.

12. He M., Zhang G., Wang G., Xu Y., Wu C., Tang Q. Research on mechanism and application to floor heave control of deep gateway. Chinese Journal of Rock Mechanics and Engineering, 28 (Suppl.1) (2009), pp. 2593-2598.

13. Wang J. H., Huang Z. H. The Recent Technological Development of Intelligent Mining in China. Engineering 3 (2017) 439 - 444.

14. Wu L., Wang Y., Ding E., Zhu W., Zhang R., Zhang S., et al. Thirdly study on digital mine: Serve for mine safety and intellimine with support from IoT. Journal of the China Coal Society, 37 (3) (2012), pp. 357-365.

15. Xie H., Gao F., Ju Y., Ge S., Wang G., Zhang R., et al. Theoretical and technological conception of the fluidization mining for deep coal resources. Journal of the China Coal Society, 42 (3) (2017), pp. 547-556.

16. Xie H., Ju Y., Gao F., Gao M., Zhang R. Groundbreaking theoretical and technical conceptualization of fluidized mining of deep underground solid mineral resources. Tunnelling and Underground Space Technology, 67(2017), pp. 68-70.

ORIGINAL PAPERS

DOI: 10.17073/2500-0632-2019-1-23-30

The Study of Geomechanical Condition of Unstable Rocks in the Vicinity of Mine Working Junctions

V. V. Basov

Siberian State Industrial University (SibSIU), Novokuznetsk, Russia, ✉vadimbasov@yahoo.com

Abstract: The relevance of research of material strain nature based on physical models equivalent to rocks is substantiated. To identify the dependencies and mechanism of unstable rock strain in the vicinity of mine working junctions, an experimental technique has been developed and presented. The method of physical modeling using equivalent materials was applied in the research. Strength characteristics of the rock equivalent material were calculated using the formulas proposed by G.N. Kuznetsov. The equivalent material was prepared based on two components, sand and paraffin. The mix formulation was selected, and ultimate compressive strength of the equivalent material was determined. The experiment was performed for three options of the physical models: an intact rock mass, a rock mass with a single mine working, and a rock mass with mine working junctions. Testing of the models made of the equivalent material was performed through uniaxial vertical loading using a hydraulic press. Based on the model testing findings, the dynamics of fracture propagation and crushing of the enclosing equivalent material in the vicinity of an artificial cavity, simulating a mine working, has been demonstrated. Besides, the graphs of relative strain versus vertical loading for each stage of the stepwise loading of these three model options were produced. The findings of the strain-stress distribution modeling for the equivalent material around the cavities simulating mine working junctions were analyzed. The strain testing findings for the materials simulating rock behavior are expected to be used as the initial data for analysis of physical and numerical simulation, as well as for developing engineering documentation with regard to the selection of parameters for supporting mine working junctions.

Keywords: physical modeling, testing device, rocks, relative strains, vertical load, equivalent material, similarity criterion, model, method of photographic evidence.

For citation: Basov V. V. The study of geomechanical condition of unstable rocks in the vicinity of mine working junctions. *Mining Science and Technology*. 2019;4(1):23-30. (In Russ.). DOI: 10.17073/2500-0632-2019-1-23-30.

Исследование геомеханического состояния неустойчивых пород в окрестности сопряжений горных выработок

Басов В. В.

Сибирский государственный индустриальный университет (СибГИУ), Новокузнецк, Россия, ✉vadimbasov@yahoo.com

Аннотация: Обоснована актуальность исследований характера деформирования материала на физических моделях, эквивалентных горным породам. Для выявления зависимостей и закономерностей деформирования неустойчивых горных пород в окрестности сопряжений горных выработок разработана и представлена методика экспериментального исследования. В работе был принят метод физического моделирования на эквивалентных материалах. Рассчитаны прочностные характеристики эквивалентного материала для исследуемых пород по формулам, предложенным Г.Н. Кузнецовым. Эквивалентный материал выбран из двух составляющих – песка и парафина. Подобрана рецептура состава смеси и определены пределы прочности эквивалентного материала при сжатии. Эксперимент проводился для трех вариантов физических моделей: нетронутого массива горных пород, массива с одиночной горной выработкой и массива с сопряжением горных выработок. Испытания моделей из эквивалентного материала проводились путем одноосного вертикального нагружения при помощи гидравлического пресса. По результатам испытания моделей из эквивалентного материала представлена динамика развития трещин и разрушения вмещающего эквивалентного материала в окрестности искусственной полости, имитирующей горную выработку. Также получены графики зависимости относительных деформаций от вертикальной нагрузки для каждого поэтапного нагружения трёх моделей. Проведена оценка результатов физического моделирования параметров НДС эквивалентного материала вокруг полостей, имитирующих сопряжения горных выработок. Полученные результаты деформирования материалов, эквивалентных горным породам, предполагается использовать в качестве исходных данных при тестировании результатов физического и численного моделирования, а также при разработке технической документации в части выбора параметров крепления сопряжений горных выработок.

Ключевые слова: физическое моделирование, стенд, горные породы, относительные деформации, вертикальная нагрузка, эквивалентный материал, критерий подобия, модель, метод фотофиксации.

Для цитирования: Басов В. В. Исследование геомеханического состояния неустойчивых пород в окрестности сопряжений горных выработок. *Горные науки и технологии.* 2019;4(1):23-30. DOI: 10.17073/2500-0632-2019-1-23-30.

Introduction

At present, in coal mines, at working face sweep rate of up to 300 m per month, the pace of construction of development workings and their junctions is a constraining factor. The main factors that negatively affect the rate of mine workings development are downtimes due to rupture of coal pillars, collapse of roof and sides of a working [4, 5, 12, 13]. Within the extraction front of a complex mechanized working face (KMZ), the number of junctions of development workings reaches 40, more than 80% of which are affected by the weight of the roof rocks snubbed by the working face [16].

Mine working junctions are rather complex objects in mines. However, methods for assessing their stability do not always ensure safe operational state of the workings, since many factors are not fully taken into account: the shape and dimensions of the junctions of the workings, the seam structure, the properties of the side rocks, etc. [2, 3, 4, 7].

The main types of downtimes were identified at the junction of the working face and stoping workings, which need installing reinforcement support, strengthening of the enclosing rocks, elimination of domes and inrushes, etc.

In this regard, it is relevant to study the geotechnical state of unstable rocks in the vicinity of the junctions of mine workings to ensure their trouble-free operation.

For this purpose, identifying the dependencies and mechanism of unstable rock strain in the vicinity of mine working junctions should be performed. This will allow, at the stage of development of design documentation, to make decisions that ensure the stability of the host rocks at mine workings junctions, reduce downtimes of working faces and ensure safe working conditions.

The purpose of this study is to develop a methodology for substantiating the parameters of the support of underground mine workings at the junctions in the course of extraction of coal seams with unstable host rocks.

To achieve this goal, at the first stage of the study, the following challenge was met by physical modeling: the stress-strain dependence of rock equivalent material (EM) in the vicinity of cavities imitating mine workings junctions was revealed.

Table 1.

Types and properties of the simulated rocks

Rock type	Ultimate compressive strength $\sigma_н$, MPa	Rock bulk density $\gamma_н$, kg/m^3
Siltstone	40	2500
Coal	8.2	1200

Experimental approach. For the study, a physical modeling method was adopted, which allows to save time and costs necessary to identify the stress-strain dependences of rock equivalent material (EM) in the vicinity of cavities imitating mine workings junctions [6, 7, 8, 11].

Types and properties of simulated rocks, as well as physico-mechanical parameters of the EM, satisfying the similarity criteria [10], are presented in Tables 1, 2.

In accordance with Table 1, strength characteristics of the rock equivalent material for each rock type were calculated using the formulas proposed by G.N. Kuznetsov [10].

Strength characteristics of the rock equivalent materials were calculated using the formula:

$$\sigma_{\text{пч.с}} = (R_{\text{с}})_{\text{м}} = \frac{l}{L} \cdot \frac{\gamma_{\text{м}}}{\gamma_{\text{н}}} (R_{\text{с}})_{\text{н}}, \qquad (1)$$

where $\sigma_{\text{пч.с}} = (R_{\text{с}})_{\text{м}}$ – ultimate compressive strength of the equivalent material;

$(R_{\text{с}})_{\text{н}}$ – ultimate compressive strength of the native rock samples;

$\frac{l}{L}$ – linear scale of the model;

$\gamma_{\text{м}}$ – bulk density of the material;

$\gamma_{\text{н}}$ – bulk density of the rocks.

Bulk density of the model material was calculated by formula:

$$\gamma_{\text{м}} = 0{,}6\gamma_{\text{н}}. \qquad (2)$$

The equivalent material was prepared based on two components, sand and paraffin. For this purpose, quartz sand with grain diameter of 0.30–0.16 mm was used. Technical paraffin STO 00148636-004-2007 was used.

In accordance with the results of the calculation and tests performed on the samples using the BP-29 Azimut hydraulic press, the composition of the mixture was selected and the ultimate compressive strengths of the equivalent material corresponding to coal and siltstone were determined (Table 2).

A special stand for physical modeling was developed (Fig. 1) [9, 14].

Table 2

Physical and mechanical parameters of the EM

Physical and mechanical parameters	**Simulated rock type**	
	Siltstone (roof-bottom)	**Coal (seam)**
EM composition	sand+paraffin (97 : 3)	sand+paraffin+paint (98,52 : 1,48)
EM blending conditions	with heating to 140 °C	
Laboratory ultimate compressive strength of EM, σ_{M}, MPa	0,24	0,10
EM stress-strain modulus E_{ss}, MPa	25	15

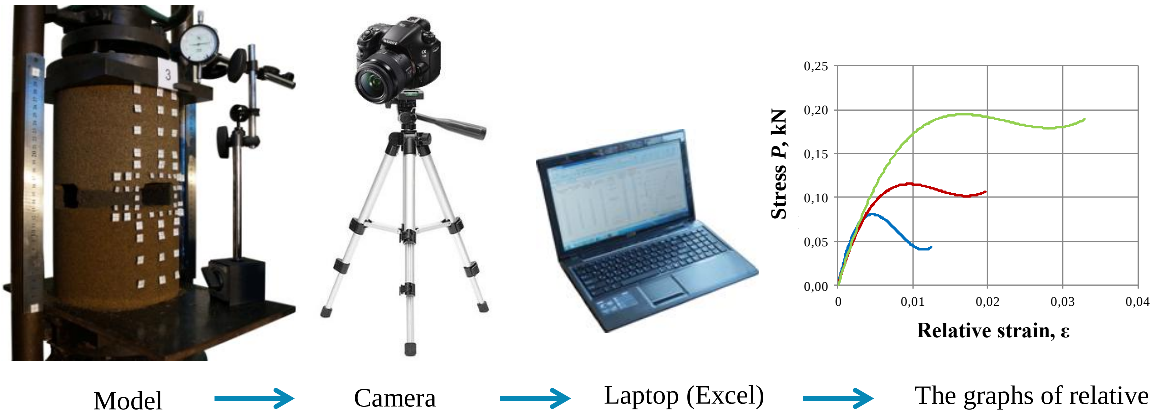

Fig. 1. Stand for physical modeling

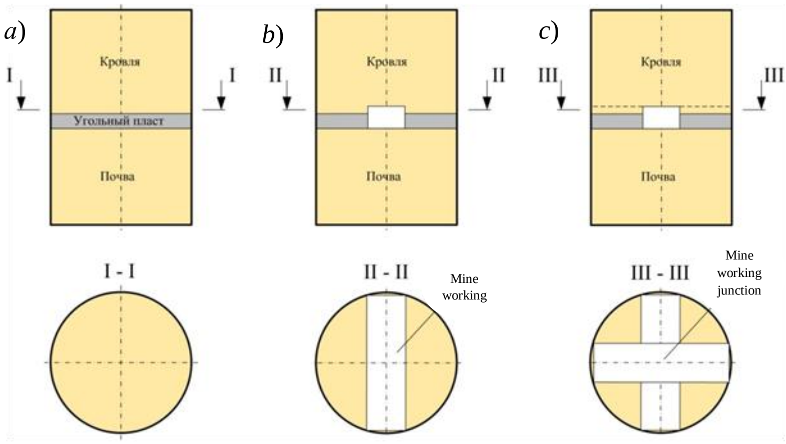

Fig. 2. Schematics of the models for physical modeling:
a – model 1, an intact rock mass; *b* – model 2, a rock mass including a single mine working; *c* – model 3, a rock mass with a mine working junction

The experiment was performed for three options of physical models made of equivalent material (Fig. 2): a) model 1 – an intact rock mass; b) model 2 - a rock mass including a single mine working; c) model 3 - a rock mass with a mine working junction

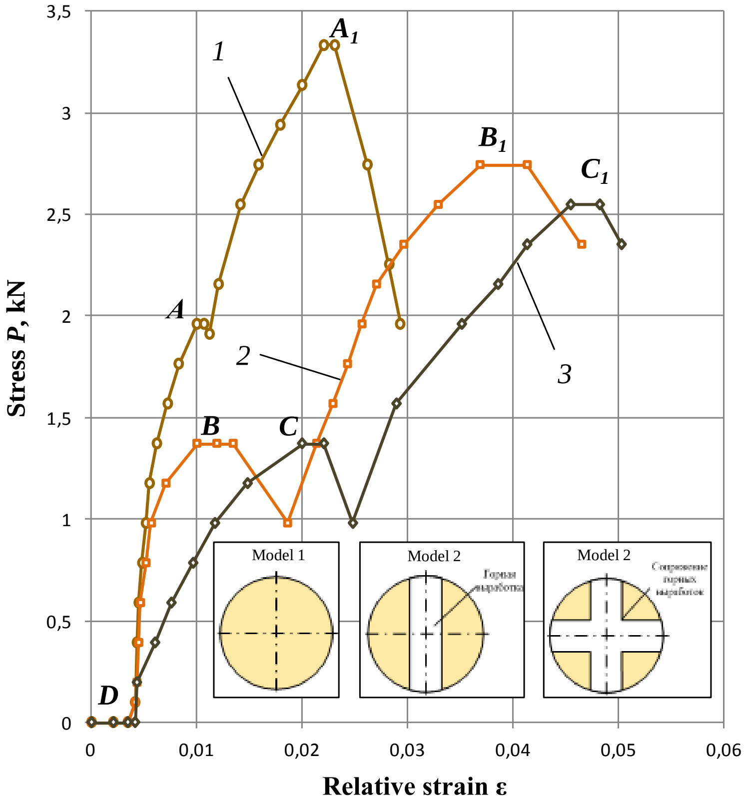

Fig. 3. The graphs of relative strain versus stress for the equivalent material (EM) of the physical models

a) *b*)

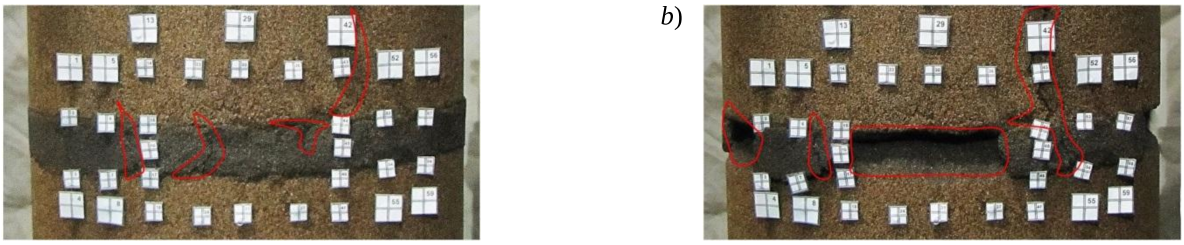

Fig. 4. Seam EM deformation schematic – intact rock mass

a) *b*)

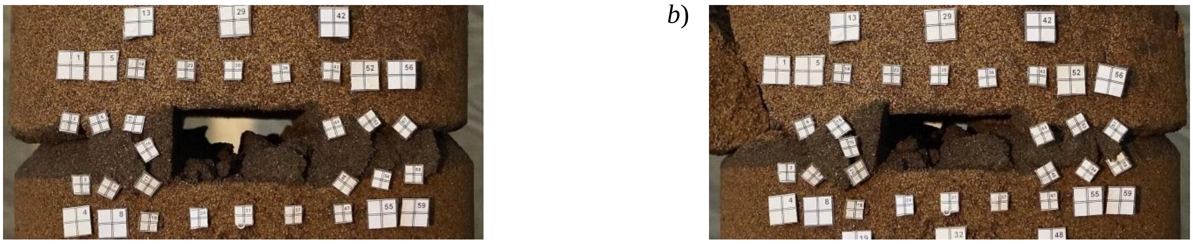

Fig. 5. Seam EM deformation schematic – rock mass including a single mine working

a) *b*)

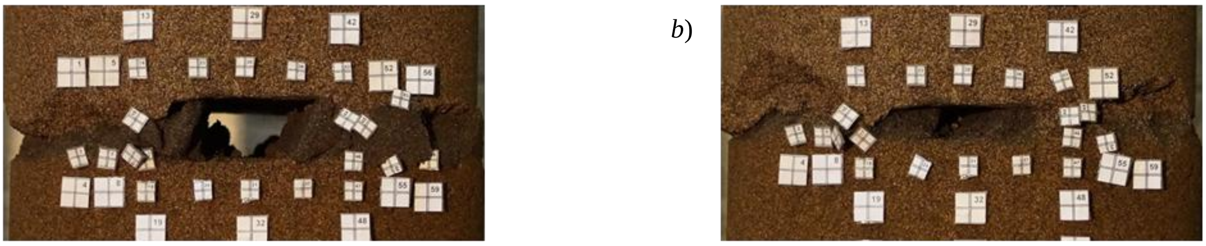

Fig. 6. Seam EM deformation schematic – rock mass with a mine working junction

The study findings. Based on the physical modeling findings, the vertical specific load of three models was determined, as well as the following parameters of the stress-strain behavior of the equivalent material around the cavities simulating mine workings: vertical displacements, relative strains.

Based on the findings of testing models made of the equivalent material and in accordance with the recommendations [15, 18], graphs of the dependence of relative strain on the vertical specific load were built and presented in Fig. 3.

Based on the works [11, 17], the analysis of the research findings was carried out in the following sequence.

During loading of model 1, the EM compression occurs, as can be seen in the graph (OD section), then the EM changes to the elastic state (DA section); when the first fractures appear, the model (rock mass) is compacted; after intensive development of fractures in the formation, it is extruded (Fig. 4a); the load is distributed on the overlying EM layers, elasto-plastic strain begins (section AA_1); after changing the zone (point A1 passed), the EM is ruptured (Fig. 4b); after a fracture appears in the upper layer (in the roof) of the model, stress relaxation occurs.

When loading model 2, weakened by one through cut (a cavity simulating a mine working), intensive propagation of fractures in the seam (section DB) is observed, with extrusion of the EM on the sides of the working (Fig. 5, a); then the EM, similar to siltstone, whose strength is 3–5 times greater than the coal strength, changes to elastic-plastic condition (section BB_1) and, with increasing vertical pressure, reaches the ultimate strength state (point B_1) and finally collapses (Fig. 5, b).

The distribution of strain in the EM, weakened by two cavities imitating junction of mine workings, is shown in graph 3 (Fig. 3). The strain rate of the material equivalent to coal in model 3 is higher compared to models 1 and 2, since the EM (coal seam) was extruded with voids replaced with coal at the intersection (junction) of two cavities; as a result, the upper and lower EM layers (roof-bottom) almost joined (Fig. 6, a, b).

Conclusions.

1) The method of physical modeling allows to save time and costs required to identify the strain mechanism and stress-strain dependences of rocks in the vicinity of mine workings junctions.

2) The strain testing findings for the materials simulating rock behavior are expected to be used as the initial data for analysis of physical and numerical simulation, as well as for developing engineering documentation (specifications) with regard to the selection of parameters for supporting mine working junctions.

References

1. Akhmetkhanov R. S. Probabilistic modeling in system engineering. IntechOpen, London, 2018, 278 p.

2. Basov V. V., Petrov A. A., Vasiliev P. V. Comparative assessment of correlation of the calculated and in-situ measured displacements of rocks of roof in underground workings: Science-intensive technologies for extraction and use of mineral resources: Collection of scientific articles based on the materials from the International Scientific and Practical Conference, June 7-10, 2016; under the general editorship of Fryanov V.N.: Novokuznetsk, SibGIU Press, 2016, No. 2, pp. 136-140. (in Russ.)

3. Ermakov A. Yu., Vasiliev P. V., Fryanov V. N., Senkus V. V., 2015, Technology for drifting and supporting of heavy gauge workings at coal mines: Novokuznetsk, NFI KemGU, 135 p. (in Russ.)

4. Zhukov E. M., Luginin I. A., Kropotov Y. I., Zyryanov K. A., Basov V. V., 2015, Assessment of the effect of fractures on the stability of rocks in the roof of coal mine development workings: Vestnik (Bulletin) SibGIU, No. 4 (14), p. 26-30. (in Russ.)

5. Zaslavsky Yu. Z. The study of rock pressure manifestations in permanent workings of Donbas deep mines: Moscow, Nedra Press, 1966, 180 p. (in Russ.)

6. Kazanin O. I, Zuev B. Yu., Meshkov A. A., 2012, Physical model-based study of displacement processes at underground mining of coal seams in the field of Krasnoyarskaya mine of SUEK-Kuzbass OJSC: Miming information-analytical bulletin (scientific and technical magazine), No. 5, p. 26-32. (in Russ.)

7. Kostyuk S. G., Kovalev N. B., Bedarev N. T., Lyubimov O. V., Sementsov V. V., Sitnikov G. A., 2014, Simulation of extraction of a syncline-folded coal seam using a model made of equivalent materials: KuzGTU Bulletin, No. 5 (105), p. 67-70. (in Russ.)

8. Ke Yang, Guangxiang Xie. An asymmetrical bolt supporting designof retreating coal roadway based on physical simulation in large dip coal seam/ AGH Journal of Mining and Geoengineering. vol. 36. №3 2012. pp. 453–461.

9. Lailiang Cai, Kan Wu., Qisheng Yu. A new method of equivalent material model deformation observation. International Journal of Modern Education and Computer Science (IJMECS), 2011, vol. 40-46, no. 5. Available at: http://www.mecs-press.org/ijmecs/ijmecs-v3-n5/v3n5-6.html (Accessed 02 March 2019)

10. Kuznetsov G. N., Budko M. N., Vasilyev Yu. I., Shklyarsky M. F., Yurevich G. G. Simulation of rock pressure manifestations: Edited by Kuznetsov, G.N.,L., Nedra Press, 1968, 279 p. (in Russ.)

11. Nan Li, Enyuan Wang, Maochen Ge, Jie Liu. The fracture mechanism and acoustic emission analysis of hard roof: a physical modeling study. Arabian Journal of Geosciences, 2015, vol. 1895-1902, No. 8. Available at: https://link.springer.com/article/10.1007/s12517-014-1378-y (Accessed 02 March 2019)

12. Polevshchikov G. Ya. "Deformation-wave" processes in rock mass when stoping face moving in coal seams: Physical and technical issues of mining, 2013, No. 5, p. 50-60. (in Russ.)

13. Rib S. V., Basov V. V., Nikitina A. M., 2016, Researh of the effect of disjunctive dislocations on a rock mass condition in the vicinity of a development working: SibGIU Bulletin, No. 1 (15), p. 17-20. (in Russ.)

14. Rib S. V. The influence of rock interlayer location on the stress-strain state of the rock massif near the underground mine / S.V. Rib // IOP Conference Series: Earth and Environmental Science. 2018. Vol. 206. Pp. 1-4(012011). Available at: http://library.sibsiu.ru

15. Seryakov V. M. Stress State of a Coal Pillar in Fully Mechanized Longwall Mining in Dislocation Zone / V. M. Seryakov, S. V. Rib, V. N. Fryanov // Journal of Mining Science. 2017. No. 6. Pp. 1001-1008. (in Russ.)

16. Singh R., Singh T. N. Investigation into the behaviour of a support system and roof strata during sublevel caving of a thick coal seam. Geotechnical and Geological Engineering 17. 1998, vol. 21-35.

17. Tereshchuk R. N., Naumovich A. V. Ensuring stability of development workings in deep coal mines: Dnepropetrovsk, 2015,134 p. (in Russ.)

18. Tsvetkov A. B., Pavlova L. D., Fryanov V. N. Construction of the approximant of complete diagram for rock deformation // IOP Conference Series: Earth and Environmental Science. 2016. Vol. 45, pp. 1-7 (012009). Available at: http://iopscience.iop.org/article/10.1088/1755-1315/45/1/012009/pdf (date of the applic. 02.03.2019). (in Russ.)

Библиографический список

1. Akhmetkhanov R. S. Probabilistic modeling in system engineering. IntechOpen, London, 2018, 278 p.

2. Басов В. В., Петров А. А., Васильев П. В. Сравнительная оценка соответствия расчётных и измеренных в натурных условиях смещений пород кровли подземных выработок // Наукоемкие технологии разработки и использования минеральных ресурсов: сборник научных статей по материалам Междунар. науч.-практ. конф., 7-10 июня 2016 г.; под общ. ред. В.Н. Фрянова. Новокузнецк: Изд. центр СибГИУ, 2016. № 2. С. 136-140.

3. Ермаков А. Ю., Васильев П. В., Фрянов В. Н., Сенкус В. В. Технология проведения и поддержания горных выработок большого сечения угольных шахт. Новокузнецк: НФИ КемГУ, 2015. 135 с.

4. Жуков Е. М., Лугинин И. А., Кропотов Ю. И., Зырянов К. А., Басов В. В. Оценка влияния трещин на устойчивость пород в кровле подготовительных выработок угольных шахт // Вестник СибГИУ. 2015. №4 (14). С. 26-30.

5. Заславский Ю. З. Исследование проявлений горного давления в капитальных выработках глубоких шахт Донецкого бассейна. М.: Недра, 1966. 180 с.

6. Казанин О. И., Зуев Б. Ю., Мешков А. А.Исследование на физических моделях процессов сдвижений при подземной разработке угольных пластов в поле шахты «Красноярская» ОАО «СУЭК-Кузбасс» // Горный информационно-аналитический бюллетень (научно-технический журнал). 2012. № 5. С. 26-32.

7. Костюк С. Г., Ковалев Н. Б., Бедарев Н. Т., Любимов О. В., Семенцов В. В., Ситников Г. А. Имитация отработки угольного пласта с наличием синклинальной складки на модели из эквивалентных материалов // Вестник КузГТУ. 2014. № 5 (105). С. 67-70.

8. Ke Yang, Guangxiang Xie. An asymmetrical bolt supporting design of retreating coal roadway based on physical simulation in large dip coal seam/ AGH Journal of Mining and Geoengineering. vol. 36. №3 2012. pp. 453–461.

9. Lailiang Cai, Kan Wu., Qisheng Yu. A new method of equivalent material model deformation observation. International Journal of Modern Education and Computer Science (IJMECS), 2011, vol. 40-46, no. 5. Available at: http://www.mecs-press.org/ijmecs/ijmecs-v3-n5/v3n5-6.html (Accessed 02 March 2019).

10. Кузнецов Г. Н., Будько М. Н., Васильев Ю. И., Шклярский М. Ф., Юревич Г. Г. Моделирование проявлений горного давления / Под ред. Г. Н. Кузнецова. Л.: Недра, 1968. 279 с.

11. Nan Li, Enyuan Wang, Maochen Ge, Jie Liu. The fracture mechanism and acoustic emission analysis of hard roof: a physical modeling study. Arabian Journal of Geosciences, 2015, vol. 1895-1902, no. 8. Available at: https://link.springer.com/article/10.1007/s12517-014-1378-y (Accessed 02 March 2019)

12. Полевщиков Г. Я. Деформационно-волновые» процессы в массиве горных пород при движении очистного забоя в угольных пластах // Физико-технические проблемы разработки полезных ископаемых. 2013. № 5. С. 50-60.

13. Риб С. В., Басов В. В., Никитина А. М. Исследование влияния дизъюнктивных нарушений на состояние массива горных пород в окрестности подготовительной выработки // Вестник СибГИУ. 2016. № 1 (15). С. 17-20.

14. Rib S. V. The influence of rock interlayer location on the stress-strain state of the rock massif near the underground mine / S. V. Rib // IOP Conference Series: Earth and Environmental Science. – 2018. – Vol. 206. - P. 1-4 (012011). – Режим доступа: http://library.sibsiu.ru

15. Seryakov V. M. Stress State of a Coal Pillar in Fully Mechanized Longwall Mining in Dislocation Zone / V. M. Seryakov, S. V. Rib, V. N. Fryanov // Journal of Mining Science. 2017. № 6. P. 1001-1008.

16. Singh R., Singh T. N. Investigation into the behaviour of a support system and roof strata during sublevel caving of a thick coal seam. Geotechnical and Geological Engineering 17. 1998, vol. 21-35.

17. Терещук Р. Н., Наумович А. В. Обеспечение устойчивости подготовительных выработок глубоких угольных шахт. Днепропетровск: 2015. 134 с.

18. Tsvetkov A. B., Pavlova L. D., Fryanov V. N. Construction of the approximant of complete diagram for rock deformation // IOP Conference Series: Earth and Environmental Science. 2016. Vol. 45. P. 1-7 (012009). URL: http://iopscience.iop.org/article/10.1088/1755-1315/45/1/012009/pdf (дата обращения 02.03.2019).

ORIGINAL PAPERS

DOI: 10.17073/2500-0632-2019-1-31-41

Effects of Intermittent Inelasticity when Propagating Seismic Wave in Low Velocity Zone

E. I. Mashinskii

The Trofimuk Institute of Petroleum Geology and Geophysics, Siberian Branch of the Russian Academy of Sciences (IPGG SB RAS), Novosibirsk, Russia, ✉MashinskiiEI@ipgg.sbras.ru

Abstract: The study of atypical manifestations of rock inelasticity improves understanding of the physical mechanisms of seismic wave propagation and attenuation in real environments. In the field experiments, the propagation of longitudinal wave at frequency of 240–1000 Hz between two shallow boreholes in low speed zone was investigated. The measurements were performed using a piezoelectric pulse emitter and similar receiver tools positioned in the boreholes. "Stress-time" σ(*t*) digital responses were recorded by the open channel with microsecond temporal resolution. The unusual short-period variations of amplitude in the form of sharp flattening wave front, stress drop, or plateau of different width (tens of microseconds) were detected in the wave profile. These low-amplitude variations in the waveform were regarded as manifestations of hopping intermittent inelasticity. This inelastic process was assumed to affect the waveform transformation. The contribution of hopping inelasticity depends on the applied stress magnitude, i.e. in this case, the seismic response amplitude. The mechanism of hopping inelasticity at small strains may be explained by microplasticity of rocks. The findings obtained represent a new step in understanding of physics of seismic and acoustic wave propagation in rocks and can be useful for handling of applied problems in geophysics and mining.

Keywords: hopping strain, rock microplasticity, inelastic seismic attributes, amplitude dependence of wave velocities and attenuation.

Acknowledgements: The author thanks G. V. Egorov for conducting experiments and useful discussion.

For citation: Mashinskii E. I. Effects of intermittent Inelasticity when propagating seismic wave in low velocity zone. *Mining Science and Technology*. 2019;4(1):31-41. (In Russ.). DOI: 10.17073/2500-0632-2019-1-31-41.

Эффекты прерывистой неупругости при распространении сейсмической волны в зоне малых скоростей

Машинский Э. И.

Институт нефтегазовой геологии и геофизики имени А. А. Трофимука СО РАН, Новосибирск, Россия; ✉MashinskiiEI@ipgg.sbras.ru

Аннотация: Изучение нетипичных проявлений неупругости горных пород расширяет понимание физических механизмов распространения и затухания сейсмических волн в реальных средах. Полевые эксперименты выполнены при распространении продольной волны частотой 240–1000 Гц в пространстве между двумя неглубокими скважинами в зоне малых скоростей (ЗМС). Измерения проводились с помощью пьезоэлектрического импульсного излучателя и аналогичных приемников, размещенных в скважинах. Цифровые записи сигналов в виде «напряжение-время» σ(*t*) регистрировались открытым каналом с микросекундным разрешением во времени. На профиле волны обнаружены необычные короткопериодные вариации амплитуды в виде резкого уменьшения крутизны фронта, падения напряжения или плато различной длительности (десятки микросекунд). Эти малоамплитудные вариации на форме волны были расценены как проявления скачкообразной прерывистой неупругости. Сделано предположение, что этот неупругий процесс оказывает влияние на трансформацию формы волны. Вклад скачкообразной неупругости зависит от величины прикладываемого напряжения, т.е. в нашем случае от величины амплитуды сейсмического сигнала. Возможный механизм скачкообразной неупругости на малых деформациях может быть объяснен микропластичностью горных пород. Полученные результаты представляют новый шаг в понимании физики распространения сейсмических и акустических волн в горных породах и могут быть полезными для решения прикладных задач в геофизике и горном деле.

Ключевые слова: скачкообразная деформация, микропластичность горных пород, неупругие сейсмические параметры, амплитудная зависимость скоростей волн и затухания.

Благодарности: Автор благодарит Егорова Г. В. за проведение экспериментов и полезную дискуссию при обсуждении работы.

Для цитирования: Машинский Э. И. Эффекты прерывистой неупругости при распространении сейсмической волны в зоне малых скоростей. *Горные науки и технологии.* 2019;4(1):31-41. DOI: 10.17073/2500-0632-2019-1-31-41.

Introduction

The study of the physical manifestation of seismic waves propagation and attenuation mechanisms, despite its long history, is still a crucial task. To solve this problem, the modern approach uses new knowledge on rock strain obtained at the micro-scale level. The classical viscoelastic model describes dispersion and relaxation well [5, 23]. However, this model does not explain the mechanism, for example, of the ambiguity of the amplitude dependence of the wave velocity and attenuation. This suggests the existence of some disregarded inelasticity mechanism.

The study of the dynamic characteristics of rocks is quite fully described in [2]. The data were obtained at large and moderate strains, however, amplitude and other atypical effects are not considered here. The study of nonlinear effects in seismic showed the possibility of their action even at small strains [4, 8]. These works gave impetus to the further study and search for the physical causes of these effects.

A review of the amplitude dependence of wave velocities and attenuation [26] presents experiments performed on rock samples under harmonic oscillations, and theoretical ideas. Most data indicate decreasing wave velocity and increasing attenuation with increasing amplitude [23, 31, 34]. A few data for rocks show, on the contrary, increasing wave velocity and decreasing wave attenuation with increasing amplitude [20, 37]. The possibility of non-standard behavior of wave velocities was substantiated in theoretical studies [24, 20; 18]. It is shown here that a decrease or increase in the modulus of elasticity occurs in accordance with the positive or negative nature of the $\sigma(\varepsilon)$ graph curvature.

There are few field experiments on the amplitude dependence of wave velocities, which were carried out in the subsoil layer in shallow pits or on the shore of a reservoir [37]. The records show that as the signal amplitude increases, the wave velocity may both increase and decrease. There is also a residual hysteresis of the wave velocities that indicates irreversible strains caused by the seismic wave. Unusual data on the amplitude dependence were also obtained in the laboratory experiments [7]. It was found that in dry and water-saturated sandstone in the ultrasonic frequency range, the attenuation parameter is more sensitive to amplitude variations than the wave velocity.

The data indicate that non-standard effects are due to defective rocks, demonstrating microheterogeneity, the presence of thin films, microcracks, and the complexity of the phase composition. The experiments using modern equipment for recording the wave process and electron microscopy confirm this [19]. For example, the data for crystalline olivine show the effect of nanometer intergranular contacts on the shear wave attenuation parameter. These intergranular contacts have abnormal elasticity modulus values and cause unusual transformations of the attenuation parameter $Q^{-1}(\omega)$. Some theoretical approaches and experimental work have also been performed in this regard [35; 11; 36].

The aim of the paper is to establish the manifestations of intermittent inelasticity in rocks caused by a seismic wave, and to compare these data with the findings of quasistatic experiments and other recent studies.

The experiment techniques and procedure

The experiments were performed at the Bystrovsky field test site in the Novosibirsk Region. The upper part of the sequence (ZMS) is relatively homogeneous (there are no reflecting boundaries) and composed of loam several tens of meters thick. The loam consists of sand, silt and clay in proportions of about 40 : 15 : 45 %, respectively. The size of clay particles and sand grains is from five to tens of micrometers. The loam to a depth of ~3 m is relatively dry, to ~8.5 m partially water saturated, and then completely water saturated. The velocity of longitudinal wave in dry and partially water saturated loams is V_p = 240–500 m/s, and in fully water saturated loam $V_p \approx 1500$ m/s.

The emitting source was located in a pit about 1 m deep. The first seismic response receiver was located near the source at a distance of 0.4–1 m. The second receiver was located in the borehole at a depth of 1 m and at a distance of 6 or 14 m from the source. The pulse source consists of a set of piezoelectric disks. The predominant frequency of the emitted pulse in the near receiver is ~1100–3300 Hz, and in the distant receiver ~120–340 Hz. The emission passes through an elastic shell with a liquid, contacting with the borehole wall. The piezoelectric pressure receiver contacts the borehole wall in a similar manner that provides good contact with the medium. Seismic records is the stress as a function of time, $\sigma(t)$, quantization time t_{quant} = 20 μs and t_{quant} = 125 μs. The amplitude quantization step (A_{quant}) in the ADC is 78 mV. The amplitude values in volts were converted to mechanical stresses using the conversion factor K_{conv} = 100μ V/Pa. The seismic response receiver has a preamplifier with a gain of K = 100. The seismic responses in digital form were recorded on a computer. The amplitude of the input waveform (seismic responses) varied discretely from minimum to maximum: $A_1 \rightarrow A_2 \rightarrow A_3 \rightarrow A_4$. The amplitude increases as $A_2/A_1 = 1.5$; $A_3/A_1 = 2.0$; $A_4/A_1 = 2.5$. At a distance of 14 m from the source, the stress in the medium is approximately several tens of Pascals, and the strain range is $\sim 10^{-8}$–10^{-6}. These are small strains being below the conditional elastic limit.

The Findings and Discussion

The analysis of seismic records was carried out using a digital high-resolution signal (seismic response) displaying (mapping) on an enlarged scale. The mapping is obtained by connecting all the quantization points (t_{quant}) of the digital amplitude values along the seismic trace by straight lines (without smoothing). Such a representation of the signal allows a detailed analysis of the dynamic process, i.e. the process of development of stress (strain) in time. The illustrations are provided in both analog and digital imageries.

Findings

Fig. 1 shows six simultaneously received signal records in analog form, recorded at three amplitude values (A_1, A_2, A_3). Of these, three seismic traces are records of the first (closest to the source) receiver installed in the borehole at a depth of 1 m, and three seismic traces were recorded by the second receiver, located in the other borehole in 1 m from the source, at a depth of 6 m.

Analysis of the records in digital displaying shows the following. Due to the impossibility of placing the entire record in one picture, it is illustrated in separate parts. Fig. 2 shows the sections of records of the first pulse semiperiod, recorded near source *a*, and the first pulse – semiperiod at a depth of 6 m (below the source) *b*. Comparison of *a* and *b* records shows their qualitative difference.

At all amplitudes, the primary signal $\sigma_s(t)$ profile is quite smooth. The profile $\sigma_\gamma(t)$ has complications in the form of a plateau 1 of various lengths, a local stress drop 2 (marked with a dashed oval) and areas of sharp changes in the steepness of the wave 3 front (marked with arrows). Here, the front steepness changes by a factor of 9 during one t_{quant}. The listed complications are of significant expansion here.

Fig. 3 shows the sections of the records of the second (positive) semiperiod of the near pulse *a* and the similar distant pulse semiperiod *b*, recorded at a depth of 6 m. Comparison of these records produces the same result as described above. The first and repeated records at the same amplitude A_2, recorded by the distant receiver, are shown in Fig. 4. These pulses in analog form are presented in Fig. 4, *a*. A detailed picture in digital imagery can be seen at three recording intervals, where section *b* represents the record of the first minimum, sections *c* and *d* are fragments of the ascending and descending pulse fronts, respectively. Here the same non-standard manifestations take place and the same peculiarities of the first and repeated recordings are observed, which are described above. The stress drop is replaced by the flat region (in Fig. 4 it is marked by arrows in the rectangle). There are sections of the pulse front that are free from non-standard manifestations (Fig. 4, *d*).

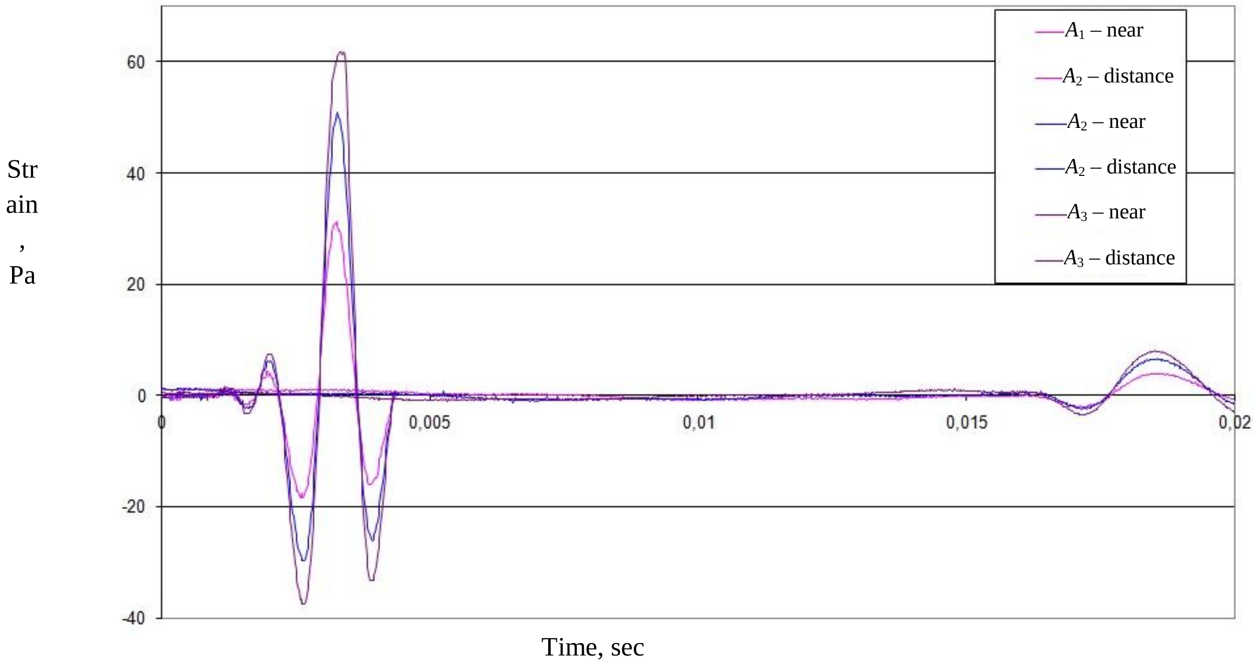

Fig. 1. Seismic response analog records at three values of amplitudes (A_1, A_2, A_3) obtained near the source (pulse emitter) and at a distance from it

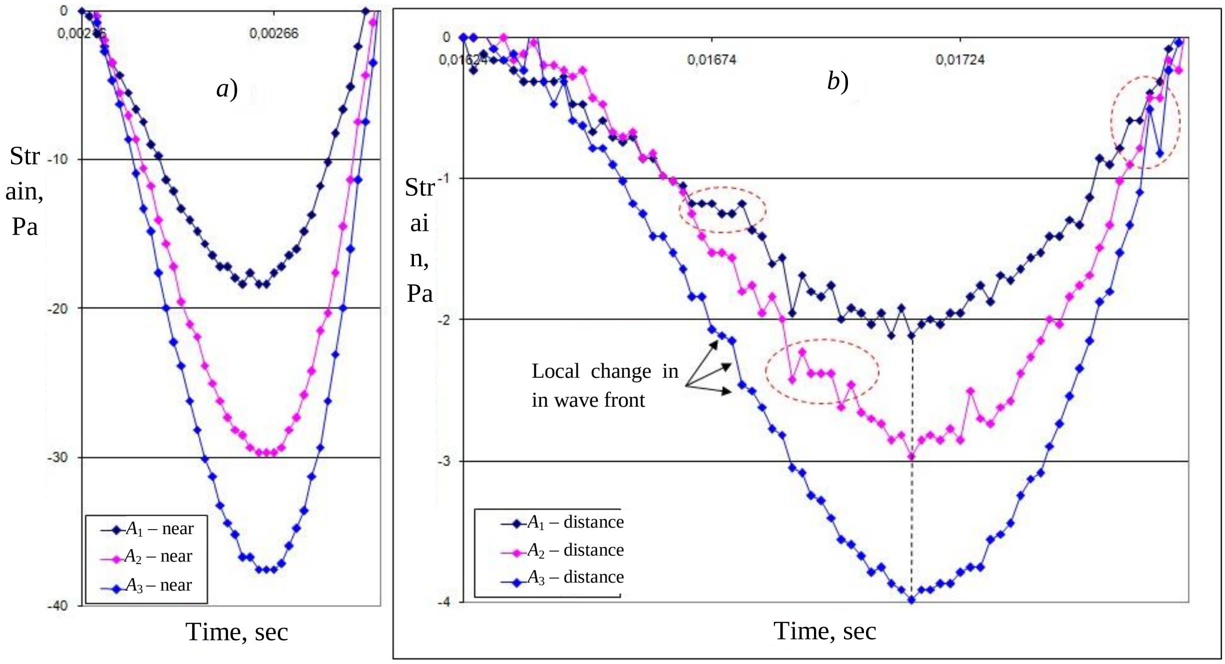

Fig. 2. Sections of the records of the first semiperiod of the pulse closest to the source (*a*) and the pulse recorded at a depth of 6 m (*b*)

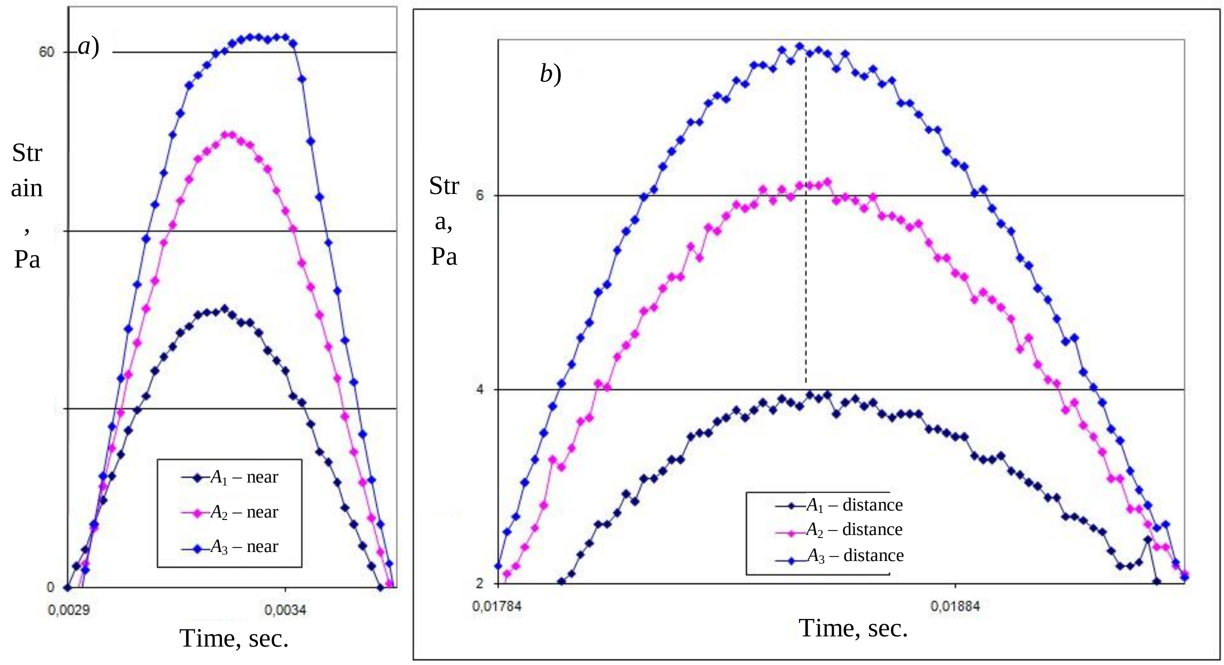

Fig. 3. Sections of the records of the positive semiperiod of the pulse closest to the source (*a*) and the analog semiperiod of the pulse recorded at a depth of 6 m (*b*)

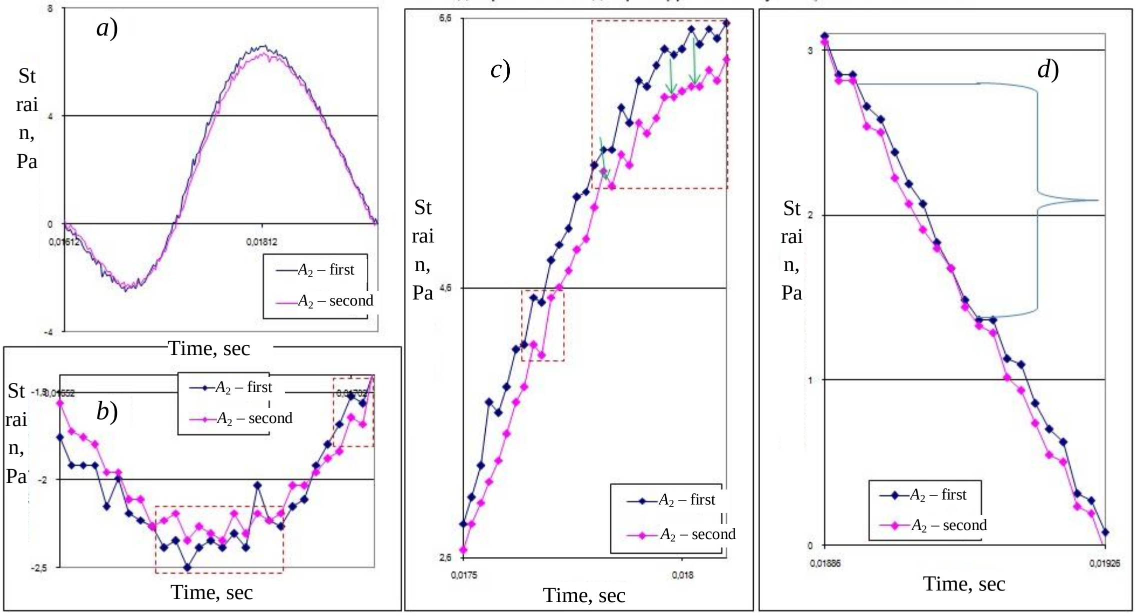

Fig. 4. The first and repeated records at the same amplitude (A_2), recorded by the far receiver tool:
a – the analog pulse record; *b* – the first minimum; *c*, *d* – fragments of the pulse ramp and downgoing front, respectively

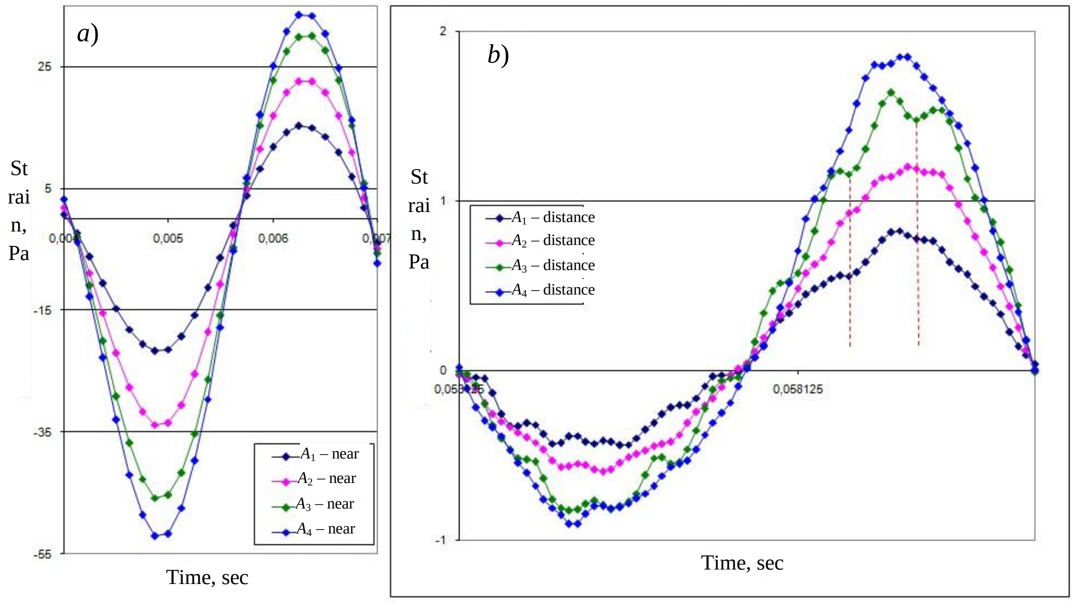

Fig. 5. Stress pulses recorded by the receiver tool closest to the source (*a*) and the far receiver (*b*), located in 1-m borehole at a distance of 14 m from the source

Fig. 5 shows the recordings of the near receiver *a* and the distant receiver *b*, located at distances of 1 m and 14 m from the source, respectively. The wave profile far from the source is complicated by the plateau and the areas of stress drop at all amplitudes. The descending front of the positive semiperiod demonstrates practically no complications. Figure 6 shows an example of the recording of an impulse at a distance of 14 m from the source, where there is an extended complication at the ascending wavefront, and no complications at the descending front. In the time interval $\Delta t = t_2 - t_1$, at all magnitudes of the amplitude, decreasing the front steepness is observed, which has a structured character. Here the complications are presented in the form of a plateau and a stress drop of a sawtooth shape. Beyond this region, the behavior of the stress profile is relatively monotonic. With increasing the amplitude, the magnitude of the sawtooth shape manifestations increases. The beginning of the stress drop occurs at point ***a***. The following drops occur at points ***b*** and ***c***. It is observed that the "micro-front" of the following, after the points ***a***, ***b***, ***c***, stress increase has the same slope with respect to the time axis, i.e. the same steepness of the front (the dashed lines are parallel).

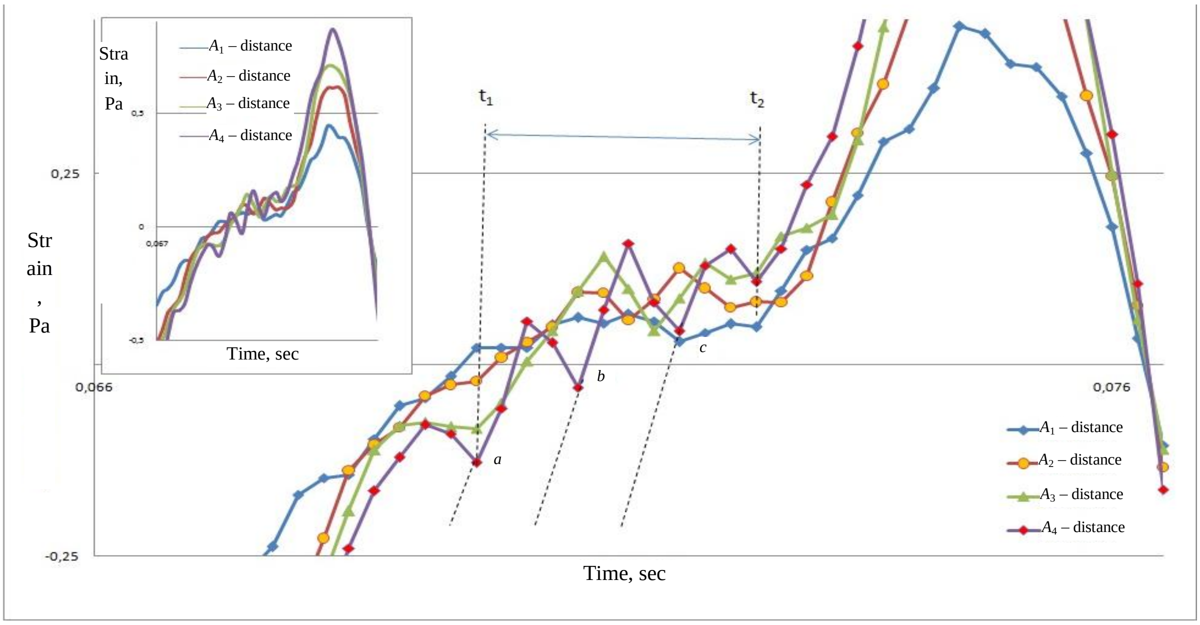

Fig. 6. Pulse records at four amplitude values recorded at a distance of 14 m from the source at a depth of 1 m

Discussion

The study of $\sigma(t)$ seismic records showed that the waveform is complicated by the inserts in the form of the plateau with boundaries marked by abrupt changes in the stress amplitude. Such an effect is supposedly attributed to the manifestation of hopping intermittent inelasticity due to rock microplasticity. Numerous data in solid state physics and materials science also indicate the mechanism of plasticity and hopping strain [1; 3; 6; 9; 14; 29; 27; 33]. It has been experimentally shown that the process of microplasticity is amplitude-dependent in nature [16, 37, 22, 25]. An intermittent change in amplitude in the form of a seismic pulse is similar to a stress stop when it reaches a critical value σ_{cr} on the curve [28]. The effective slope of the pulse front is formed with the joint participation of elasticity and inelasticity of a hopping nature. This coincides with the data obtained in material sciences. The sudden appearance of a yield plateau on the $\sigma(\varepsilon)$curves, called a sudden “displacement jump“ when loading and unloading (“pop-in” and “pop-out event”), was found in many experiments [12; 21].

Duplication of records, registration of the signal with accumulation ensures the reliability of the measurements and removes the involvement of arbitrary noise events. Repeated recording within a single time quantum does not always coincide with the first recording, as, for example, shown in Fig. 4. This is acceptable for recording with high detailing in complex material such as a rock. The effect of the same slope of the local section at the wave front after a local stress drop (Fig. 6, parallel dashed lines from points **a, b,** and **в**) was predicted in [14]. It is shown here that the sections of the stress drop in the $\sigma(\varepsilon)$ diagram are followed by the sections of elastic strain that are parallel to each other. Besides, the transition of the plateau to the stress drop (their mutual replacement), which is shown in Fig. 4, *в,* is also known. It should be noted that the ascending front of the pulse at all amplitudes has complications, while the descending front is free of them (see Fig. 6). The input pulse is always also practically “clean”.

The hopping strain and stress plateau were also found in natural materials, such as silicon [32], stishovite [30], sapphire, diorite, graphite, mica, and others [10]. Quartz grains and other minerals are present both in hard rocks and in poorly consolidated medium. Using electron microscopy, it was shown that quartz single crystals contain inclusions of various chemical composition of micrometer sizes. When a low-intensity wave propagates, quartz demonstrates signs of nonclassical inelasticity, which was recorded in the parameters of amplitude-frequency-dependent attenuation using electron microscopy [22]. It is noteworthy that the strain hopping and plateau were found in such a weak material as nanoclay [15], as well as in gypsum [13] and granite. These facts can also be regarded as an indirect confirmation of the possibility of such effects in a poorly consolidated medium. A theoretical justification of the propagation of seismic waves involving the microplasticity process was developed in [36]. It is necessary to consider other possible mechanisms, such as the acousto-plastic effect in metals and alloys [28]. In this work, experimental material was analyzed, and justifications and approaches for solving the problem of the mechanism of intermittent (hopping) inelasticity in rocks were proposed.

Conclusion

New data on the physics of seismic wave propagation in a real medium were obtained in this study. There are many mechanisms of seismic waves attenuation, however, the mechanism of intermittent (hopping) strain is not yet included in the seismic model. The new knowledge can be used to develop a rheological model and theoretical researches. It is likely that the amplitude dependence of wave velocities and attenuation is connected with intermittent inelasticity and, in particular, with microplasticity. This is evidenced by the hopping and stress-dependent nature of the strain process. The cause of waveform transformation may be microplasticity.

The problem of the nature of microplasticity in geological materials remains open so far. The mechanism of inelasticity may be the same as in solids (the motion of dislocations and other defects of the microstructure), or completely different. However, the detected manifestations of seismic microplasticity in the loams are very similar to the manifestations of microplasticity in ordinary solids. This issue needs further clarification. Microplasticity has respect to the little-known inelastic processes of propagation of low-amplitude waves in natural materials. New knowledge about elastic-inelastic processes is required not only for the theory development, but also for obtaining more effective diagnostic features for solving various applied problems by seismic and acoustic methods.

References

1. Barannikova S. A., Nadezhkin M. V., Zuev L. B. On localization of plastic deformation during compression of LiF crystals: Solid State Physics, 2010, v. 52, No. 7, pp. 1291-1294. (in Russ.)

2. Voznesensky E. A. Soil behavior under dynamic loads: Moscow, Moscow University Press, 1998, 320 p.

3. Golovin, Yu. I., Dub O. N., Ivolgin V. I., Korenkov V. V. Tyurin A. I. Kinetic features of deformation of solids in nano-micro-volumes, Solid-state physics, 2005, v. 47, No. 6, pp. 961-973. (in Russ.)

4. Gushchin V. V., Pavlenko, O. V. Study of nonlinear elastic properties of rocks by seismic data, Modern Seismology, Achievements and Challenges: Moscow, 1998, v. 13. (in Russ.)

5. Kondratyev O. K., 1986, Seismic waves in absorbing media: Nedra Press, Moscow, 176 p. (in Russ.)

6. Lebedev S. V., Savich S. V., Alloy Al-3%Mg intermittent deformation parameters in the temperature range (210–350) K: Visnyk KhNU, No. 915, "Physics" series, 2010, v. 14, pp. 91-95. (in Russ.)

7. Mashinsky E. I. Amplitude-dependent attenuation of longitudinal and transverse waves in dry and saturated sandstone under pressure: Geology and Geophysics, 2009, v. 50, pp. 950-956. (In Russ.)

8. Nikolaev A. V. Problems of nonlinear seismic: Moscow, Nauka Press, 1987, 288 p. (in Russ.)

9. Peschanskaya N. N., Smirnov B. I., Shpeizman V. V. Hopping microdeformation in nanostructured materials: FTT, 2008, v. 50, No. 5, pp. 815-819. (in Russ.)

10. Barsoum M. W. MAX Phases: Properties of Machinable Ternary Carbides and Nitrides, Wiley-VCH Verlag GmbH, 2013.

11. Braccini S., *et al*.. The maraging-steel blades of the Virgo super attenuator. Meas. Sci. Technol., 2000, 11, pp. 467–476.

12. Bradby J. E. and Williams J. S., 2004, Pop-in events induced by spherical indentaton ib compound semiconductors. J. Mater. Res., 19. No 1, pp. 380–386.

13. Brantut N., Schubnel A., and Y. Gueguen, 2011. Damage and rupture dynamics at the brittle-ductile transition: The case of gypsum. Journal of Geophysical Research, Vol. 116, B01404.

14. Derlet P. M., Maaf R., 2013, Micro-plasticity and intermittent dislocation activity in a simplied micro structural model, arXiv:1205.1486v2 [cond- mat.mtrl-sci] 8 Feb 2013, pp. 1 - 33.

15. Dhakal H. N., Zhang Z. Y., Richardson M.O.W., 2006. Nanoindentation behaviour of layered silicate reinforced unsaturated polyester nanocomposites. Polymer Testing, 25, pp. 846 – 852.

16. Golovin I. S., Sinning H.-R., Goken J., Riehemann W., 2004. Fatigue-related damping in some cellular metallic materials. Materials Science and Engineering, A 370, p. 537 - 541.

17. Guyer R. A., McCall K. R., Boitnott G. N., 1995. Hysteresis, Discrete Memory and Nonlinear Wave Propagation in Rock: a New Paradigm, *Phys. Rev. Lett.*, 74, 17, pp. 3491–3494.

18. Guyer R. A., Johnson P. A., 1999. Nonlinear mesoscopic elasticity: Evidence for a new class of materials *Physics Today* 52**,** 4, pp. 30–36.

19. Jackson I., Faul U. H., Fitz Gerald J. D., Tan B. H. Shear wave attenuation and dispersion in melt-bearing olivine polycrystals: 1. Specimen fabrication and mechanical testing // *J. Geophys. Res.*, 2004, v. 109, B06201, pp. 1–17.

20. Johnston D. H., Toksoz M. N., 1980. Thermal cracking and amplitude dependent attenuation. Journal of Geophysical Research, 85, pp. 937 - 942.

21. Lorenz D., Zeckzer A., Hilpert U., Grau P., 2003, Pop-in effect as homogenous nucleation of dislocationsduring nanoidentation. Physical Review, B 67, 172101.

22. Mashinskii E. I., 2008. Amplitude-frequency dependencies of Wave Attenuation in Single-Crystal Quartz: Experimental Study. Journal of Geophysical Research, 113, B11304.

23. Mavko G. M, 1979. Friction Attenuation: An Inherent Amplitude Dependence. Journal of Geophysical Research 84 (9), pp. 4769–4775.

24. McCall K.R., Guyer, R. A., 1994. Equation of State and Wave Propagation in Hysteretic Nonlinear Elastic Materials, *J. Geophys. Res.*, 99, B 12. 23,887–23,897.

25. Nishino Y., Asano, S., 1996. Amplitude-dependent internal friction and microplasticity in thin-film materials. Journal de Physique IV, 6, pp. 783–786.

26. Ostrovsky L. A., Johnson, P. A., 2001. Dynamic nonlinear elasticity in geomaterials. La Rivista del Nuovo Cimento 24, 4, 7.

27. Qiang J. B., Xie G. Q., Zhang W., Inoue A., 2007. Unusual room temperature ductility of a Zr-based bulk metallic glass containing nanoparticles. Applied Physics Letters, 90, 231907, pp. 1–3.

28. Sapozhnikov K. V., Vetrov V. V., Pulnev S. A., Kustov S. B., 1996. Acousto-pseudoelastic effect and internal friction during stress-induced martensitic transformations in Cu-Al-Ni single crystals. Scripta Materialia., 34 (10), p. 1543–1548.

29. Smirnov B. I., Shpeizman V. V., Peschanskaya, N. N., Nikolaev R. K., 2002. Effect of magnetic field on microplastic strain rate for C_{60} single crystals. Physics of the Solid State, 44 (10), pp. 2009–2012.

30. Sheng-Nian Luo J.G. Swadener, Chi Ma, Oliver Tschauner, 2007. Examining crystallographic orientation dependence of hardness of silica stishovite. Physica, B 390, 138–142.

31. Tutuncu, A.N., Podio, A.L., Sharma, M.M., 1994. An experimental investigation of factors influencing compressional- and shear-wave velocities and attenuations in tight gas sandstones. Geophysics, 59 (1), pp. 77–86.

32. Vodenitcharova T., Zhang L.C., 2004. A new constitutive model for the phase transformations in mono-crystalline silicon. International Journal of Solids and Structures, 41, pp. 5411–5424.

33. Wang W., 2003. Deformation behavior of Ni3Al single crystal during nanoindentation. Acta Materialia, 51, pp. 6169–6180.

34. Winkler, K.W., Nur, A., Gladwin, M., 1979. Friction and seismic attenuation in rock. Nature 274, pp. 528–531.

35. Xu H., Day S.M., Minster, J.-B.H., 1998. Model for Nonlinear Wave Propagation Derived from Rock Hysteresis. Measurements Journal of Geophysical Research, 103, (B 12), 29,915–29,929.

36. Yarushina V.M., Podladchikov Y.Y., 2010, Plastic yielding as a frequency and amplitude independent mechanism of seismic wave attenuation. Geophysics, 75, 3, pp. 51–63.

37. Zaitsev V. Yu., Nazarov V. E., Talanov V. I., 1999. Experimental Study of the self-action of seismoacoustic waves. Acoustic Physics, 45 (6), pp. 720–726.

Библиографический список

1. Баранникова С. А., Надежкин М. В., Зуев Л. Б. О локализации пластической деформации при сжатии кристаллов LiF // Физика твердого тела. 2010. Том 52. Вып. 7. С. 1291–1294.

2. Вознесенский Е.А. Поведение грунтов при динамических нагрузках. М.: Издательство Московского университета, 1998. 320 с.

3. Головин Ю.И., Дуб С.Н., Иволгин В.И., Коренков В.В., Тюрин А.И.. Кинетические особенности деформации твердых тел в нано-микрообъемах // Физика твердого тела. 2005. Том 47. Вып. 6. С. 961–973.

4. Гущин В. В., Павленко О. В. Изучение нелинейно-упругих свойств земных пород по сейсмическим данным // Современная сейсмология. Достижения и проблемы. М.: 1998. Т. 13

5. Кондратьев О. К. Сейсмические волны в поглощающих средах. М.: Недра, 1986. 176 с.

6. Лебедев С. В., Савич С. В. Параметры скачкообразной деформации сплава Al- 3% Mg в интервале температур (210–350) К. // Вісник ХНУ. 2010. № 915. Серія «Фізика». Вип. 14. С. 91–95.

7. Машинский Э. И., Амплитудно-зависимое затухание продольных и поперечных волн в сухом и насыщенном песчанике под давлением // Геология и Геофизика. 2009. Т. 50. С. 950–956.

8. Николаев А. В. Проблемы нелинейной сейсмики. М.: Наука, 1987. 288 с.

9. Песчанская Н. Н., Смирнов Б. И., Шпейзман В.В.. Скачкообразная микродеформация в наноструктурных материалах // ФТТ. 2008. Т. 50. Вып. 5. С. 815–819.

10. Barsoum M. W. MAX Phases: Properties of Machinable Ternary Carbides and Nitrides, Wiley-VCH Verlag GmbH., 2013

11. Braccini S., *et al.*. The maraging-steel blades of the Virgo super attenuator. Meas. Sci. Technol., 2000, 11, pp. 467–476.

12. Bradby J. E. and Williams J. S. Pop-in events induced by spherical indentaton ib compound semiconductors. J. Mater. Res., 19, 2004, No. 1, pp. 380–386.

13. Brantut N., Schubnel A., and Y. GueguenDamage and rupture dynamics at the brittle-ductile transition: The case of gypsum. Journal of Geophysical Research, 2011, Vol. 116, B01404.

14. Derlet P. M., Maaf R. Micro-plasticity and intermittent dislocation activity in a simplied micro structural model, arXiv:1205.1486v2 [cond- mat.mtrl-sci] 8 Feb 2013, 2013, pp. 1-33.

15. Dhakal H. N., Zhang Z. Y., Richardson M. O. W. Nanoindentation behaviour of layered silicate reinforced unsaturated polyester nanocomposites. Polymer Testing, 2006, 25, pp. 846-852.

16. Golovin I. S., Sinning H.-R., Goken J., Riehemann W. Fatigue-related damping in some cellular metallic materials. Materials Science and Engineering, , 2004, A 370, pp. 537 - 541.

17. Guyer R. A., McCall K. R., Boitnott G. N. Hysteresis, Discrete Memory and Nonlinear Wave Propagation in Rock: a New Paradigm, *Phys. Rev. Lett.*, 1995, 74, 17, pp. 3491–3494.

18. Guyer R. A., Johnson P. A. Nonlinear mesoscopic elasticity: Evidence for a new class of materials *Physics Today* 52**,** 1999, 4, pp. 30–36.

19. Jackson I., Faul U. H., Fitz Gerald J. D., Tan B. H. Shear wave attenuation and dispersion in melt-bearing olivine polycrystals: 1. Specimen fabrication and mechanical testing // *J. Geophys. Res.*, 2004, v. 109, B06201, pp. 1–17.

20. Johnston D. H., Toksoz M. N., 1980. Thermal cracking and amplitude dependent attenuation. Journal of Geophysical Research, 85, pp. 937-942.

21. Lorenz D., Zeckzer A., Hilpert U., Grau P. Pop-in effect as homogenous nucleation of dislocationsduring nanoidentation. Physical Review, B 67, 172101, 2003.

22. Mashinskii E. I. Amplitude-frequency dependencies of Wave Attenuation in Single-Crystal Quartz: Experimental Study. Journal of Geophysical Research, 113, B11304, 2008.

23. Mavko G. M. Friction Attenuation: An Inherent Amplitude Dependence. Journal of Geophysical Research 84 (9), pp. 4769–4775, 1979.

24. McCall K. R., Guyer, R. A. Equation of State and Wave Propagation in Hysteretic Nonlinear Elastic Materials, *J. Geophys. Res.*, 1994, 99, B 12. 23,887–23,897.

25. Nishino Y., Asano, S., 1996. Amplitude-dependent internal friction and microplasticity in thin-film materials. Journal de Physique IV, 6, pp. 783–786.

26. Ostrovsky L. A., Johnson P. A. Dynamic nonlinear elasticity in geomaterials. La Rivista del Nuovo Cimento 24, 2001, 4, 7.

27. Qiang J. B., Xie G. Q., Zhang W., Inoue A., 2007. Unusual room temperature ductility of a Zr-based bulk metallic glass containing nanoparticles. Applied Physics Letters, 90, 231907, pp. 1–3.

28. Sapozhnikov K. V., Vetrov V. V., Pulnev S. A., Kustov S. B. Acousto-pseudoelastic effect and internal friction during stress-induced martensitic transformations in Cu-Al-Ni single crystals. Scripta Materialia., 1996, 34(10), pp. 1543–1548.

29. Smirnov B. I., Shpeizman, V. V., Peschanskaya, N. N., Nikolaev R. K., 2002. Effect of magnetic field on microplastic strain rate for C_{60} single crystals. Physics of the Solid State, 44 (10), pp. 2009–2012.

30. Sheng-Nian Luo J. G. Swadener, Chi Ma, Oliver Tschauner, 2007. Examining crystallographic orientation dependence of hardness of silica stishovite. Physica, B 390, 138–142.

31. Tutuncu, A.N., Podio, A.L., Sharma, M.M., 1994. An experimental investigation of factors influencing compressional- and shear-wave velocities and attenuations in tight gas sandstones. Geophysics, 59 (1), pp. 77–86.

32. Vodenitcharova T., Zhang L.C., 2004. A new constitutive model for the phase transformations in mono-crystalline silicon. International Journal of Solids and Structures, 41, pp. 5411–5424.

33. Wang W., 2003. Deformation behavior of Ni3Al single crystal during nanoindentation. Acta Materialia, 51, pp. 6169–6180.

34. Winkler, K.W., Nur, A., Gladwin, M., 1979. Friction and seismic attenuation in rock. Nature 274, pp. 528–531.

35. Xu H., Day S.M., Minster, J.-B.H., 1998. Model for Nonlinear Wave Propagation Derived from Rock Hysteresis. Measurements Journal of Geophysical Research, 103, (B 12), 29,915–29,929.

36. Yarushina V.M., Podladchikov Y.Y., 2010, Plastic yielding as a frequency and amplitude independent mechanism of seismic wave attenuation. Geophysics, 75, 3, pp. 51–63.

37. Zaitsev V. Yu., Nazarov V. E., Talanov V. I., 1999. Experimental Study of the self-action of seismoacoustic waves. Acoustic Physics, 45 (6), pp. 720–726.

ORIGINAL PAPERS

DOI: 10.17073/2500-0632-2019-1-42-56

Analysis of Hydrocarbon Saturation Nature in a Heterogeneous Reservoir as Exemplified in AC10 Formation of Priobskoe Field

I. B. Ratnikov, N. S. Yarkova, E. A. Romanov

Ltd. "Coretest service", Tyumen, Russia, ✉IBRatnikov@mail.ru

Abstract: The main factors affecting the nature of uneven hydrocarbon saturation of the AC10 formation reservoir at Priobskoye field located in Western Siberia are considered. The formation is characterized by extreme heterogeneity caused by macro- and microstructure, which is determined by the lithofacial and structural-morphological conditions of sedimentation. The formation is characterized by high variability of lithological-mineralogical composition and textural and structural features. To bring to light the nature of the uneven hydrocarbon saturation of the reservoir, the combined analysis of the findings obtained from the study of the size of capillary channels and pores, as well as the investigation of the degree of their filling with clay and carbonate material, was performed. The analysis has shown that the filler composition, its amount in the pore space, and the (core) hydrocarbon saturation collectively evened the AC10 formation electrical resistance in different saturation zones, which led to distortion of the hydrocarbon saturation of the reservoir as a whole.

Keywords: heterogeneity, hydrocarbon saturation, pore and pore channel sizes, porosity, permeability, clayiness, carbonate content.

For citation: Ratnikov I. B., Yarkova N. S., Romanov E. A. Analysis of hydrocarbon saturation nature in a heterogeneous reservoir as exemplified in AC10 formation of Priobskoe field. *Mining Science and Technology*. 2019;4(1):42-56. (In Russ.). DOI: 10.17073/2500-0632-2019-1-42-56.

Анализ характера насыщенности пород в неоднородном коллекторе на примере пласта АС10 Приобского месторождения

Ратников И. Б., Яркова Н. С., Романов Е. А.

ООО «Коретест сервис», Тюмень, Россия, ✉IBRatnikov@mail.ru

Аннотация: Рассматриваются основные факторы, оказывающие влияние на природу неравномерной насыщенности углеводородами (УВ) коллектора пласта АС10 Приобского месторождения, расположенного на территории Западной Сибири. Отложения залежи характеризуются чрезвычайной неоднородностью, обусловленной макро- и микростроением, которое определено литолого-фациальными и структурно-морфологическими условиями осадконакопления. Данная залежь отличается широкой изменчивостью литолого-минералогического состава и текстурно-структурных особенностей. С целью выявления природы неравномерной насыщенности коллектора УВ выполнен совместный анализ результатов, полученных по размерам капиллярных каналов и пор, а также степени их заполнения глинистым и карбонатным материалом. Исследования показали, что состав цемента, его количество в поровом пространстве и насыщенность керна УВ в совокупности нивелировали электрическое сопротивление пласта АС10 в различных зонах насыщения, что привело к искажению насыщенности коллектора в целом.

Ключевые слова: неоднородность, насыщенность, размеры пор и поровых каналов, пористость, проницаемость, глинистость, карбонатность.

Для цитирования: Ратников И. Б., Яркова Н. С., Романов Е. А. Анализ характера насыщенности пород в неоднородном коллекторе на примере пласта АС10 Приобского месторождения. *Горные науки и технологии.* 2019;4(1):42-56. DOI: 10.17073/2500-0632-2019-1-42-56.

Introduction

Rock heterogeneity is a fundamental property of matter. M.V. Rats noted that heterogeneity is inherent in any rock from the moment of its origination and disappears only with the disappearance of the rock itself. The problem of heterogeneity of rocks and the variability of their physical properties at different levels of the material structural organization and under various thermodynamic conditions is fundamental in petrophysics [13]. G. I. Petkevich emphasized that when describing heterogeneous and different-scale geological objects, there is an urgent need for new approaches, improvement of concepts and terms, the introduction of formal constructs and quantitative indicators.

The heterogeneity attracts the attention of geologists of all specializations (including petrophysicists) since the inception of geological sciences. Most researchers studying the petrographic, lithological, hydrodynamic and other features of rocks, in fact, are engaged in nothing more than the study of heterogeneity of rocks. Geophysicists are not the exception.

One of the important properties of the geological environment (GE) is its time-to-time and spatial variability. Variability determines the heterogeneity of an object, which is determined by the difference in its properties at different points. Modern modeling in geological sciences imposes strict requirements on the study and obtaining of source information. First of all, this is a detailed description of thin layers and microlayers of a rock and quantitative assessment of all the required parameters of these layers. The parameters studied at individual point in the GE do not always suit specialists. In laboratory practice, the study of rock properties is carried out precisely based on a point-to-point discrete principle, although it is far from always possible to select samples for analysis from a thin layer.

It was repeatedly noted in [14, 15, 18–20] that, in essence, all petrophysical characters are of the inherited character of lithofacial variability. This is due to the heterogeneity formed during the diagenesis of sedimentary rocks that occur at different points in the GE in different ways (under different conditions). As a result, the further course of epigenesis is “superimposed” on the diagenesis process. Hence the heredity of the heterogeneity of rocks arises, which determines the variability of petrophysical (and not only) features.

At present, the study of rock heterogeneity in petroleum geology is becoming increasingly important, since the main reserves of oil and gas are accumulated in reservoirs with low permeability (poroperm properties or reservoir quality (RQ)), complicated by structural heterogeneity. Along with resolving issues of the methodology, the influence of heterogeneity of reservoir rocks on the reservoir properties, the rock permeability, hydrocarbon saturation, and displacement efficiency is studied. The pictures of the movement of oil-water contact, ways to increase oil recovery are also studied – all these issues are very important for successful development of a field. When assessing the mentioned parameters of reservoir rocks, description and analysis of heterogeneity are of crucial importance. A number of researchers [1–3, 5, 8] have done a great job of analysis and assessment of geological heterogeneity in the design of oil field development. However, in theory and practical aspects of hydrocarbon reserve estimation, this issue remains less studied and is only limited to determining the factors characterizing heterogeneity, and typifying oil deposits based on them [5, 9]. Attention should also be paid to the ambiguous interpretation of the concepts of "geological heterogeneity" and "confidence of oil and gas reserves" [1, 5, 7, 9; 21–23].

The influence of heterogeneity on sediment productivity was noted by many experts [4, 9, 13, 26–28]. It has been established that increasing the degree of heterogeneity of reservoir rocks leads to decreasing productivity. In petroleum geology, micro- and macro-heterogeneity is usually distinguished [6, 7, 10, 21].

Micro-heterogeneity of rocks is studied, as a rule, in laboratory conditions by traditional methods: in thin sections, on images of a scanning electron microscope, by capillarimetry, X-ray phase analysis, and acoustic measurements, as well as using devices designed to determine effective porosity and permeability coefficient. These are the basic methods. There are also special ones: immersion, thermal, X-ray fluorescence, IR spectrometric, and other methods of analysis.

To study macro-heterogeneity, geophysical well logging data for all drilled wells and seismic data are used. Macro-heterogeneity is studied vertically (along the thickness of a horizon) and along the strike of the formations (by area).

Geologists (geophysicists) pay special attention to macro-heterogeneity with a detailed breakdown of reservoir horizons by impermeable sublayers.

The aim of this work is an attempt to identify the nature of uneven hydrocarbon saturation of the AC10 formation reservoir and the impact of heterogeneity on the rock physical properties.

The findings discussion

Analysis of hydrocarbon saturation nature the AC10 formation rocks was performed based on two boreholes of the Priobskoe field.

In the process of the AC10 formation origination, the sea basin was sharply differentiated in depth. This was due to its partial shallowing in the eastern and southeastern parts of the region due to the accumulation of significant masses of terrigenous material. The edge of the shelf was located within the considered territory. The amount of fragmental product entering the basin increased. The formation of sand bodies during this period was connected both with the accumulation of the fragmental product in the shelf area, especially in its frontal part, and with the activity of turbidite flows of various hydrodynamic activity. The sand strata of various genesis may be spatially separated, connected by "channels" or represent a single body. The conditions of sedimentation determined the rather intricate spatial (in plan view and cross-section) nature of the distribution of the sand bodies.

The area of the sand body occurrence in the lower part of the AC10 formation belongs to the shelf zone, which was very flat and apparently represented an alluvial-delta plain. The inflow of material occurred from the southeast through two channels with its redistribution along the frontal zone. The sea basin in the period under review retained differentiation in depth. At the stage of completion of the AC10 formation origination, the differentiation of the sea basin in depth successively decreased that was connected with the accumulation of terrigenous material in the previous time. The amount of the fragmental product supplied decreased, and basin processes began to prevail in its redistribution, under the influence of which bar systems were formed. The activity of turbidite flows is observed only in the western part of the area, confined to the slope and lower part of the terrain.

It becomes clear from the foregoing that the conditions of the AC10 formation origination suggest wide variability of its lithological and mineralogical composition and textural-and-structural features.

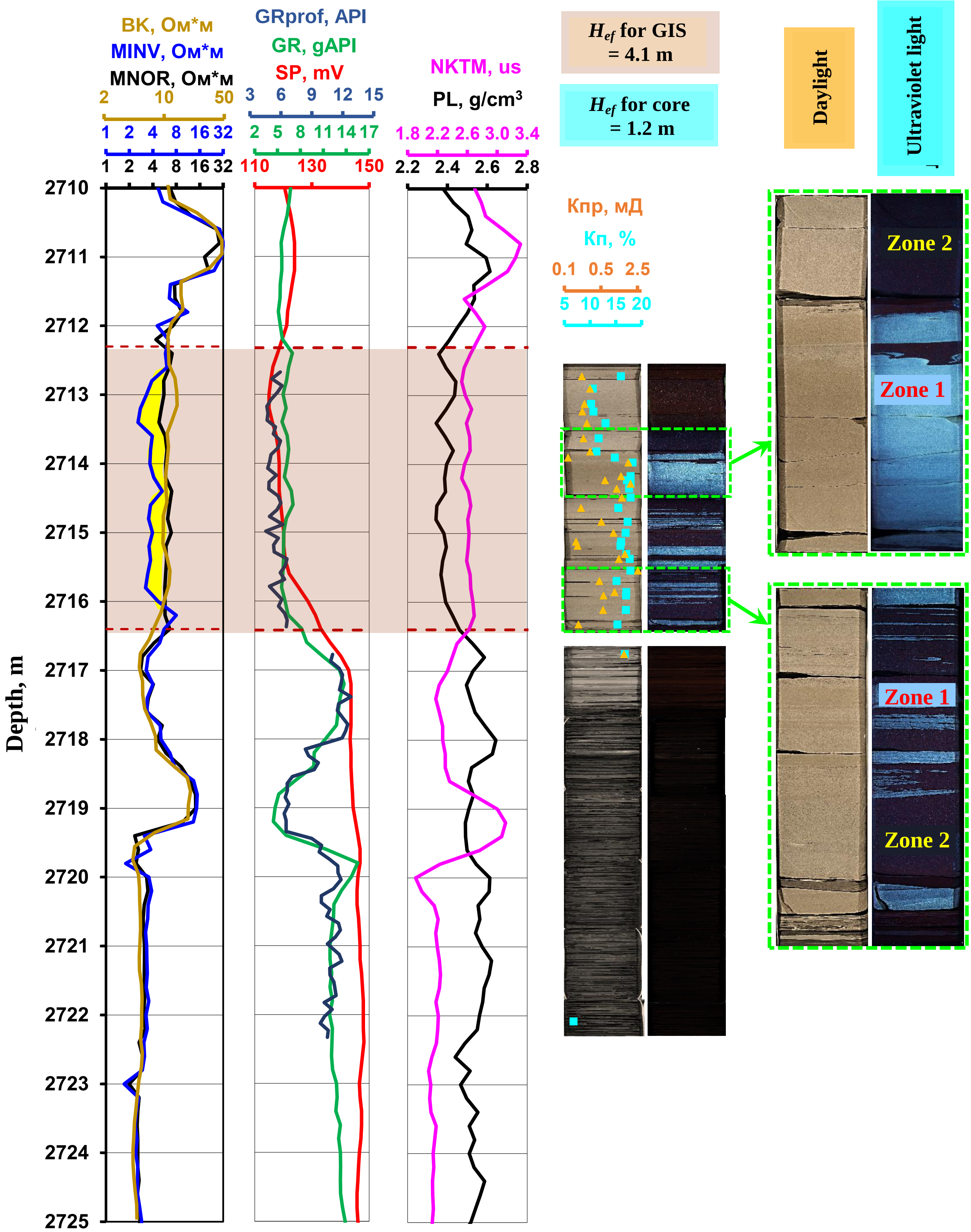

Fig. 1. Geophysical logging data and core photographs in daylight and ultraviolet light for the rocks of AC10 formation in borehole 1 at Priobskoe field

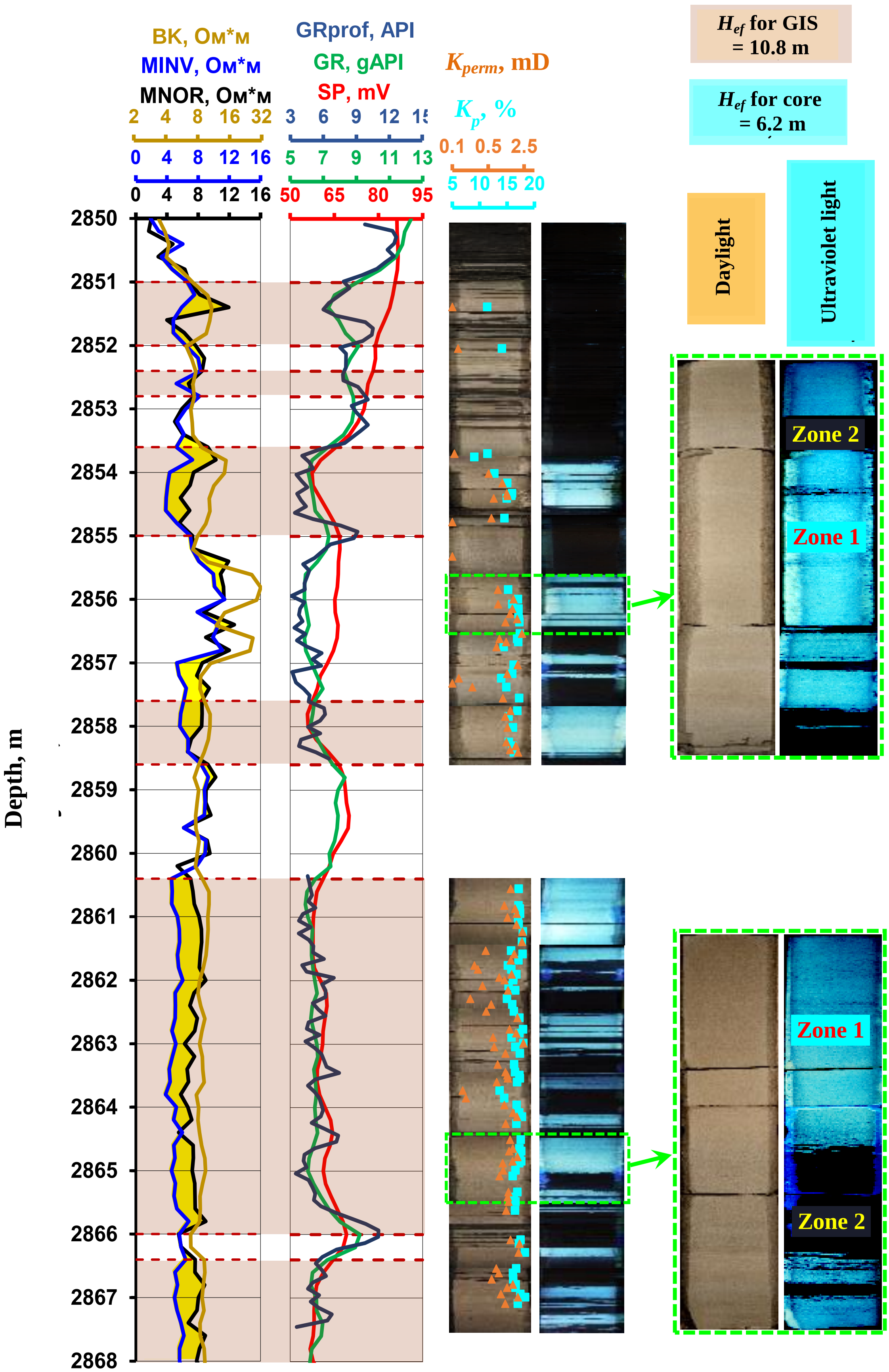

Fig. 2. Geophysical logging data and core photographs in daylight and ultraviolet light for the rocks of AC10 formation in borehole 2 at Priobskoe field

Fig. 1 and 2 show the comparison of the geophysical well logging data with core photographs in daylight and ultraviolet light for the rocks of the AC10 formation from two boreholes at the Priobskoe field. In the given intervals of depth, the total effective thickness H_{ef} determined by the logging data was 14.9 m, whereas from the core photographs in ultraviolet (UV) light H_{ef} of the oil-saturated interlayers is 7.4 m only, i.e. by 50.0 % less. It can be seen in the photographs in daylight that the core of the AC10 formation is predominantly homogeneous. However, the photographs in ultraviolet light showed island core saturation with hydrocarbons. In the photograph in UV light, 2 zones are clearly distinguished: bright glowing (zone 1) and dark glowing (zone 2).

Let's try to comprehend why the core visually homogenous in photographs in daylight, shows island core saturation with hydrocarbons in the photographs in UV light.

Lithologically, the rocks of zone 1 are represented by sandstone and siltstone with clay and carbonate-clay cement, and those of zone 2 are siltstone with clay and carbonate cement (Fig. 3).

For the rocks of zone 1, the sand fraction amounts to from 40.4 to 59.2% (the average value is 44.6 %), the silt fraction amounts to from 33.2 to 49.2 % (45.0 %), and the clay fraction, from 7.3 up to 12.7 % (10.3 %); the carbonate content varies within 2.5–9.6% (4.9 %).

For the rocks of zone 2, the sand fraction amounts to from 23.6 to 47.9 % (the average value is 35.4 %), the silt fraction amounts to 38.7 to 59.6 % (50.4 %), and the clay fraction, from 10.5 up to 24.1 % (14.2 %), the carbonate content varies within 4.6–30.9 % (9.3 %) (Fig. 4).

The rocks of zone 1 and zone 2 are of poor grading (Fig. 5). The grading factor is often used as an indicator of sedimentation conditions. However, in most cases, it gives only comparative characteristics.

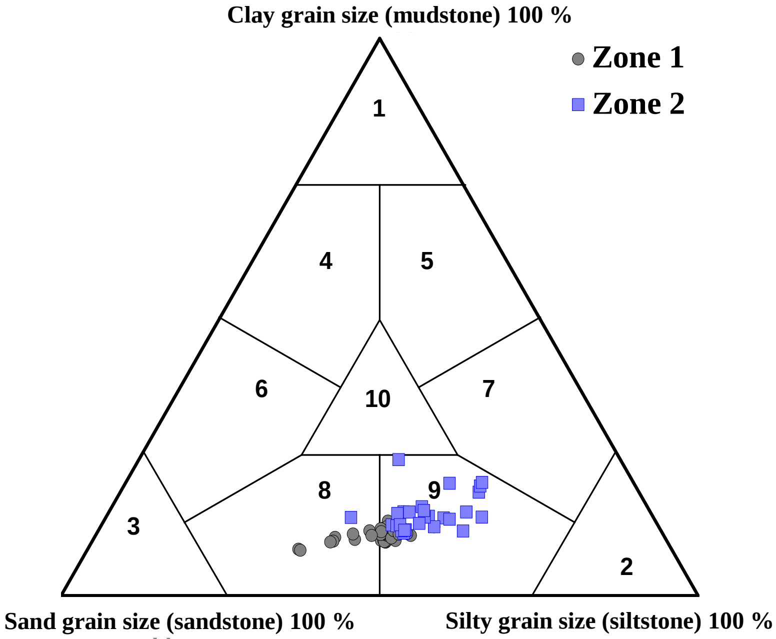

Fig. 3. Classification graphic chart of sandy-silty-clay rocks according to F. Shepard [12]:
1 – mudstone; *2* – siltstone; *3* – sandstone; *4* – sandy mudstone; *5* – silty mudstone; *6* – clayey sandstone; *7* – clayey siltstone; *8* – silty sandstone; *9* – sandy siltstone; *10* – sandy-silty mudstone

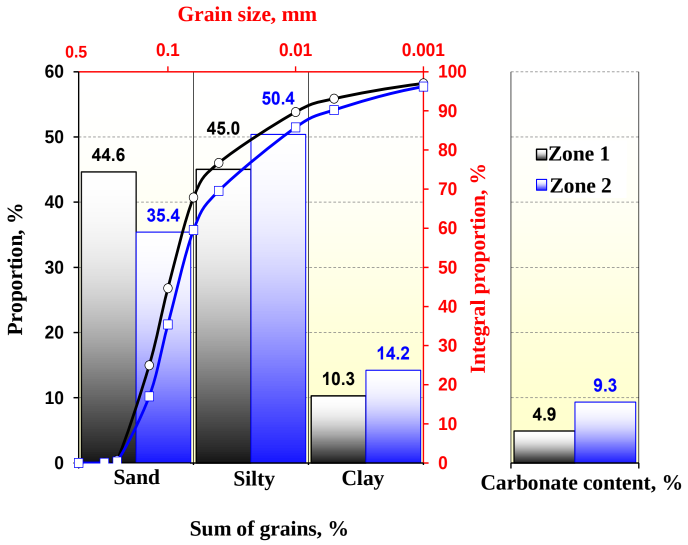

Fig. 4. Grain-size and carbonate content distribution in rocks of AC10 formation of Priobskoe field

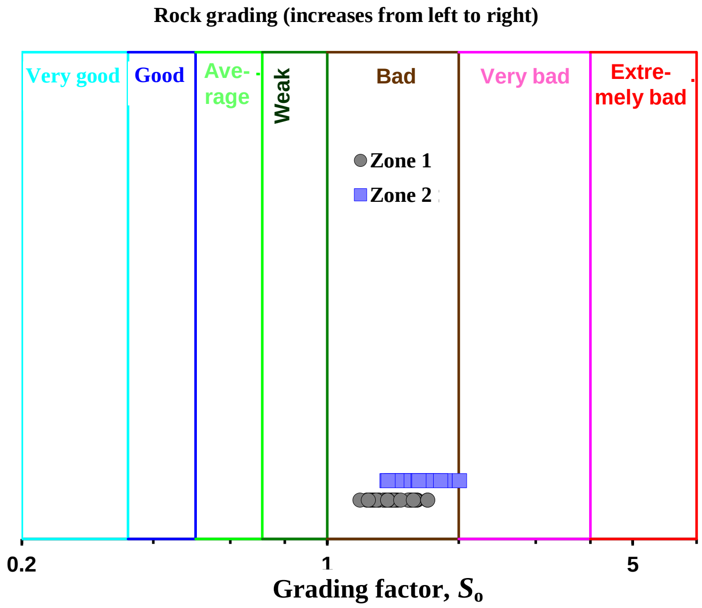

Fig. 5. Sorting of the AC10 formation rocks according to R.L. Folk and W.C. Ward [24]

The clastic rock grain size distribution has a certain genetic significance, since it reflects the nature of transportation and the dynamics of sedimentation medium. Paired combinations of grain size factors are used to compile “genetic diagrams” that reflect, with varying degree of confidence, the dynamic conditions of the sedimentation medium. The most famous diagrams are those of R. Passsega and G.F. Rozhkov.

Dynamic diagram developed by R. Passsega involves such characteristics as median grain size *M* and grain size/centile *S*, µm, reflecting the maximum flow capacity. This takes into account the way of transporting the fragmental product by particle rolling, saltation, transfer in the form of a graded or homogeneous suspension. Dynamic genetic diagram by G.F. Rozhkov is based on the principle of natural mechanical differentiation of particles of sand and silt size (aeolian processes are also taken into account). The diagram is based on the asymmetry and excess relationships, which are determined by the statistical moment formulas [11].

According to the diagrams by R. Passsega and G.F. Rozhkov, the AC10 formation sediments mainly correspond to the type of suspension sediment type and, to a lesser extent, to the type of rolling sediment of the littoral facies complex (Fig. 6, 7).

Based on the analysis of porosity and permeability, the rocks of the selected zones belong to different petrophysical types (Fig. 8). The estimation of the pore space in thin sections showed that the rocks of zone 1 have larger pores relative to the rocks of zone 2 (Fig. 9).

To bring to light the nature of the uneven hydrocarbon saturation of the reservoir in the distinguished zones, the combined analysis of the findings obtained from the study of the size of capillary channels and pores, as well as the investigation of the degree of their filling with clay and carbonate material, was performed.

The sizes of pores and pore channels and the nature of their distribution in size are one of the important indicators in petrophysics. The distribution of phases in the reservoir largely depends on these indicators. The petrophysical parameters mainly depend on the size of the pore channels composing the pore space. It is known that the more heterogeneous the sizes of the reservoir pore channels, the greater the residual hydrocarbon saturation and the lower the displacement efficiency. This phenomenon in mudded-off reservoirs is primarily due to the Laplace effect [16].

With the aim of studying the structural features of the pore space in the distinguished zones, an analysis of scanning electron microscope (SEM) images was performed (Fig. 10). In the rocks of zone 1, predominance of inter-microaggregate-grain, inter-grain and intra-grain micropores, as well as cavernous-expanded leaching pores with average size of 14 μm, very few pores with cross-section of up to 70 μm, anisometric and slot-shaped, connecting with each other through ultracapillary and narrow slot-like pore channels is observed.

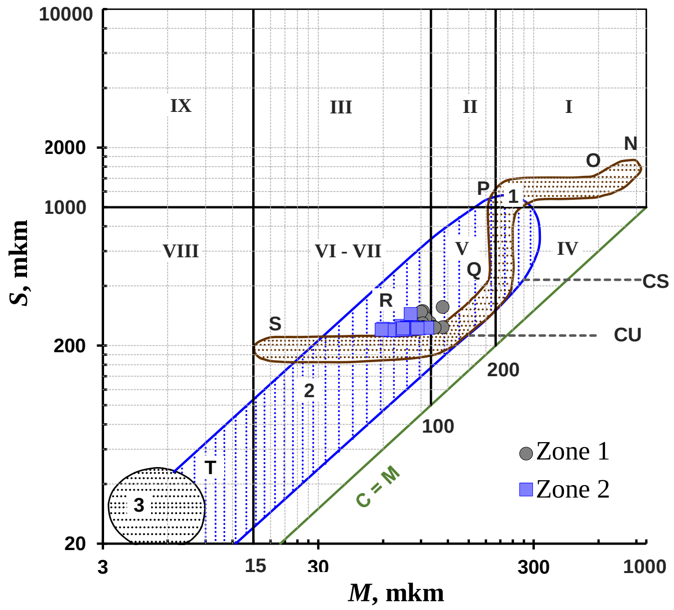

Fig. 6. Genetic S-M diagram by R. Passega [25]

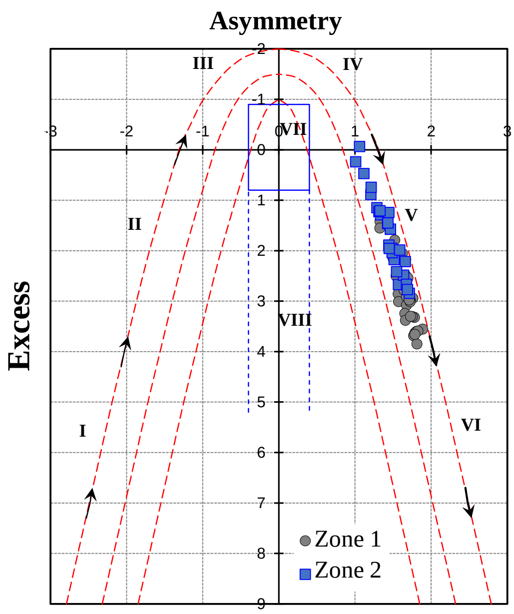

Fig. 7. Dynamic genetic diagram by G.F. Rozhkov [17]

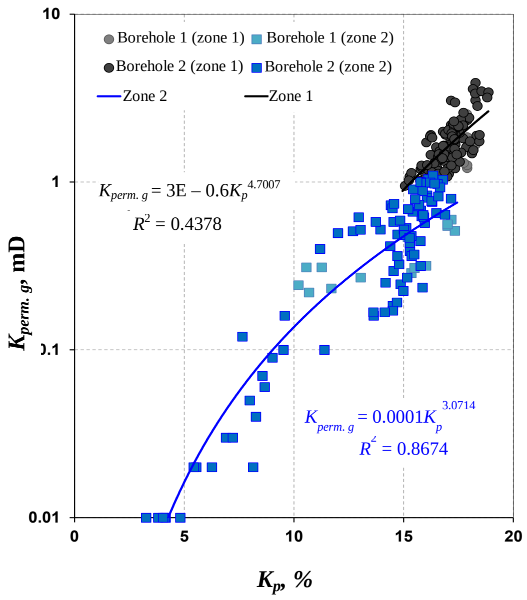

Fig. 8. Comparison of absolute permeability for gas ($K_{perm.\,g}$) with open porosity (K_p)

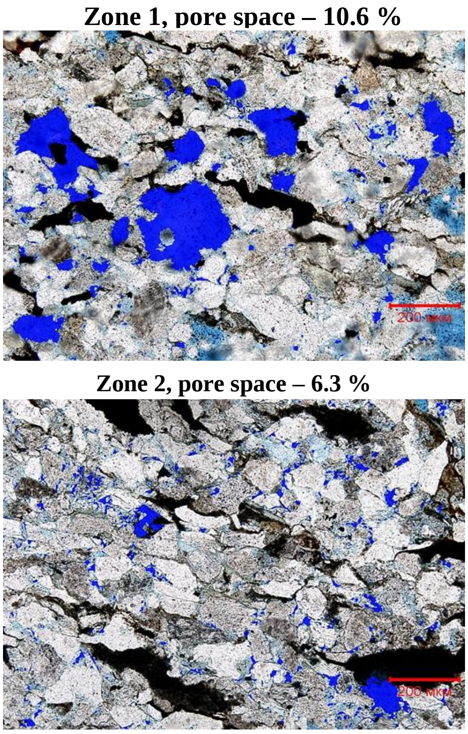

Fig. 9. Calculation of pore space using thin section photographs in transmitted light with "mask overlay"

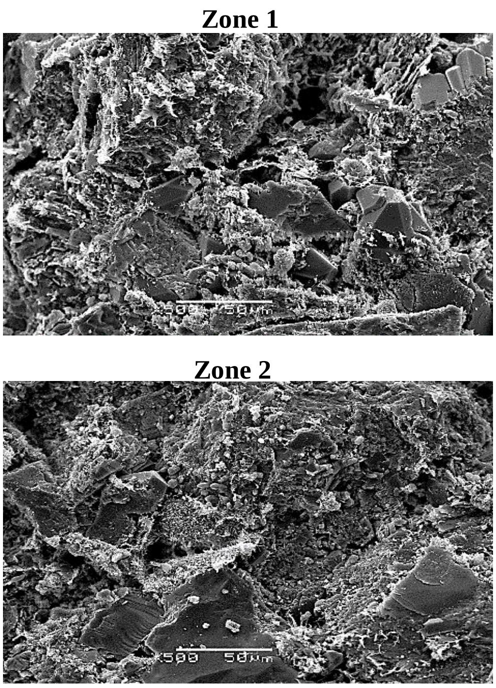

Fig. 10. Electron-scan microscope image photographs General rock texture and the pore space structure features, zooming of 500x

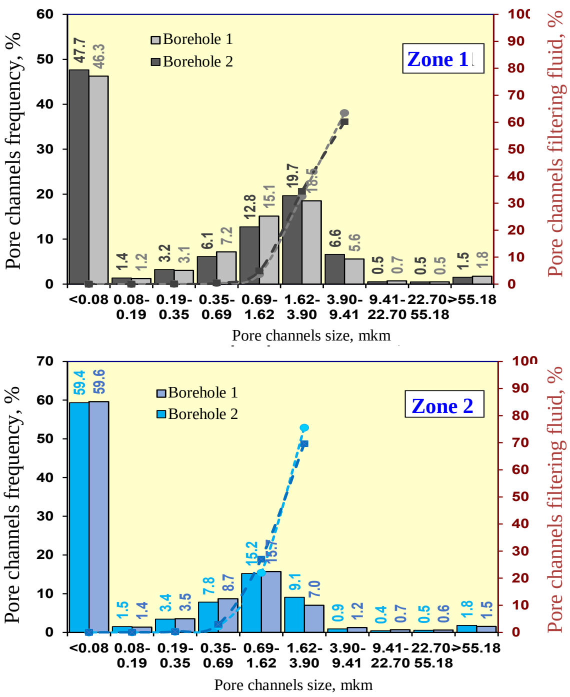

Fig. 11. Distribution of pore channels by size and their participation in oil filtration

In the rocks of zone 2, predominance of inter-grain and inter-microaggregate-grain micropores, more rarely intra-grain micropores, with average size of 8 μm, very few pores with cross-section of up to 20 μm, anisometric and sinuous-slot-shaped, closed and connecting with each other through ultracapillary pore channels is observed.

The study of the pore space structure by centrifugation revealed that in the rocks of zone 1, pore channels from 1.62 to 3.90 μm in size prevail, and the main role in liquid filtration is played by pore channels of size from 3.90 to 9.41 μm, while in the rocks of zone 2, pore channels from 0.69 to 1.62 μm in size predominate, and liquid filtration mainly occurs through pore channels of size from 1.62 to 3.90 μm (Fig. 11).

The analysis of the pore space structural features revealed that the rocks of zone 1 have larger pores and have better filtration channels (pore throats) relative to the rocks of zone 2.

Based on the data on the distribution of the pore channels and their participation in the liquid filtration, the average radii of the pore channels were calculated by the method of statistical moments, and their comparison with the absolute gas permeability was performed (Fig. 12). The statistical moment method is based on the rigorous probabilistic theory of estimating statistical characteristics [16].

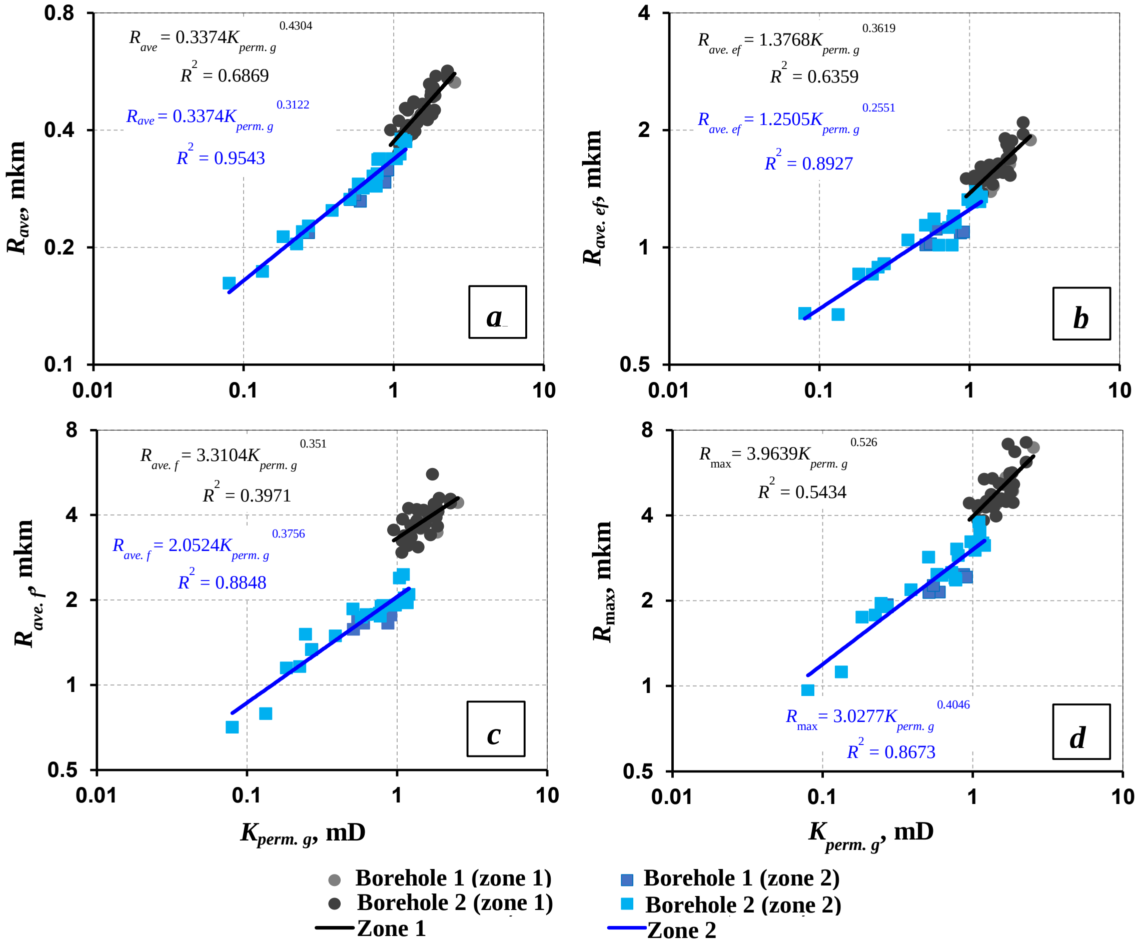

Fig. 12. Average (R_{ave}) (*a*), average effective ($R_{ave.\,ef}$) (*b*), average filtering ($R_{ave.\,f}$) (*c*), and maximum (R_{max}) (*d*) radii of the pore channels versus absolute permeability for gas ($K_{perm.\,g}$)

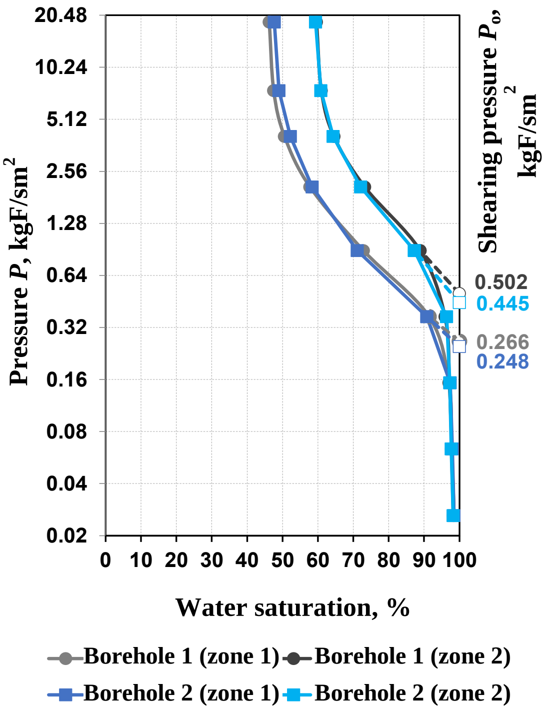

Fig. 13. Graphic determination of shearing pressure (P_o) for selected zones

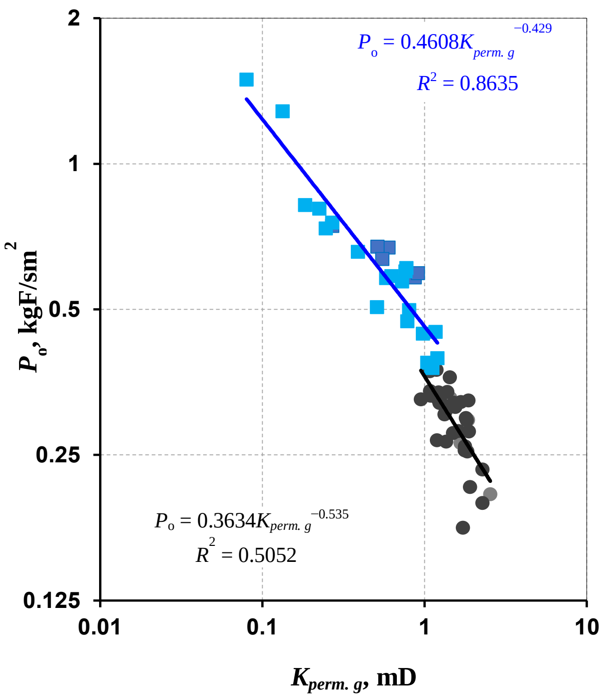

Fig. 14. Shearing pressure (P_o) versus absolute permeability for gas ($K_{perm.\,g}$)

Fig. 15. Pore space filling with carbonate material based on thin section photographs in transmitted light

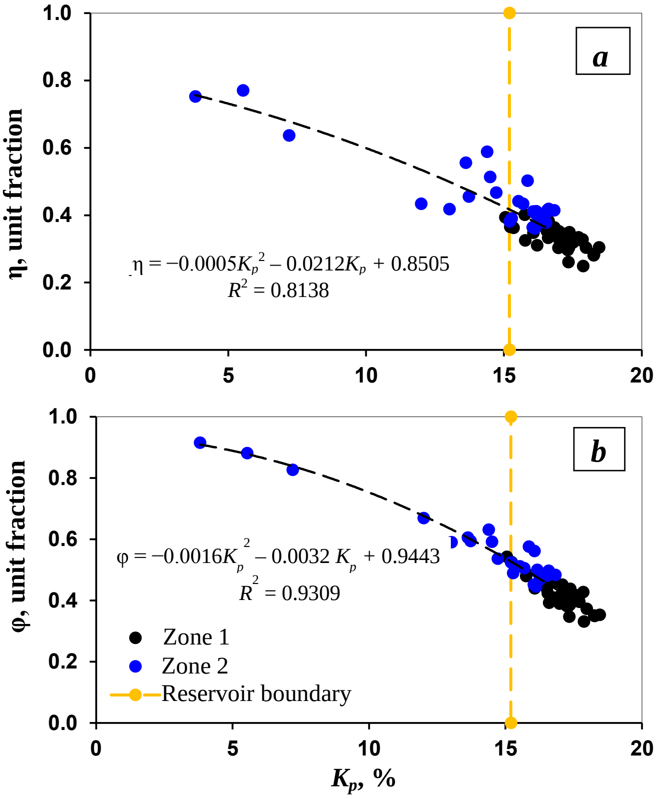

Fig. 16. Relative clay content (η) (*a*) and clay-carbonate content (φ) (*b*) versus open porosity (K_p)

Fig. 12 shows that in the rocks of zone 1, most of the filtration channels connecting the pores to each other has average radius ranging from 2.9 to 5.6 microns, whereas in the rocks of zone 2, from 0.7 to 2.5 microns. The analysis of the pore channel average radii showed that the size of the filtration channels of zone 1 is two times the size of the filtration channels of zone 2.

The pressure at which the liquid displacement begins (shear pressure) for the rocks of zone 1 ranges from 0.177 to 0.375 kgf/cm^2 (the average value is 0.297 kgf/cm^2), and that for the rocks of zone 2, from 0.378 to 1.494 kgf/cm^2 (0.641 kgf/cm^2) (Fig. 13, 14). At the pressure levels below the shear pressure, liquid displacement will not occur, and, as a result, oil will not displace water.

The analysis of the material composition showed that the content of clay and carbonate material in the pore space of the rocks has a fundamental effect on the size of the filtration channels (Fig. 15).

The clay volume K_{clay} and the carbonate volume K_{carb} values vary within the following ranges: for the rocks of zone 1, K_{clay} ranges from 6.1 to 10.5 % (the average value is 8.5 %) and K_{carb} ranges from 2.0 to 8.9 % (4,1 %); and for the rocks of zone 2, K_{clay} ranges from 9.1 to 20.5 % (12.1 %) and K_{carb}, from 3.3 to 31.1 % (8.4 %).

For the purpose of determining the degree of filling the rock pore space with clay and carbonate material, we calculated the relative clay content η and clay-carbonate content φ and compared them with the open porosity K_p (Fig. 16). The degree of filling the pore space with clay and carbonate material for the rocks of zone 1 ranges within 35–54 % (42 % on average), and that for the rocks of zone 2, 45–92 % (57 %).

Fig. 16 shows that in the rocks of zone 1, the degree of filling of the pore space with clay and carbonate material is much less than that in the rocks of zone 2.

Conclusion

Based on the implemented analysis, we conclude that the uneven hydrocarbon saturation of the AC10 formation is due to the microheterogeneity of these rocks.

The sediments of the AC10 formation correspond to the littoral facies complex, whose origination conditions determine wide variability of the lithological and mineralogical composition and textural-and-structural features, that led to the microheterogeneity of these rocks.

The high content of clay and carbonate material in the pore space of the rocks of the AC10 formation produced fundamental effect on the size of the filtration channels and, as a result, determined the uneven hydrocarbon saturation.

Since the geophysical well logging data are aimed at studying macroheterogeneity, the filler composition, its amount in the pore space, and the (core) hydrocarbon saturation collectively evened the AC10 formation electrical resistance in different saturation zones that led to distortion of the hydrocarbon saturation of the reservoir as a whole.

To increase the confidence of hydrocarbon saturation estimation for the AC10 formation rocks, the lithological-petrophysical and geophysical data should be applied in combination. It is necessary to formulate the systematic approach to solving such problems.

References

1. Azamatov V. I. Investigation in estimation of oil reserves of large fields for the design of their development: Dr.Sci. geol.-min. thesis, 1975, Moscow, MINKhiGP, 38 p. (In Russ.)

2. Borisov Yu. P. Taking into account the formation heterogeneity in the design of oil reservoir development:

Proceedings of the VNII, vol. XXI, State Technical Publishing House, 1959, pp. 245-260. (In Russ.)

3. Borisov Yu. P., Voinov V. V., Ryabinina Z. K. The effect of formation heterogeneity on oil field development : Moscow, Nedra Press, 1970, 288 p. (In Russ.)

4. Borisov Yu. P., Ryabinina Z. K., Voinov V. V. Features of the design of oil field development taking into account their heterogeneity: Moscow, Nedra Press, 1976, 285 p. (In Russ.)

5. Vlasenko V. V. Improving the method of estimating formation geological heterogeneity for exploration and development of oil fields (as exemplified in oil fields of the Ural-Volga and Western Siberia oil fields): 1974, PhD. geol.-min. thesis, Moscow, VNII, 14 p. (In Russ.)

6. Dementiev L. F. On the concept of "geological heterogeneity" of productive strata and methods of its study: Proceedings of the Perm branch of Giprovostokneft, vol. 1, Moscow, Nedra Press, 1965, pp. 3-10. (In Russ.)

7. Zheltov Yu. V., Kuznetsov A. V. Heterogeneity of oil-bearing formations and tasks for its study: In the book: Physical and geological factors in development of oil and gas condensate fields, Moscow, Nedra Press, 1969, pp. 7-12. (In Russ.)

8. Zhdanov M. A., Ovanesov M. G., Tokarev M. A. Multifaceted consideration of geological heterogeneity in the analysis of oil recovery: Geology of oil and gas, No. 3, 1974, pp. 19-23. (In Russ.)

9. Melik-Pashayev V. S., Klimushin I. M., Breev V. A., *et al.* Study of geological heterogeneity of oil fields for their development: Proceedings of VNII, v. LIX, 1974, pp. 3-12. (In Russ.)

10. Kovalev A. G., Vashurkin A. I. On heterogeneity of oil-containing reservoirs: Proceedings of VNII, v. 44-196, pp. 13-22. (In Russ.)

11. Krasheninnikov G. F., Volkova A. N., Ivanova N. V. Doctrine of facies with the basics of lithology: Moscow State University, 1988, 215 p. (In Russ.)

12. Kuznetsov V. G. Sedimentary rocks and their study: Manual for graduate students, Moscow, Nedra-Business Center LLC, 2007, 511 p. (In Russ.)

13. Petkevich G. I. Informativeness of acoustic characteristics of heterogeneous geological environments: Kiev: Naukova Dumka Press, 1976, 213 p. (In Russ.)

14. Ratnikov I. B, Korytov V. S. Determination of lithologic and petrophysical parameters of heterogeneous rocks by the method of core micro-profiling: Challenges of petrophysics and quantitative interpretation of logging data (Proceedings of the review competition in memory of Mikhail Mikhailovich Ellansky and memories of him), Moscow, CJSC Pangea, 2007, pp. 52-59. (In Russ.)

15. Ratnikov I. B, Shulga R. S., Romanov, E. A., Bastrikov S. N., 2016, Analysis of porosity parameter with the involvement of elements of regional petrophysics (electrofacies) and clay content type: Mining sciences and technologies, No. 2, pp. 50-65. (In Russ.)

16. Ratnikov I. B., Shulga R. S., Romanov E. A. Interpretation of capillar study data: Mining sciences and technologies No. 4, 2016, pp. 24-39. (In Russ.)

17. Rozhkov G. F., Geological interpretation of grain-size parameters based on data of fractional sieve analysis: Grain-size analysis in geology. Moscow, 1978, pp. 5-25. (In Russ.)

18. Semenov V. V., Moreva E. V., Ratnikov I. B. Study of structural and textural heterogeneities in core by the method of non-destructive testing (micro-profiling) for increasing reliability of borehole logging data interpretation: Ways of realization of the oil and gas potential of the Khanty-Mansi Autonomous Okrug, IX Scientific-Practical Conference, Khanty-Mansiysk, NaukaServis Publishing House, 2006, v. 2, pp. 235-242. (In Russ.)

19. Semenov V. V., Moreva E. V., Ratnikov I. B. Study of heterogeneous reservoirs based on the core by micro-profiling method: Geophysics, 2006, No. 2, pp. 48-52. (In Russ.)

20. Semenov V. V., Ratnikov I. B., Sokova K. I. New technologies for experimental study of complex structure reservoirs: Actual issues of petrophysics of complex structure reservoirs, Edited by Dr. Sci. in Geology and Mineralogy Shnurman, I.G., Krasnodar: Prosveshchenie-Yug Press, 2010, pp. 110-170. (In Russ.)

21. Stasenkov V. V., Klimushin I. M., Breev V. A. Methods for studying geological heterogeneity of oil measures: Moscow, Nedra Press, 1972, 168 p. (In Russ.)

22. Frolov E. F., Bykov N. E., Egorov R. A., Fursov A. Ya. Optimization of oil-field exploration: Moscow, Nedra Press, 1976, 303 p. (In Russ.)

23. Frolov E. F., Egorov R. A., Fursov A. Ya., 1972, On methods for assessing reliability of parameters of oil and gas accumulations: Geology of oil and gas, No. 3, pp. 31-36. (in Russ.)

24. Fo1k R. L., Ward W. C. Brazos River bar: a study in the significance of grain size parameters // J. Sediment. Petrol, 1957, Vol. 27, No. 1, pp. 3-27. (In Russ.)

25. Passega R., Byramjee R. Grain size image of clastic deposits // Sedimentology, 1969, Vol. 13, N 3/4, pp. 233-252.

26. Saner S., Kissami M., Al Nufaili S. Estimation of Permeability From Well Logs Using Resistivity and Saturation Data // SPEFE, March 1997, 27 p.

27. Timur A. An Investigation of Permeability, Porosity, and Residual Water Saturation Relationships for Sandstone Reservoirs // The Log Analyst, 1968, Vol. 9, No. 4, pp. 8-17.

28. Xue G. Optimal Transformations for Multiple Regression: Application to Permeability Estimation from Well Logs // SPEFE, June 1997, 85 p.

Библиографический список

1. Азаматов В. И. Исследование вопросов оценки запасов нефти крупных месторождений в связи с проектированием их разработки. Автореф. дис. … д-ра геол.-минерал. наук. М., МИНХиГП, 1975. 38 с.

2. Борисов Ю. П. Учет неоднородности пласта при проектировании разработки нефтяной залежи // Труды ВНИИ, вып. XXI, Госпотехиздат, 1959. С. 245–260.

3. Борисов Ю. П., Воинов В. В., Рябинина З. К. Влияние неоднородности пластов на разработку нефтяных месторождений. М.: Недра, 1970. 288 с.

4. Борисов Ю. П., Рябинина З. К., Воинов В. В. Особенности проектирования разработки нефтяных месторождений с учетом их неоднородности. М.: Недра, 1976. 285 с.

5. Власенко В. В. Совершенствование методики оценки геологической неоднородности пластов при разведке и разработке нефтяных месторождений (на примере нефтяных месторождений залежей Урало-Поволжья и Западной Сибири). Автореф. дис. … канд. геол.-минерал. наук. М., ВНИИ,1974. 14 с.

6. Дементьев Л. Ф. О понятии «геологическая неоднородность» продуктивных пластов и методах ее изучения // Труды Пермского филиала Гипровостокнефти, вып. 1. М.: Недра, 1965. С. 3–10.

7. Желтов Ю. В., Кузнецов А. В. Неоднородность нефтеносных горизонтов и задачи по ее изучению. В кн.: Физико-геологические факторы при разработке нефтяных и нефтегазоконденсатных месторождений. М.: Недра, 1969. С. 7–12.

8. Жданов М. А., Ованесов М. Г., Токарев М. А. Комплексный учет геологической неоднородности при анализе выработки нефтеотдачи // Геология нефти и газа. 1974 . № 3. С. 19-23.

9. Мелик-Пашаев В. С., Климушин И. М., Бреев В. А. и др. Изучение геологической неоднородности нефтяных залежей в связи с их разработкой // Труды ВНИИ. 1974. Вып. LIX . С. 3–12.

10. Ковалев А. Г., Вашуркин. А. И. О неоднородности нефтесодержащих коллекторов // Труды ВНИИ. Вып. 44, 196. С. 13–22.

11. Крашенинников Г. Ф., Волкова А. Н., Иванова Н. В. Учение о фациях с основами литологии. Издательство московского университета, 1988. 215 с.

12. Кузнецов В. Г. Литология. Осадочные горные породы и их изучение: Учеб. пособие для вузов. – М.: ООО «Недра-Бизнесцентр», 2007. 511 с.

13. Петкевич Г. И. Информативность акустических характеристик неоднородных геологических сред. Киев: Наукова думка, 1976. 213 с.

14. Ратников И. Б., Корытов В. С. Определение литолого-петрофизических параметров неоднородных пород методом микропрофилирования керна // Вопросы петрофизики и количественной интерпретации данных каротажа (материалы смотра-конкурса памяти Михаила Михайловича Элланского и воспоминания о нем). М.: ЗАО «Пангея», 2007. С. 52–59.

15. Ратников И. Б., Шульга Р. С., Романов Е. А., Бастриков С. Н. Анализ параметра пористости с привлечением элементов региональной петрофизики (электрофаций) и типа глинистости // Горные науки и технологии. 2016. № 2. С. 50–65.

16. Ратников И. Б., Шульга Р. С., Романов Е. А. Интерпретация данных капиллярных исследований // Горные науки и технологии. 2016 . № 4. С. 24–39.

17. Рожков Г. Ф. Геологическая интерпретация гранулометрических параметров по данным дробного ситового анализа // Гранулометрический анализ в геологии. М.: 1978. С. 5–25.

18. Семенов В. В., Морева Е. В., Ратников И. Б. Изучение структурно-текстурных неоднородностей на керне методом неразрушающего контроля (микропрофилирования) с целью повышения достоверности результатов интерпретации ГИС // Пути реализации нефтегазового потенциала ХМАО. IX науч.-практ. конф. Ханты-Мансийск: Изд-во «ИздатНаукаСервис», 2006. Т. 2. С. 235–242.

19. Семенов В.В., Морева Е.В., Ратников И.Б. Изучение неоднородных коллекторов на керне методом микропрофилирования // Геофизика. 2006. № 2. С. 48–52.

20. Семенов В. В., Ратников И. Б., Сокова К. И. Новые технологии экспериментального изучения сложнопостроенных коллекторов // Актуальные вопросы петрофизики сложнопостроенных коллекторов / Под ред. д-ра геол.-минерал. наук И.Г. Шнурмана. Краснодар: Просвещение-Юг. 2010. С. 110–170.

21. Стасенков В. В., Климушин И. М., Бреев В. А. Методы изучения геологической неоднородности нефтяных пластов. М.: Недра, 1972. 168 с.

22. Фролов Е. Ф., Быков Н. Е., Егоров Р. А., Фурсов А. Я. Оптимизация разведки нефтяных месторождений. М.: Недра, 1976. 303 с.

23. Фролов Е. Ф., Егоров Р. А., Фурсов А. Я. О методах оценки степени достоверности параметров залежей нефти и газа // Геология нефти и газа. 1972. № 3. С. 31–36.

24. Fo1k R. L., Ward W. C. Brazos River bar: a study in the significance of grain size parameters // J. Sediment. Petrol, 1957, Vol. 27, N 1, p. 3-27.

25. Passega R., Byramjee R. Grain size image of clastic deposits // Sedimentology, 1969, Vol. 13, N 3/4, pp. 233-252.

26. Saner S., Kissami M., Al Nufaili S. Estimation of Permeability From Well Logs Using Resistivity and Saturation Data // SPEFE, March 1997, 27 p.

27. Timur A. An Investigation of Permeability, Porosity, and Residual Water Saturation Relationships for Sandstone Reservoirs // The Log Analyst, 1968, Vol. 9, No. 4, pp. 8-17.

28. Xue G. Optimal Transformations for Multiple Regression: Application to Permeability Estimation from Well Logs // SPEFE, June 1997, 85 p.

ORIGINAL PAPERS

DOI: 10.17073/2500-0632-2019-1-57-64

Analysis of Possible Origination of Domes in Longwalls

R. I. Imranov, E. N. Khmyrova, O. G. Besimbayeva, S. P. Olenyuk, A. Z. Kapasova

Karaganda State Technical University, Karaganda, Kazakhstan, ✉hmyrovae@mail.ru

Abstract: The research is aimed at solving problems of assessing underground working stability in complicated mining and geological conditions to increase reliability and safety of mining operations. Analysis of geomechanical processes occurring in a rock mass during extraction of coal seams to determine the stability of mining block roof is the most important task. The performed digital modeling of the rock mass based on the structural logs for K1 seam and the nearest borehole log enabled highly detailed identifying the types of rocks occurred in the seam roof and their strength characteristics, compressive stresses. To determine the stability of a mining block roof, the factor of safety of the rocks was used, which was determined by modeling method using Phase 28.0 and Rockscince software. The carbonaceous argillite parting 0.09–0.12 m thick was taken as the contact of the longwall with the seam roof, and, for completeness of the analysis, the upper high-ash coal member in the seam roof up to 0.7 m thick was used. The modeling findings, presented in the graph of dependence between the safety factor and the distance between the belt heading and air drift, showed that the probability of dome formation in the longwall is high, as the factor of safety of the rocks is less than unity, that indicates the roof instability in the course of the coal seam block extraction. The modeling methods allowed assessing the mine working stability, based on which the measures to improve the reliability and safety of mining operations can be timely developed, and due technical and technological solutions shall be reached.

Keywords: longwall, seam, rock mechanical and gas-dynamic process, stress, strain, stability, modeling, factor of safety.

For citation: Imranov R. I., Khmyrova E. N., Besimbayeva O. G., Olenyuk S. P., Kapasova A. Z. Analysis of possible origination of domes in longwalls. *Mining Science and Technology*. 2019;4(1):57-64. (In Russ.). DOI: 10.17073/2500-0632-2019-1-57-64.

Анализ возможного возникновения куполов в лаве

Имранов Р. А., Хмырова Е. Н., Бесимбаева О. Г., Оленюк С. П., Капасова А. З.

Карагандинский государственный технический университет, Караганда, Казахстан, ✉hmyrovae@mail.ru

Аннотация: Исследования направлены на решение задач по оценке устойчивости горных выработок при подземной разработке в сложных горно-геологических условиях, повышающих надежность и безопасность проведения горных работ. Исследование геомеханических процессов, происходящих в горном массиве при отработке угольных пластов, с целью определения устойчивости кровли выемочного блока является важнейшей задачей. Выполнено цифровое моделирование массива горных пород по структурным колонкам пласта К1 и ближайшей скважине, которое позволило с высокой детальностью определить типы пород, залегающих в кровле пласта, и их прочностные характеристики, напряжения на сжатие. Для определения устойчивости кровли выемочного блока был использован показатель коэффициента запаса прочности пород, который определялся методом моделирования с использованием программного обеспечения Phase 28.0 и Rockscince. Контактом комплекса лавы с кровлей пласта был принят прослой углистого аргиллита мощностью 0,09–0,12 м, и для полноты анализа использовалась верхняя высокозольная пачка угля в кровле пласта мощностью до 0,7 м. Результаты моделирования, отраженные на графике изменения коэффициента запаса прочности в зависимости от расстояния между конвейерным и вентиляционными штреками, показывают, что вероятность образования куполов в лаве велика, так как коэффициент запаса прочности пород менее единицы, что указывает на неустойчивость кровли при отработке выемочного участка угольного пласта. Методами моделирования показана возможность произвести оценку устойчивости горных выработок, на основании которой своевременно разработать мероприятия, повышающие надежность и безопасность проведения горных работ, и принять правильные технические и технологические решения.

Ключевые слова: лава, пласт, геомеханический и газодинамический процесс, напряжение, деформация, устойчивость, моделирование, коэффициент запаса прочности.

Для цитирования: Имранов Р. А., Хмырова Е. Н., Бесимбаева О. Г., Оленюк С. П., Капасова А. З. Анализ возможного возникновения куполов в лаве. *Горные науки и технологии.* 2019;4(1):57-64. DOI: 10.17073/2500-0632-2019-1-57-64.

Introduction

Underground coal mining is almost always accompanied by difficult mining, geological, and geotechnical conditions, therefore, an urgent issue is studying rock mechanical and gas-dynamic processes occurring in underground workings. Determining the level of maximum effective stresses around mine workings is one of the most important tasks of rock mechanics [3, 4]. Analysis of the simulation results, taking into account the safety factor of the rocks, allows selecting the optimal parameters for the deposit mining, the opening scheme and horizon development work.

The study of the effect of rock pressure on the rock mass and powered support during extraction of a mining block of the longwall allows to determine the change in the condition of the seam roof rocks from compression to tension, which may lead to gradual caving the rock from the roof up to a sudden bulk collapse and the formation of domes.

The research tasks and objectives

The idea of the research is to study a combination of various factors: the structure and properties of a coal-rock mass, a combination of geological and mining conditions, the level of existing stresses in the rock mass, and the technological parameters of the mining block extraction [5].

In this regard, the development of methods for the integrated management of rock mechanical and gas-dynamic processes in coal mines is an urgent scientific and practical task.

The obtained scientific and practical results of the studies performed by the authors can be used as the basis for the integrated management of rock mechanical and gas-dynamic processes in mines [6–10].

Most studies are based on solving the elastic rock mechanical problem, and the resulting stresses and strains are compared with the maximum allowable for the near-outline rock mass. When solving rock mechanical problems, one of the main issues is the determination of reliable calculated values of the strength properties of a rock mass.

The research methods

By the level of stresses existing in a rock mass, it is possible to assess the stability of mine workings and determine the rock safety factor.

Cross section of permanent mine workings in the course of their drifting may change due to the influence of the stresses occurring in the surrounding rocks [11–13]. Instability of the workings is caused by high vertical stress. However, in practice, there are cases when horizontal stresses significantly exceed vertical ones that may lead to deformation of the roof and bottom rocks. The bottom deformation is manifested by bulging only, which may go practically unnoticed.

The existence of tensile stresses does not always cause failure of the rock mass in the area. The rocks themselves can to some extent resist tension, and even in case of some displacements, the rock mass retain some stability (the so-called residual rock strength) [3, 17].

Deformation of the roof rock (Fig. 1) may be accompanied by intensive rock failure, initially in the form of flaws, and then with the transition to collapses. The transition to collapses is connected with decreasing the bearing area when approaching the crest part of the roof.

It should be noted that with the dynamic manifestation of instability in the form of gradual phased roof rock collapse, a sudden bulk collapse may happen.

In the areas where vertical and lateral stresses σ_v and σ_l can simultaneously affect the formation of the cross-sectional shape of a working, the physics of the deformation process is fully determined by the physico-mechanical properties of the rocks.

Therefore, both the level of effective stresses and the properties of rocks, in each case, are individual in nature.

The research subject is K1 coal seam being extracted by 46 K1 longwall. Extraction of a mining block leads to changing rock pressure on rock mass and powered support. This in turn causes periodic changing the rock condition from compression to tension, inducing changing the size and number of hanging rock members in the seam roof, participating in producing abutment pressure [1, 4, 18, 19].

To determine the longwall roof stability (Fig. 1), digital simulation of the rock mass [20] was performed based on the structural logs for K1 seam (Fig. 2) and Borehole No. 11355.

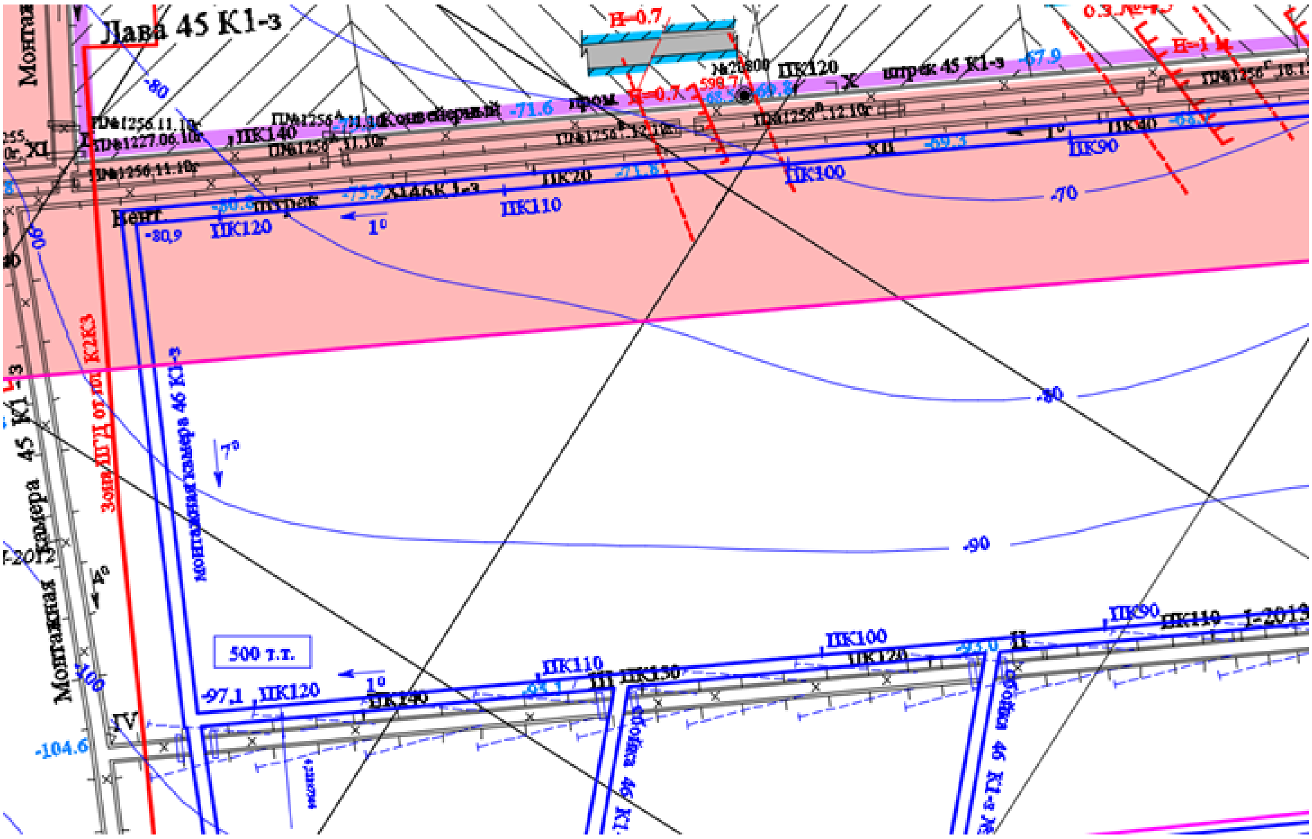

Fig. 1. Longwall 46 K1 mining plan

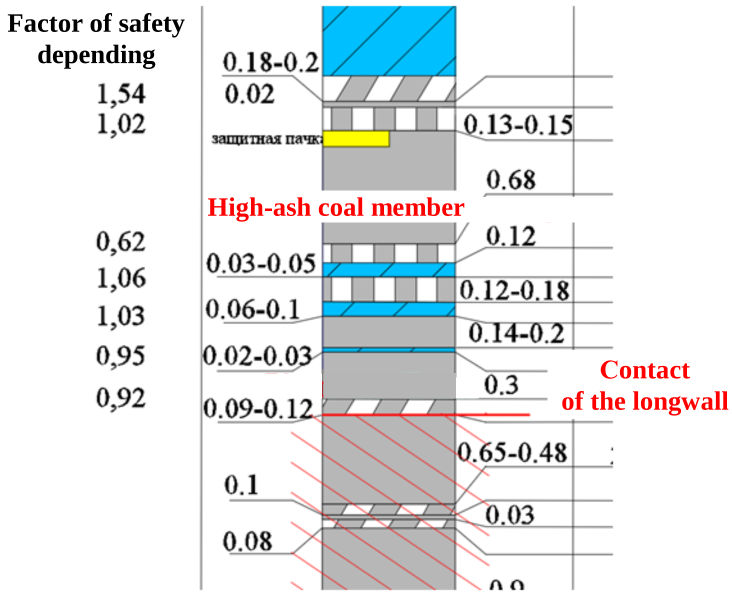

Fig. 2. K1 seam structural log

K1 seam consists of 6–7 standard and two high-ash coal members in the seam top (compressive stress σ_{comp} of 11–12 MPa). The seam top is represented by medium-grained mudstone up to 20.5 m thick (compressive stress σ_{comp} of 22–25 MPa). In the immediate top of the seam, in depth interval 1.2–1.8 m, K1´ stratum up to 0.2 m thick occurs. Sandstone and siltstone with compressive stress σ_{comp} of 35–59 MPa lie in the seam bottom.

To determine the stability of the roof of the extraction pillar, the rock safety factor values were used. The carbonaceous argillite parting 0.09–0.12 m thick was taken as the contact of the longwall with the seam roof (Fig. 2), and, for completeness of the analysis, the upper high-ash coal member in the seam roof up to 0.7 m thick was used.

Findings

Based on the study findings, we can conclude that the seam roof at contact with the carbonaceous argillite parting in the longwall is unstable and easily collapsed. The safety factor value at the contact of the longwall and the carbonaceous mudstone (Fig. 3) is 0.92 on average in the longwall.

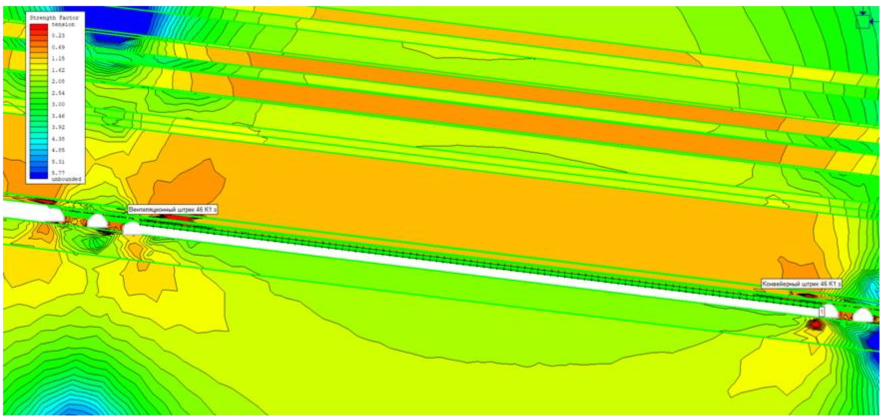

Fig. 3. Factor of safety of the modeled rock mass

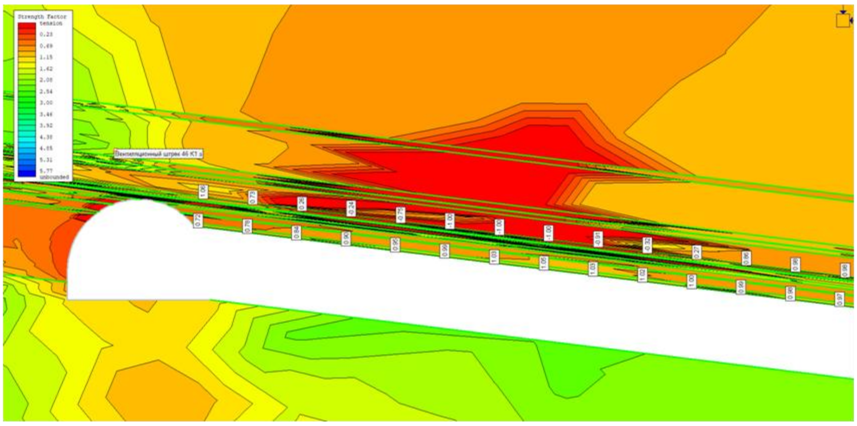

Fig. 4. Factor of safety of the air heading

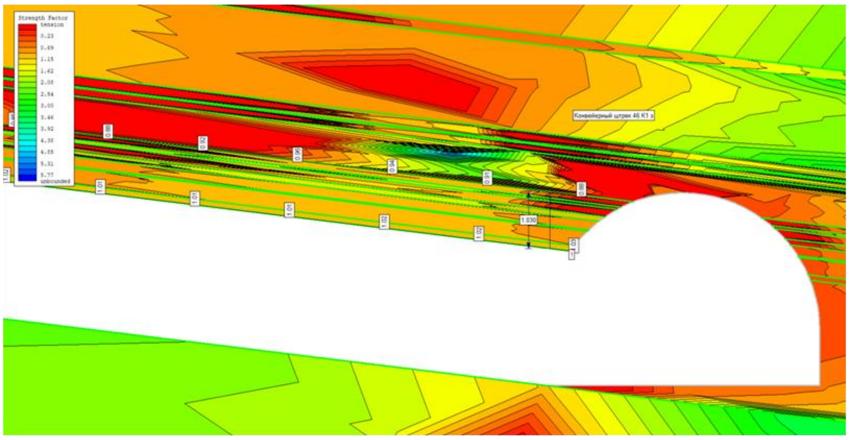

Fig. 5. Factor of safety of the belt heading

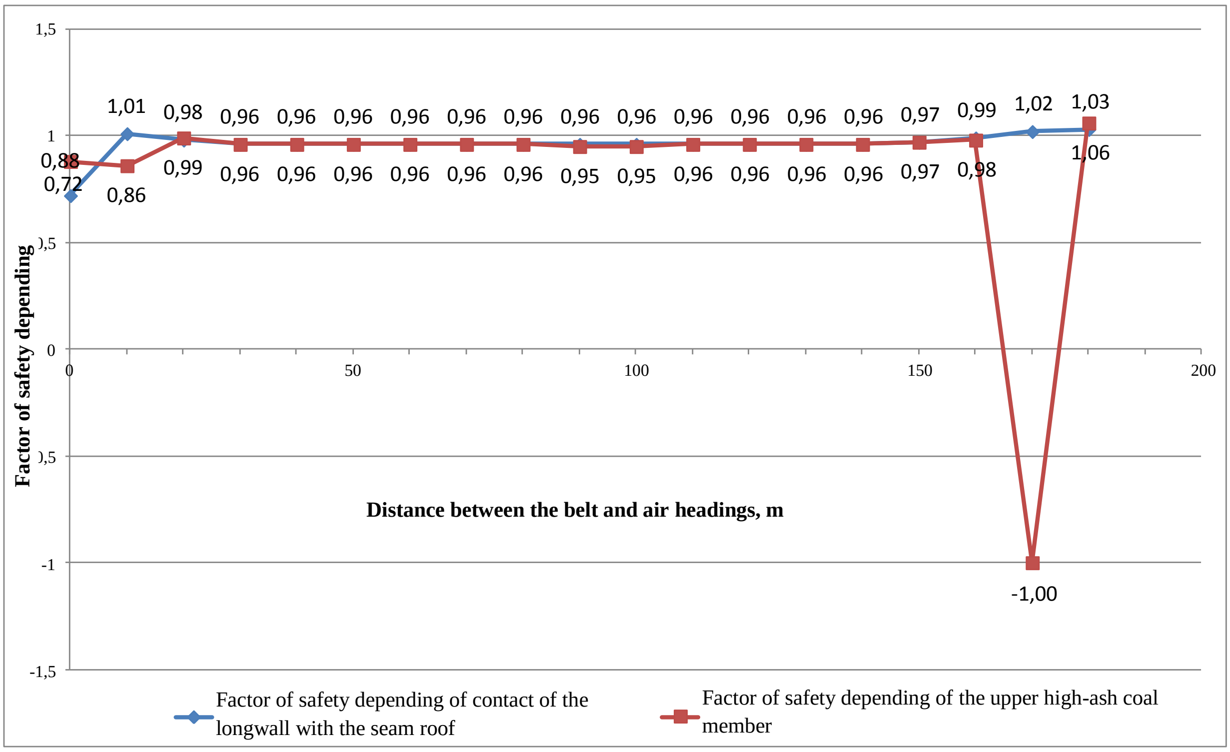

Fig.6. The change in factor of safety depending on the distance between the belt and air headings

The safety factor of the upper high-ash coal member is less than unity and in some places becomes negative in a section 25 m long from the air heading towards the extraction block (Fig. 4). Such value of the safety factor is an indicator that the roof rocks during mining of the extraction block in this place will collapse [21–23]. A possible reason for this is that this block is located in the OGD zone of the overlying extraction block mining.

Conclusion

The modeling findings, presented in the graph of dependence between the safety factor and the distance between the belt heading and air heading, obviously demonstrate that the probability of dome formation in the extraction block roof is high, as the factor of safety of the rocks is less than unity, that indicates the longwall roof instability in the course of the coal seam extraction (Fig. 6).

Based on the findings of the performed studies of rock mechanical processes occurring in the rock mass during extraction block mining, the right decisions can be made on further coal seam mining [24]. Knowing the forecasting data for a coal seam section mining will allow predetermining the most dangerous places, namely the roof collapse points, at the design stage.

The implemented studies with the determination of the safety factor allow predicting the likelihood of domes formation in the extraction block roof and developing measures to ensure safe coal seam mining conditions, as well as preventing potential future emergencies [24, 25].

References

1. Chernyak I. L., Zaidenvarg V. E. Frequency of changes in stress-strain state of coal and rock masses at the front of production face: Mining Journal, News of Higher Educational Institutions, 1993, No. 3, pp. 25-28. (in Russ.)

2. Report on the findings of Research No. 304 185 16 Kazakhstan: DMT GmbH & Co. KG, Essen, 2016. (in Russ.)

3. Filimonov K. A. Research of the stress condition of undermined rock mass: Vestn,Kuz,GTU, 2003, No. 5, pp. 22-25. (in Russ.)

4. Polevshchikov G. Ya., "Deformation-wave" processes in rock mass when stoping face moving in coal seams: Polevshchikov G. Ya, FTPRPI, 2013, No. 5, pp. 50-60. (in Russ.)

5. Dolgonosov V. N., Pak G. A., Drizhd N. A., Aliev S. B., Nizametdinov F. K. Geomechanical and gas-dynamic processes in coal mines: Karaganda, Publishing House of KarGTU, 2012, 214 p. (in Russ.)

6. Polevshchikov G. Ya., *et al.* Fractal feature of rock mass structuring when changing pressure on near-face part of coal seam extracted by longwall face: Bulletin of Scientific Center for Safety in Coal Industry,Scientific and technical journal, Kemerovo, 2013, No. 1-1, pp. 16-23. (in Russ.)

8. Scott M., Mazumder S., Jiang J. Permeability Increase in Bowen Basin Coal as a Result of Matrix Shrinkage during Primary Depletion, SPE International SPE 158152, 2012, vol. 1, pp. 323–343.

9. Pan Z., Connell L. D., Modeling Permeability for Coal Reservoirs: A Review of Analytical Models and Testing Data, Int. J. Coal Geol., 2012, 92, pp. 1–44.

10. Nazarova L. A., Nazarov L. A., Karchesvky A. L., Vandamme M. Determining Kinetic Parameters of a Block Coal Bed Gas by Solving Inverse Problem Based on Data of Borehole Gas Measurements, J. Min. Sci., 2015, vol. 51, no. 4, pp. 666–672.

11. Eremenko A. A., Seryakov V. M., Gakhova L. R. Geomechanical substantiation of the parameters and methods for creating a damping layer in the vicinity of a mine roadway to reduce rock pressure: FTPRPI, 2014, No. 4, pp. 61–70. (in Russ.)

12. Pinkun Guo, Yuanping Cheng. Permeability Prediction in Deep Coal Seam: A Case Study on No. 3 Coal Seam of the Southern Qinshui Basin in China, The Scientific World Journal, 2013, vol. 2013.

13. Seidle J., Jeansonne M., Erickson D. Application of Matchstick Geometry to Stress Dependent Permeability in Coals, SPE Rocky Mountain Regional Meeting, Society of Petroleum Engineers, 1992.

14. Fedorov A. V., Fedorchenko I. A., Leont'ev I. V. Mathematical modeling of two problems of wave dynamics in heterogeneous media, Shock Waves Journ., 2006, Vol. 15, No. 8.

15. Oparin V. N., Tanaino A. S., Yushkin V. F. Discrete properties of entities of a geomedium and their canonical representation. Journal of Mining Science, 2007, No. 3.

16. Wang X., Pan Y., Zhang Z., A Spatial Strain Localization Mechanism of Zonal Disintegration through Numerical Simulation, J. Min. Sci., 2013, vol. 49, no. 3, pp. 357–367.

17. Reuter M. Waveform distribution of rock pressure along longwall face: Reuter, M., Kurfüst, V., Mayrhover, K., Wexler, Ju.: FTPRPI, 2009, No. 2, p. 38-44.

18. Kozyreva E. N., Shinkevich M. V. Structuring rock mass in the conditions of extracting coal seam by longwalls: Industrial Safety and Geotechnics, Kuzbass. Collected papers "Education, science, innovation", 2014, No.1. (in Russ.)

19. Kozyreva E. N. Features of gas-geomechanical processes at a mine extraction district: Kozyreva, E.N., Shinkevich, M.V.: Bulletin of Scientific Center for Safety in Coal Industry, Kemerovo, 2010, No. 2, p. 28-35.

20. Leontyeva Ye,V. Evaluation of the possibilities of computer simulation of a geomechanical process in a hosting rock mass [Electronic resource]: Kemerovo. Innovative Convention. (in Russ.)

21. Zakharov V. N., Malinnikova O. N., Trofimov V. A., Filippov Yu. A. The dependence of coal seam permeability on gas content and effective stresses: Physical and technical issues of mining, 2016, No.2, pp. 16-26. (in Russ.)

22. Pak G. A., Drizhd N. A., Dolgonosov V. N. Method of main roof caving step calculation and forecast of gas release in the mines of Karaganda basin: Labor Safety in Industry, 2010, No. 10, pp. 31-34. (in Russ.)

23. Shpakov P. S., Pak G. A., Dolgonosov V. N. Interrelation of main roof caving steps and gas release intensity in Sokurskaya and Saranskaya mines of Karaganda basin: Mine surveying and subsoil use, 2009, No. 6, pp. 70-72. (in Russ.)

24. Instructions for safe extraction of dangerous (in coal-and-gas outburst) seams: Ministry of Energy and Coal Industry of Kazakhstan, 1995, 92 p. (in Russ.)

25. Rules for protection of structures and natural objects from harmful effects of underground coal mining: Moscow, Nedra Press, 1981, 288 p. (in Russ.)

Библиографический список

1. Черняк И. Л. Периодичность изменения напряжённо-деформированного состояния массивов угля и пород впереди очистного забоя / И. Л. Черняк, В. Е. Зайденварг // Горный журнал. Изв. высших учебных заведений. 1993. № 3. С. 25−28.

2. Отчет о результатах исследования № 304 185 16 Казахстанская ДМТ ГмбХ энд Ко. КГ, Эссен. 2016 г.

3. Филимонов К. А. Исследование напряженного состояния подрабатываемого массива // Вестник Куз-ГТУ. 2003. № 5. С. 22-25.

4. Полевщиков Г. Я. Деформационно-волновые» процессы в массиве горных пород при движении очистного забоя в угольных пластах / Г. Я Полевщиков // ФТПРПИ. 2013. № 5. С. 50–60.

5. Долгоносов В.Н., Пак Г.А., Дрижд Н.А., Алиев С.Б., Низаметдинов Ф.К. Геомеханические и газодинамические процессы в угольных шахтах. Караганда: Изд-во КарГТУ, 2012. 214 с.

6. Полевщиков Г. Я. и др. Фрактальная особенность структуризации массива горных пород в изменениях давления на призабойную часть отрабатываемого длинным очистным забоем угольного пласта // Вестник научного центра по безопасности работ в угольной промышленности. Научно-технический журнал. Кемерово. 2013. Вып. 1-1. С. 16–23.

8. Scott M., Mazumder S., Jiang J. Permeability Increase in Bowen Basin Coal as a Result of Matrix Shrinkage during Primary Depletion, SPE International SPE 158152, 2012, vol. 1, pp. 323–343.

9. Pan Z., Connell L. D., Modeling Permeability for Coal Reservoirs: A Review of Analytical Models and Testing Data, Int. J. Coal Geol., 2012, 92, pp. 1–44.

10. Nazarova L. A., Nazarov L. A., Karchesvky A. L., Vandamme M. Determining Kinetic Parameters of a Block Coal Bed Gas by Solving Inverse Problem Based on Data of Borehole Gas Measurements, J. Min. Sci., 2015, vol. 51, no. 4, pp. 666–672.

11. Еременко А. А., Серяков В. М., Гахова Л. Р. Геомеханическое обоснование параметров и способа создания демпферного слоя в окрестности выработки для снижения уровня горного давления // ФТПРПИ. – 2014. № 4. С. 61–70.

12. Pinkun Guo, Yuanping Cheng. Permeability Prediction in Deep Coal Seam: A Case Study on No. 3 Coal Seam of the Southern Qinshui Basin in China, The Scientific World Journal, 2013, vol. 2013.

13. Seidle J., Jeansonne M., Erickson D. Application of Matchstick Geometry to Stress Dependent Permeability in Coals, SPE Rocky Mountain Regional Meeting, Society of Petroleum Engineers, 1992.

14. Fedorov A. V., Fedorchenko I. A., Leont'ev I. V. Mathematical modeling of two problems of wave dynamics in heterogeneous media, Shock Waves Journ., Vol. 15, No. 8, 2006.

15. Oparin V. N., Tanaino A. S., Yushkin V. F. Discrete properties of entities of a geomedium and their canonical representation. Journal of Mining Science, No. 3(2007).

16. Wang X., Pan Y., Zhang Z., A Spatial Strain Localization Mechanism of Zonal Disintegration through Numerical Simulation, J. Min. Sci., 2013, vol. 49, no. 3, pp. 357–367.

17. Ройтер М. Волнообразное распределение горного давления вдоль забоя лавы / М. Ройтер, В. Курфюст, К. Майрховер, Ю. Векслер // ФТПРПИ. 2009. № 2. С. 38−44.

18. Козырева Е. Н., Шинкевич М. В. Структуризация массива горных пород в условиях отработки угольного пласта длинными столбами // Промышленная безопасность и геомеханика. – Кузбасс. Сборник трудов «Образование, наука, инновации». 2014. №1.

19. Козырева, Е. Н. Особенности газогеомеханических процессов на выемочном участке шахты / Е. Н. Козырева, М. В. Шинкевич // Вестник Научного центра по безопасности работ в угольной промышленности. Кемерово. 2010. № 2. С. 28–35.

20. Леонтьева Е. В. Оценка возможностей методов компьютерного моделирования геомеханического процесса во вмещающем массиве [Электронный ресурс] / Кемерово. Инновационный конвент.

21. Захаров В. Н., Малинникова О. Н., Трофимов В. А., Филиппов Ю. А. Зависимость проницаемости угольного пласта от газосодержания и действующих напряжений // Физико-технические проблемы разработки полезных ископаемых. 2016. №2. С. 16–26.

22. Пак Г. А., Дрижд Н. А., Долгоносов В. Н. Методика расчета шагов обрушения основной кровли и прогноз газовыделения на шахтах Карагандинского бассейна // Безопасность труда в промышленности. 2010. № 10. С. 31–34.

23. Шпаков П. С., Пак Г. А., Долгоносов В. Н. Взаимосвязь шагов обрушения основной кровли и интенсивности газовыделения на шахтах «Сокурская» и «Саранская» Карагандинского бассейна // Маркшейдерия и недропользование. 2009. № 6. С. 70–72.

24. Инструкция по безопасному ведению горных работ на пластах, опасных по внезапным выбросам угля и газа / Министерство энергетики и угольной промышленности РК, 1995. 92 с.

25. Правила охраны сооружений и природных объектов от вредного влияния подземных горных разработок на угольных месторождениях. М.: Недра, 1981. 288 с.

ORIGINAL PAPERS

DOI: 10.17073/2500-0632-2019-1-65-75

The Method of Detection of Clay Minerals and Iron Oxide Based on Landsat Multispectral Images (as Exemplified in the Territory of Thai Nguyen Province, Vietnam)

Le Hung Trinh[1], V. R. Zabloskii[2]

[1]Le Quy Don Technical University, Ha Noi city, Vietnam; ✉trinhlehung125@gmail.com;
[2]Moscow State University of Geodesy and Cartography, Moscow, Russia, v-r-zablotskii@ya.ru

Abstract: Landsat multispectral images have been successfully used for discovering some mineral deposits in different regions of the world. Some minerals, including clay minerals and iron oxide, can be detected by multispectral surveys due to their spectral characteristics. This paper presents the results of the application of principal component analysis and Crosta technique for detecting accumulations of clay minerals and iron oxide based on a Landsat 8 Oli multispectral image of Thai Nguyen Province, north of Vietnam. The obtained results have demonstrated the feasibility and suitability of prompt detecting mineral deposits based on the remote sensing data. The image processing methods and facilities tested in this study can be used to create maps of distribution of clay minerals and iron oxide for effective and expedient prospecting and exploration for minerals.

Keywords: remote sensing, principal component analysis, mineral, Landsat, Vietnam.

For citation: Trinh Le Hung, Zabloskii V. R. The method of detection of clay minerals and iron oxide based on Landsat multispectral images (as exemplified in the territory of Thai Nguyen Province, Vietnam). *Mining Science and Technology*. 2019;4(1):65-75. (In Russ.). DOI: 10.17073/2500-0632-2019-1-65-75.

Методика обнаружения глинистых минералов и оксида железа по данным многозональных изображений Landsat (на примере территории провинции Тхай Нгуен, Вьетнам)

Чинь Ле Хунг[1], Заблоцкий В. Р.[2]

[1]Технический университет им. Ле Куи Дон, Ханой, Вьетнам, ✉trinhlehung125@gmail.com;
[2]Московский государственный университет геодезии и картографии, Москва, Россия, v-r-zablotskii@ya.ru

Аннотация: Многозональные изображения Landsat с успехом использовались для выявления месторождений некоторых полезных ископаемых в разных регионах мира. Некоторые минералы, в том числе глинистые минералы и оксид железа, могут быть обнаружены по данным многозональной съемки из-за их спектральных характеристик. В данной работе представлены результаты применения метода главных компонетов и технологии Crosta для обнаружения скоплений глинистых минералов и оксида железа на основе использования многозонального изображения Landsat 8 Oli провинции Тхай Нгуен, север Вьетнама. Полученные результаты показали возможность и целесообразность оперативного определения месторождения полезных ископаемых по данным дистанционного зондирования. Методы и средства обработки изображений, апробированные в этом исследовании, могут использоваться для создания карт распределения глинистых минералов и оксида железа, с целью эффективного и рационального поиска полезных ископаемых и разведки минерального сырья.

Ключевые слова: дистанционное зондирование, метод главных компонетов, минерал, Landsat, Vietnam.

Для цитирования: Чинь Ле Хунг, Заблоцкий В. Р. Методика обнаружения глинистых минералов и оксида железа по данным многозональных изображений Landsat (на примере территории провинции Тхай Нгуен, Вьетнам). *Горные науки и технологии.* 2019;4(1):65-75. DOI: 10.17073/2500-0632-2019-1-65-75.

INTRODUCTION

Minerals are the most important natural resources of any country. Mineral resources are used in many industries: in energy generation, construction, metallurgy, agriculture, etc. Prospecting and discovery of mineral resources is a difficult task. Traditional methods based on field prospecting and exploratory surveying work, solve this problem, but bear high costs. Remote sensing technology has several advantages over ground-based reconnaissanc|exploration methods, due to coverage of a wide area and short re-observation period. The studies [1–5, 7–10, 13–18, 20–23] confirms the possibility of using multispectral images (Landsat, Aster) for monitoring and detecting minerals. Scanner images capture information about the underlying surface in the visible, near and middle infrared spectral regions [6, 11, 12]. This allows investigating physical properties of the studied surface and making assumptions about soils and rocks.

Landsat multispectral image data have been used for several years in arid and semi-arid natural conditions to identify deposits of iron oxides and hydrothermal minerals. Many authors have used the spectral index method to detect minerals. For example, the spectral indices obtained from Landsat and ASTER multispectral images were used for prospecting iron oxide, clay minerals, magnetite content, ferrous minerals and calculation of Abrams, Chica-Olma and Kaufmann indices [4, 10]. Crosta (1989) [5], Mia and Fujimitsu (2012) [16] used the principal component analysis (PCA) method to detect mineral deposits. Based on the principal component analysis method, Fraser et al. (1997) [10] developed the DPCA method (directed principal component analysis) to monitor the distribution of minerals. The DPCA method was also used by Khaleighi and Ranjbar (2011) [14] to map copper content in Iran based on ASTER multispectral images. The findings obtained in these studies show that the principal component method has higher accuracy of mineral detection than the spectral index method.

This work is devoted to the detection of clay minerals and iron oxides in the Thai Nguyen Province, northern Vietnam based on the multispectral survey LANDSAT 8 data using the method of principal components. Some other image processing methods were also used in the work, including the creation of color mosaics, stretching the histograms of brightness, decorrelation, improving the edges of contours, merging images, calculating spectral indices – to estimate the mineral content in rocks and soils.

MATERIALS

The Study Area. Thai Nguyen Province is located in the northern part of Vietnam, 80 km from the Hanoi, the capital of the country (Fig. 1). The geographic coordinates: 21°20 ′ to 22°03′ N, 105°52′ to 106°14′ E The Province is crossed by several mountain ranges, stretching in the direction from the northwest to the southeast. In the southwest of the province, Tamdao mountain range of 80 km long is located. The vegetative cover in the Province, mainly presented by newly planted forests and fruit trees, occupies about 80% of the area. Natural forests remained in a small part of the territory and are common in high mountain ranges. Mountain soil occupies 48.4% of the area, is located at heights of more than 200 m and formed as a result of weathering of hard and metamorphic rocks and other formations. The soil of the hills covers 31.4 % of the area, is formed mainly over sandstone, siltstone and some ancient tectonic formations. Thai Nguyen Province is rich in mineral resources, including iron and coal. Pictures of some mineral mines in the study area are shown in Fig. 3 [24].

Initial data. In this work, we used a multispectral image received from the Landsat 8 OLI satellites; the survey date was June 15, 2017 (Fig. 2). The image was produced in cloudless weather – a necessary condition for shooting. This image was downloaded from the site of the United States Geological Survey (US Geological Survey – USGS – http://glovis.usgs.gov) with L1T processing level [25].

Landsat 8 is the eighth satellite in the Landsat program and the seventh satellite of this series, launched into the Earth orbit. Landsat 8 receives images of the Earth's surface in the visible, near-IR and thermal IR ranges, with spatial resolution of 15 to 100 m (Table 1).

METHODS AND FINDINGS

To detect iron oxides and clay minerals from Landsat 8 multispectral image data, the principal component analysis (PCA) method was used. This method allows to reduce the data dimensionality with the least loss of valuable information for decryption.

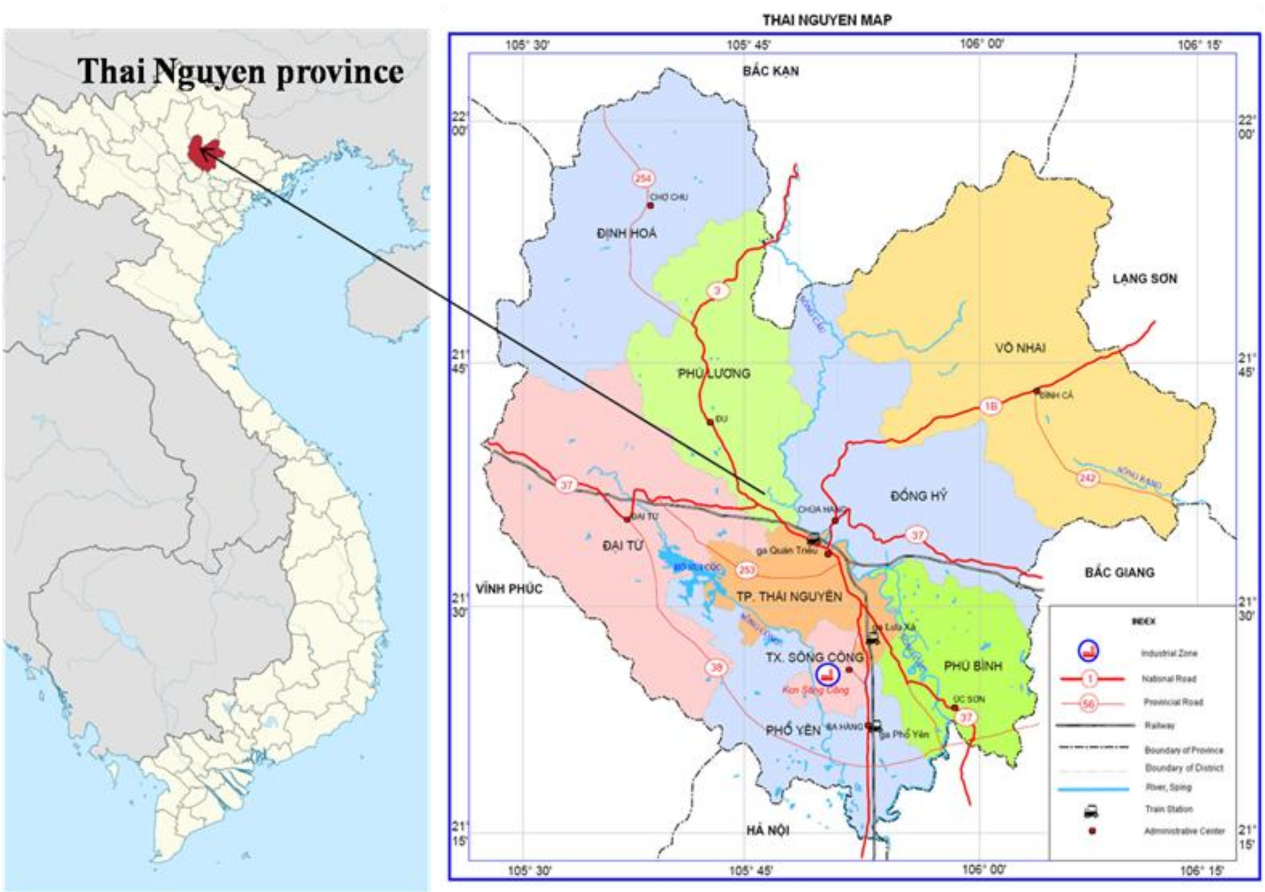

Fig. 1. Location of the study area, Thai Nguyen Province, Vietnam

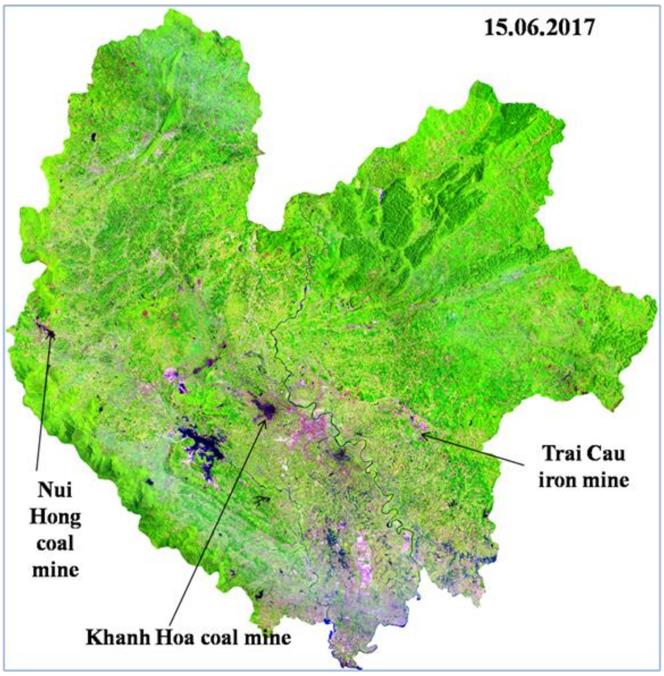

Fig. 2. Landsat 8 multispectral image in Thai Nguyen province, 15.06.2017

Fig. 3. Pictures of some mineral mines in the study area: coal mines Han Hoa (a), Nui Hong (b), and Chai Kau iron ore mine (c) [24]

Table 1

Characteristics of the multispectral image received from the Landsat 8 satellite

No.	Spectral channel	Range (μm)	Spectral resolution (m)
1	Channel 1 – shores and aerosols	0.433–0.453	30
2	Channel 2 – Blue	0.450–0.515	30
3	Channel 3 – Green	0.525–0.600	30
4	Channel 4 – Red	0.630–0.680	30
5	Channel 5 – Near-infrared	0.845–0.885	30
6	Channel 6 – Middle-infrared	1.560–1.660	30
7	Channel 7 – Middle-infrared	2.100–2.300	30
8	Channel 8 – achromatic	0.500–0.680	15
9	Channel 9 – Cirrus	1.360–1.390	30
10	Channel 10 – Thermal infrared	10.30–11.30	100
11	Channel 11 – Thermal infrared	11.50–12.50	100

In this paper, it is shown that the first principal component (PC1) consists of the positive elements of all spectral channels of the Landsat 8 image (channels 2, 3, 4, 5, 6, and 7). PC1 amounts to about 95.12 % of the eigenvalue of the total variance for the PCA data. The eigenvector for the third principal component (PC3) indicates that vegetation, which has high reflectivity in the near infrared range (channel 5) prevails in PC3. The negative value of the element in channel 5 on this principal component (−0.77223) also indicates that the vegetation pixels will be black on this principal component. Since the elements on the eigenvectors for channel 2 and channel 4 in the sixth principal component (PC6) (Table 2) are also opposite in sign, it can be assumed that the iron oxides will differ in bright pixels in PC6. Hydroxyl minerals are displayed as dark pixels in PC5 due to the fact that the contribution is negative from channel 6 and positive from channel 7 in this PC5 (Table 2). If the number of input channels is reduced to avoid a certain spectral contrast, the probability of determining an unique principal component for the detection of minerals will increase [15].

Hydroxyl minerals reflect electromagnetic radiation in the range 1.55–1.75 μm (channel 6 of the Landsat 8 image) much more intensively than in the other studied ranges, and are intensively absorbed in the range from 2.05 to 2.35 μm (channel 7) [7]. Thus, for the detection of clay minerals, spectral channels in blue (channel 2), near IR (channel 5) and mid-infrared ranges (channels 6 and 7) of Landsat 8 image are used. Channels 3 (green) and 4 (red) are not used, to avoid the effects of iron oxides and vegetation cover. The results of the conversion of the principal components in the combination of channels 2, 5, 6 and 7 of the Landsat 8 image for the territory of the Thai Nguyen Province Vietnam) are shown in Table. 3. An analysis of the results showed that PC4 with relatively strong positive load for channel 7 (0.7384) and moderate negative load for channel 6 (−0.5791) can be used to detect hydroxyl minerals. PC4 distinguishes hydroxyl minerals as dark pixels. Using the inversion method, hydroxyl minerals are represented by light pixels on PC4 (Fig. 4, *a*).

Table 2

The findings of main component analysis for 6 multispectral image channels of Landsat 8

Channel	B2	B3	B4	B5	B6	B7	Eigenvalue (%)
PC1	0.32708	0.26698	0.22964	0.38848	0.39815	0.64149	95.123
PC2	−0.14263	0.05132	0.24151	0.03498	0.60180	0.58675	2.689
PC3	0.22824	0.23004	0.46350	−0.77223	−0.15801	0.11465	1.935
PC4	−0.09365	−0.38327	−0.56946	−0.42576	0.36687	0.33932	0.196
PC5	−0.17823	0.13023	0.12403	−0.25107	−0.54775	0.06205	0.035
PC6	−0.56011	−0.53438	0.54677	0.08179	−0.08079	0.28967	0.023

Table 3

The findings of main component analysis for identifying hydroxyl minerals

Principal components	Eigen vector				Eigenvalue (%)
	B2	B5	B6	B7	
PC1	0.3566	0.6158	0.6218	0.3270	95.481
PC2	0.1340	0.6730	−0.4379	−0.5808	3.119
PC3	−0.9072	0.2833	0.2935	−0.1024	1.310
PC4	−0.1783	0.2959	**−0.5791**	**0.7384**	0.090

Table 4

The findings of main component analysis for identifying clay minerals

Principal components	Eigen vector				Eigenvalue (%)
	B2	B4	B5	B6	
PC1	0.3680	0.2381	0.6351	0.6360	95.775
PC2	0.0992	0.4337	−0.7340	0.5132	2.410
PC3	−0.7739	−0.3509	0.0548	0.5244	1.724
PC4	**0.5058**	**−0.7951**	−0.2343	0.2389	0.091

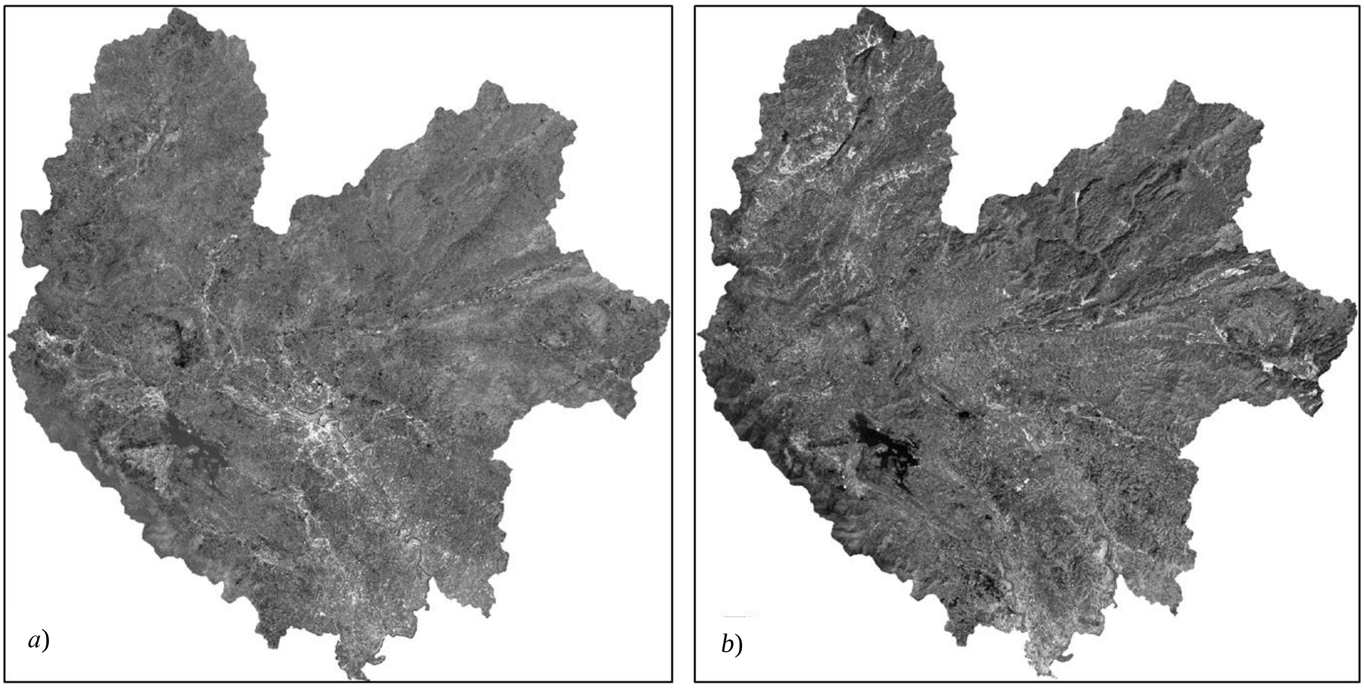

Fig. 4. Component PC4, bright pixels indicate the location of hydroxyl minerals (*a*) and iron oxides (*b*)

Similarly, for the detection of iron oxides, the spectral channels 2, 4, 5, and 6 of the Landsat 8 image are used in this study. The green channel (channel 3) is not used to avoid the effect of vegetation on the results of the detection of minerals. The results of the conversion of the principal components in the combination of channels 2, 4, 5, and 6 of the Landsat 8 image in the Thai Nguyen Province (Vietnam) are shown in Table. 4. In this case, PC4 pinpoints iron oxide as dark pixels (the eigenvector for channel 4 is −0.7951 and for channel 2, +0.5058). This image (PC4) can be inverted by brightness (brightness inverse) to show the location of iron oxides as bright pixels (Fig. 4, *b*).

Images of the principal components (PC4) for hydroxyl minerals and iron oxides are combined to create a single image displaying pixels with abnormal concentrations of both hydroxyls and oxides of iron as the brightest. This merger of two images is also obtained using the method of principal components, such as PC1, having positive eigenvalues for both input images. These images were then combined using Crosta technology to produce the three-layer image. The flowchart of the image processing method for detecting hydroxyl minerals and iron oxides from the LANDSAT 8 multispectral image data is shown in Fig. 5.

To process multispectral images, the RS-MINERALS software package was created based on the Matlab programming language. The package is intended for the analysis of satellite images by the principal component analysis method. The RS-MINERALS software package provides the ability to open and process satellite images in TIFF format, including basic modules such as View (imagery), Idicies (spectral indices), PCA (principal component analysis), DPCA (directed PCA), Interpreter (image processing). The software program interface is presented in Fig. 6.

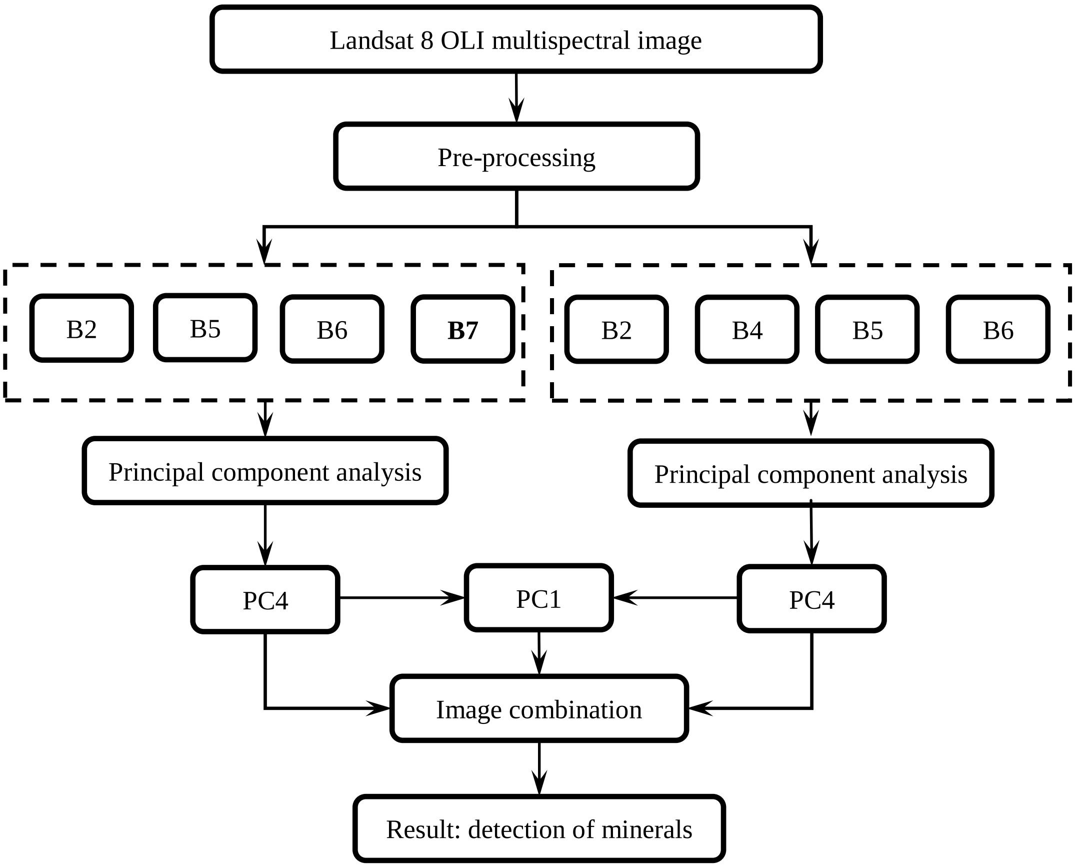

Fig. 5. Image processing method for detection of hydroxyl minerals and iron oxide using a Landsat 8 Oli multispectral image

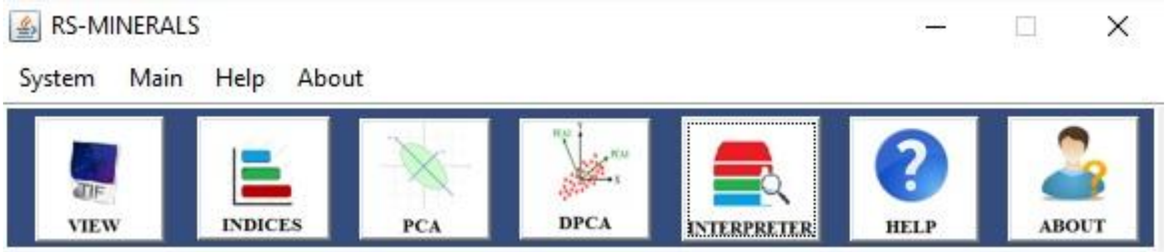

Fig. 6. RS-MINERALS software program interface

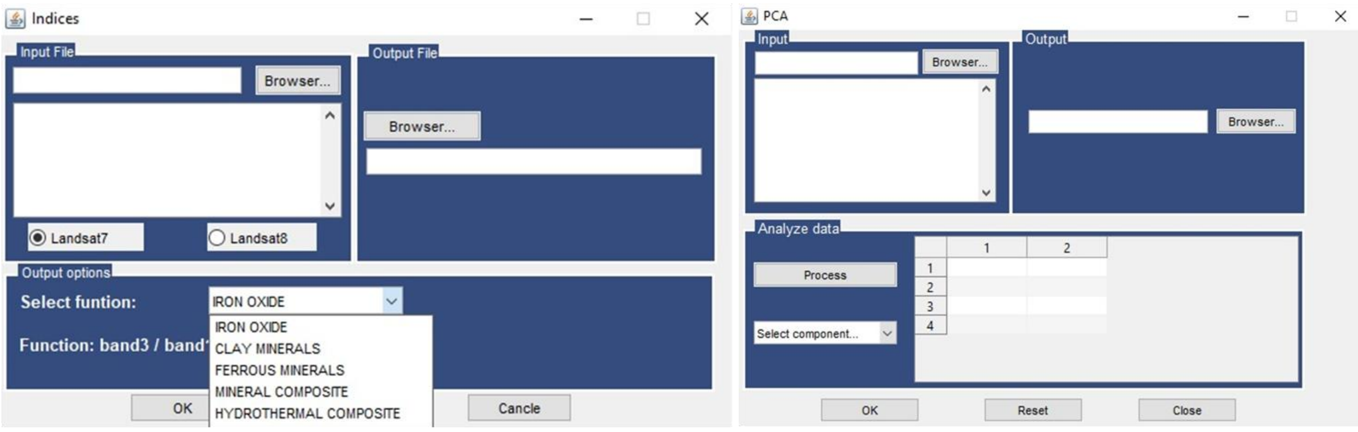

а *б*

Fig. 7. PCA (*a*) and Indices (*b*) modules in the RS-MINERALS software package

The PCA module allows calculating the principal components for Landsat images. At the output, the program displays eigenvectors and eigenvalues for the selected principal components containing the most valuable information about minerals (Fig. 7, *a*).

The Indices module allows calculating mineral indices such as those for clay minerals, iron oxide, ferrous minerals, mineral composites, Abramm index, Kaufmann index and Chica-Olma index (Fig. 7, *b*).

The Interpreter module has tools for combining the spectral channels of a multispectral image (Band combinations) and Brightness inversion. The Brightness inversion tool allows inverting the brightness of pixels to highlight the location of minerals in the image of the principal component.

The DPCA module allows highlighting the location of minerals using the DPCA method described by Fraser and Green (1987). In this method, PC1 is calculated from the ratios of the Landsat TM spectral channels: (channel 4/channel 3) and (channel 5/channel 7). The image (channel 5/channel 4) and the image (channel 7 + channel 1) were used to create the color RGB image.

The result of the combination of the images for the detection of hydroxyl minerals and iron oxide was shown in Fig. 8. In this image, white pixels represent areas rich in both hydroxyl and iron minerals. The areas containing many hydroxyl minerals are shown by bright red to orange color, and the areas rich in iron are shown in bright blue to blue color [15].

To assess the accuracy of the detection of hydroxyl minerals and iron oxide from Landsat 8 multispectral survey data, we used the mineral map of Thai Nguyen Province, Vietnam, at a scale of 1:200,000 (Fig. 9). The obtained results showed that iron minerals are distributed over most of the Thai Nguyen Province. The location of large iron ore mines such as Trai Cau, Hoa Trung, Linh Nham, Thanh Chu, Tien Bo is clearly displayed in the image after color combination with the use of Crosta technology. The results also showed that hydroxyl minerals are concentrated in the areas where large coal mines are located, such as Nui Hong, Khanh Hoa, Phan Me (see Fig. 8).

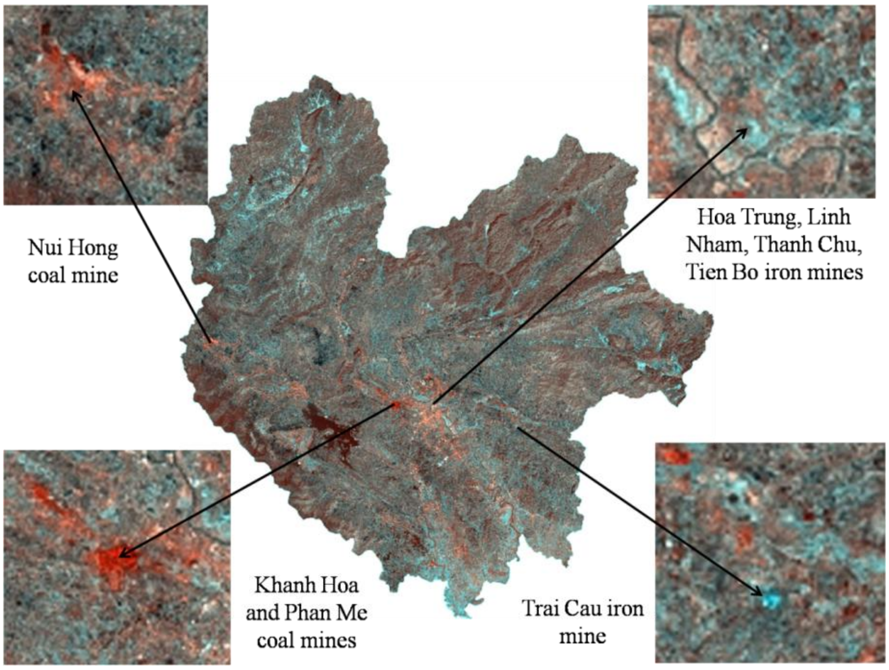

Fig. 8. Crosta-based image combination

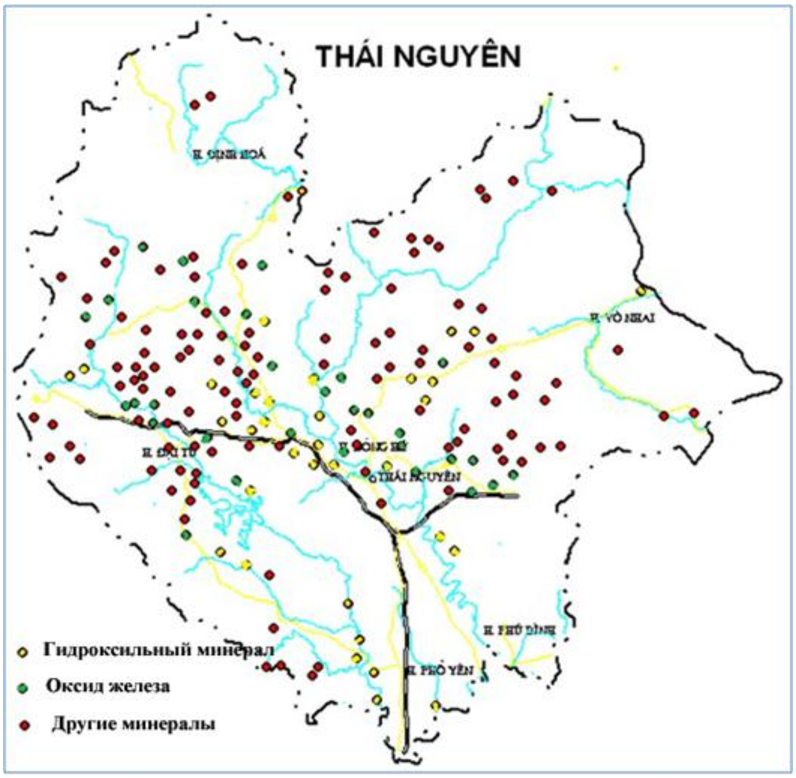

Fig. 9. Map of minerals of Thai Nguyen province (Vietnam), scale 1 : 200.000

CONCLUSIONS

LANDSAT 8 multispectral images can be effectively used to detect and forecast the hydroxyl mineral and iron oxide deposits. The method of the principal component analysis is capable to detect minerals with greater reliability due to the elimination of duplicate information in the spectral channels. In this study, hydroxyl minerals and iron oxide were detected in rocks, as well as in open soils in the vicinity of mining enterprises. Rock emissions around mines are very well decrypted on images of the principal components based on Crosta technology. In the Thai Nguyen Province, in the territory with sparse vegetation, hydroxyl minerals and iron oxide can also be detected based on decryption of hard rock and arenacaous formations. The findings obtained in this study can be used to create and update a map of minerals distribution for forecasting new concentrations of mineral raw materials.

Библиографический список / References

1. Oparin V. N., Potapov V. P., Ginliyatullina O. L., On comprehensive assessment of environmental condition based on data of earth remote sensing in regions with high man-induced impact: Physical and technical issues of mining, 2014, No. 6, pp. 199-209. (in Russ.)

2. Usikov V. I., Lipina L. N. Evaluation of geoecological situation in the area of Maly Khingan based on data of remote sensing of the earth's surface: Physical and technical issues of mining, 2018, No. 2, pp. 154-160. (in Russ.)

3. Abrams M. J. Remote sensing of porphyry copper in Southern Arizona, Economic Geology, 1983, No. 78, pp. 591–604.

4. Alasta A. F. Using remote sensing data to indentify iron deposits in central western Libya, International conference on Emerging trends in Computer and Image processing, Bangkok, 2011, pp. 56–61.

5. Crosta A. P., Moore J. M. Enhancement of LANDSAT Thematic Mapper imagery for residual soil mapping in SW Minas Gerais State Brazil: a prospecting case history in greenstone belt terrain, Proceedings of the 9th Thematic Conference on Remote Sensing for Exploration Geology, Calgary (Ann Arbor, MI: Environmental Research Institute of Michigan), 1989, pp. 1173–1187.

6. Clark R. N., Swayze G. A., Wise R., Livo K. E., Hoefen T. M., Kokaly R. F., Sutley S. J. USGS Digital Spectral library, USGS Open file Rep, 1989.

7. Dematte J. A. M., Fiorio P. R., Ben-Dor E. Estimation of soil properties by orbital and laboratory reflectance means and its relation with soil classification, The Open Remote Sensing Journal, 2009, Vol. 2, pp.12–23.

8. Dogan H.D. (2012). Mineral composite assessment of Kelkit River Basin in Turkey by means of remote sensing, Journal Earth System Science, Vol. 118(6), pp.701–710.

9. Fongaro C., Dematte J., Rizzo R., Safanelli J., Mendes W., Dotto A., Vicente L., Franceschini M., Ustin S. Improvement of Clay and Sand Quantification Based on a Novel Approach with a Focus on Multispectral Satellite Images, Remote Sensing, 2018, 10, 1555; doi:10.3390/rs10101555.

10. Fraster S. J., Green A. A. A software defoliant for geological analysis of band ratio, International journal of remote sensing, 1997, Vol.8, pp. 525–532.

11. Goetz A. F., Rock F. H., Rowan B. N. Remote sensing for exploration: An overview, Economic Geology, 1983, Vol. 78, 573–590.

12. Hunt G. R., Ashley R. P. Spectra of altered rocks in the visible and near infrared, Economic Geology, 1979, Vol. 74, pp. 1613-1629.

13. Kaufman H. Mineral exploration along the Agaba-Levant structure by use of TM-data concepts, processing and results, International Journal of Remote Sensing, 1988, 9:1630–1658.

14. Khaleghi M., Ranjbar H. Alteration mapping for exploration of porphyry copper mineralization in Sarduiyed area, Kerman province, Iran using ASTER SWIR data, Australian Journal of Basic and Applied Sciences, 2011, 5(8), pp. 61–69.

15. Loughlin W. P. Principal component analysis for alteration mapping, Photogrammetric Engineering and Remote Sensing, 1991, 57(g), pp. 1163–1169

16. Mia M. B., Fujimitsu Y. Mapping hydrothermal altered mineral deposits using LANDSAT 7 ETM+ image in and around Kuju volcano, Kyushu, Japan, Journal Earth System Science, 2012, Vol. 121(4), pp.1049–1057.

17. Pour A. B., Hashim M. Integrating PALSAR and ASTER data for mineral deposits exploration in tropi-

cal environments: a case study from Central Belt, Peninsular Malaysia, International Journal of Image and Data Fusion, 2015, 6(2), pp. 170–188.

18. Pour A. B., Park T., Park Y., Hong J., Zoheir B., Pradhan B., Ayoobi I., Hashim M. Application of Multi-Sensor Satellite Data for Exploration of Zn–Pb Sulfide Mineralization in the Franklinian Basin, North Greenland, Remote Sensing, 2018, 10(8), 1186; doi:10.3390/rs10081186.

19. Singh A., Harrison A. Standarlized principal components, International Journal of Remote Sensing, 6(6), 1985, pp. 883–896.

20. Sridhar B. B., Vincent R. K. Mapping and estimation of phosphorus and copper concentrations in Fly Ash spill area using LANDSAT TM data, Photogrammetric Engineering and Remote Sensing, 2009, Vol. 75(9), pp. 1030-1033.

21. Trinh L. H. Application of remote sensing technique to detect and map iron oxide, clay minerals and ferrous minerals in Thai Nguyen province, Горные науки и технологии, 2016, Vol. 1, 60 – 66.

22. Trinh L. H. Application of band ratio method to detect iron oxide, clay minerals and ferrous minerals, Mining Industry Journal, 2014, Vol. 4, pp. 19-24.

23. Van der Meer F. D., van der Werff H. M. A., van Ruitenbeek F. J. A. Potential of ESA's Sentinel-2 for geological applications, Remote Sensing of Environment, 2014, 148, 124–133

24. Vietnam national coal-mineral industries holding corporation limited (Vinacomin). Available at: www.vinacomin.com.vn.

25. The official website of GloVis. Available at: http://glovis.usgs.gov.